Technische Universität Dortmund

Higher-order corrections to the energy loss cross sections of high-energy muons

Dissertation zur Erlangung des akademischen Grades eines

Doktors der Naturwissenschaften
(Dr. rer. nat.)

vorgelegt von

M. Sc. Alexander Sandrock
geboren in Arnsberg

Lehrstuhl für Experimentelle Physik V
Fakultät Physik
Technische Universität Dortmund

Dortmund, September 2018.

Contents

Abstract

In this thesis corrections to the energy loss cross sections of high-energy muons are calculated. Over a large part of the energy range investigated by very large volume neutrino telescopes such as IceCube, pair production and bremsstrahlung dominate the energy loss. The theoretical uncertainties on the energy loss cross sections influence the experimental results as systematic uncertainties. These corrections are important for the energy reconstruction of high-energy muons which are observed in particle and astroparticle detectors.

The leading-order cross sections of bremsstrahlung and pair production have been parametrized with less approximations than in previous works. In the case of bremsstrahlung the differences are most pronounced at low muon energies, where bremsstrahlung is a very subdominant process, while at higher energies the difference to previous works is negligible. For pair production, the new parametrizations lead to changes of up to a percent to the cross section differential in the lost energy, and the differences are present at all energies.

For bremsstrahlung, the next-to-leading-order (NLO) corrections have been calculated for the average energy loss and the differential cross section. The average energy loss is increased by about 2% in the high-energy limit due to these corrections. The relative effect on the differential cross section is independent of the energy of the muon in the approximation used here. The correction increases the cross section for large relative energy losses.

For the inelastic nuclear interaction, NLO corrections have also been calculated. The correction to the cross section is also most pronounced for large relative energy losses; the correction is not independent of the muon energy for this process.

For bremsstrahlung and pair production, Coulomb corrections, i. e. corrections to all orders in the coupling $Z\alpha$ to the electric field of the nucleus have been calculated and parametrized, taking into account the nuclear formfactor. The qualitative behavior has been predicted earlier by other authors using simplified models for the nuclear charge distribution; this is the first quantitative calculation of Coulomb corrections for realistic extended nuclei.

Zusammenfassung

In dieser Arbeit werden Korrekturen zu den Wirkungsquerschnitten der Energieverlustprozesse hochenergetischer Myonen berechnet. Die theoretischen Unsicherheiten auf die Wirkungsquerschnitte der Energieverlustprozesse beeinflussen experimentelle Ergebnisse als systematische Unsicherheiten. Die in dieser Arbeit bestimmten Korrekturen sind daher von Bedeutung für die Energierekonstruktion hochenergetischer Myonen, wie sie in Detektoren von Teilchenphysik- und Astroteilchenphysikexperimenten beobachtet werden. Der Energieverlust wird über einen Großteil des Energiebereichs großvolumiger Neutrinoteleskope, wie IceCube, durch Paarproduktion und Bremsstrahlung dominiert

Die Wirkungsquerschnitte für Bremsstrahlung und Paarproduktion in führender Ordnung werden mit weniger Näherungen als in früheren Arbeiten parametrisiert. Im Falle der Bremsstrahlung sind die Unterschiede am bedeutendsten bei kleinen Energien, wo Bremsstrahlung ein subdominanter Prozess ist, während bei hohen Energien die Unterschiede zu früheren Arbeiten vernachlässigbar

sind. Im Fall der Paarproduktion führt die neue Parametrisierung zu Unterschieden von bis zu etwa einem Prozent im in der verlorenen Energie differentiellen Wirkungsquerschnitt, die bei allen Energien auftreten.

Strahlungskorrekturen werden für den mittleren Energieverlust und den differentiellen Wirkungsquerschnitt der Bremsstrahlung berechnet. Der mittlere Energieverlust von Myonen durch Bremsstrahlung steigt durch diese Korrekturen um etwa 2%. Der relative Effekt auf den differentiellen Wirkungsquerschnitt ist in der hier genutzten Näherung unabhängig von der Energie des Myons. Die Korrekturen erhöhen den Wirkungsquerschnitt für große relative Energieverluste.

Ebenfalls wurden Strahlungskorrekturen für den Wirkungsquerschnitt der inelastischen nuklearen Wechselwirkung berechnet. Die Korrekturen sind auch in diesem Fall bei großen relativen Energieverlusten bedeutend, jedoch sind die Korrekturen in diesem Fall nicht unabhängig von der Myonenergie.

Für Bremsstrahlung und Paarproduktion wurden Coulombkorrekturen, d. h. Korrekturen zu allen Ordnungen im Kopplungsparameter $Z\alpha$ zum elektrischen Feld des Kerns berechnet, wobei der nukleare Formfaktor berücksichtig wurde. Die qualitativen Eigenschaften der Ergebnisse stimmen mit früheren näherungsweisen Vorhersagen überein; diese Arbeit führt die erste quantitative Bestimmung von Coulombkorrekturen für realistische ausgedehnte Atomkerne durch.

Chapter 1

Introduction

One of the central problems of astroparticle physics is the energy reconstruction of muons and neutrinos. The energy spectra of muons and neutrinos produced in the atmosphere in extended air showers provide the possibility to study hadronic interactions at energies inaccessible to present accelerators, and the energy spectra of astrophysical neutrinos offer insights into the acceleration processes of such extreme environments as active galactic nuclei and gamma ray bursts, which are assumed to be the production sites of ultra-high energy charged cosmic ray particles.

The determination of these spectra depends on the energy reconstruction of the muon events and, in the case of muon neutrino spectra, the determination of the neutrino energy from the muon energy. The energy reconstruction of muons is based on the energy loss of muons. The processes which contribute to the energy loss of muons are ionization, pair production, bremsstrahlung and inelastic nuclear interaction.

The average energy loss is approximately a first-order polynomial of the energy and thus well correlated to the energy of the muon [15]. However, the energy is not lost continuously but stochastically. This makes the determination of the muon energy an ill-posed inverse problem. The algorithms used to solve this problem [5, 51] depend on accurate simulations [63, 64] of the energy loss patterns and their effects in detectors. The uncertainties of the energy loss cross sections affect the results of these algorithms as systematic uncertainties. To reduce the uncertainties, the cross sections are calculated more exactly in this thesis.

The production processes and energy spectra of atmospheric muons and of atmospheric and astrophysical neutrinos are described in Chapter 2, together with a brief account of astroparticle physics in general. The characteristics of the different energy loss processes and the parametrizations commonly used for the simulation of muon propagation are reviewed in Chapter 3, where also improved parametrizations of the leading-order cross sections for bremsstrahlung and pair production are presented and the influence of other processes is estimated. In Chapter 4 a modified Weizsäcker-Williams method is presented, which is used in Chapter 5 to investigate the effect of radiative corrections on the average energy loss and cross section of bremsstrahlung. Additionally, in this chapter the radiative correction to the cross section of inelastic nuclear interaction is calculated. The effect of Coulomb corrections on the pair production and bremsstrahlung

cross section is investigated in Chapter 6.

Chapter 2

Muon production

Muons in astroparticle detectors are produced in the atmosphere via decay of hadrons, where the spectral behaviour depends on the decaying hadron, via pair production in photon-nucleus interactions in the atmosphere, production of muon pairs by other muons or in charged current interactions of muon neutrinos.

2.1 Muons from pions and kaons

Pions and kaons decay predominantly into muons and muon neutrinos

$$\pi^{\pm} \to \mu^{\pm} + \nu_{\mu}(\bar{\nu}_{\mu}) \quad (\sim 100\,\%) \tag{2.1}$$

$$K^{\pm} \to \mu^{\pm} + \nu_{\mu}(\bar{\nu}_{\mu}) \quad (\sim 63.5\,\%). \tag{2.2}$$

Typically these decays occur in heights of $\sim$ 15 km [46]. For muon energies above $E_{\mu} \sim 2.5\,\mathrm{GeV}$ the decay length is longer than the distance to the ground and the muon can be considered as stable.

The form of the muon flux is determined by the competition between the decay of the parent mesons according to the above equations and the interaction of the mesons with the surrounding air. The critical energy where the interaction probability exceeds the decay probability of the hadron i is approximately given by [46]

$$\varepsilon_i^{\mathrm{crit}} = \frac{\varepsilon_i}{\cos\theta^*} = \frac{m_i c^2 h_0}{\cos\theta^* c\tau_i}, \tag{2.3}$$

where θ^* is the local zenith angle at the production site to account for the curvature of the Earth, m_i and τ_i are the mass and lifetime of the hadron i and $h_0 = RT/Mg = 29.62\,\mathrm{m/K} \times T \approx 6.4\,\mathrm{km}$ is the scale height in an exponential approximation of the density at high altitudes, where R is the universal gas constant, g the gravitational acceleration, T the temperature and M the molar mass of the atmosphere. The local zenith angle θ^* at production is related to the zenith angle θ on ground by

$$\cos\theta = \frac{(R_E + h)\cos\theta^* - R_E}{\sqrt{(R_E + h)^2 + R_E^2 - 2(R_E + h)R_E\cos\theta^*}} \tag{2.4}$$

with R_E the earth radius and h the production height. The leptons from these light hadrons are commonly referred to as conventional muons and neutrinos. The spectrum of leptons from air showers can then be expressed as[1] [45]

$$\varphi_\ell(E_\ell) = \varphi_N(E_\ell) \times \left\{ \frac{A_{\pi\ell}}{1 + B_{\pi\ell} \cos\theta E_\ell/\varepsilon_\pi} + \frac{A_{K\ell}}{1 + B_{K\ell} \cos\theta E_\ell/\varepsilon_K} + \frac{A_{\mathrm{charm}\ell}}{1 + B_{\mathrm{charm}\ell} \cos\theta E_\ell/\varepsilon_{\mathrm{charm}}} \right\}, \tag{2.5}$$

where the weakly energy-dependent A-factors consist of the spectrum-weighted moments of the production and decay of mesons, accounting for both the kinematics and branching ratios, the denominator accounts for the interaction and the energy dependence of the decay distributions, and $\varphi_N(E) = dN_N/dE$ is the number spectrum of cosmic-ray nucleons interacting with the atmsophere.

Air shower arrays such as the Pierre Auger Observatory [1] and Telescope Array [8] observe a flux of nuclei which can be described approximately by a broken law [46] (Fig. 2.1)

$$\frac{dN}{dE} \propto \begin{cases} E^{-2.7} & 10\,\mathrm{GeV} \lesssim E \lesssim 1\,\mathrm{PeV}, \\ E^{-3.1} & 10\,\mathrm{PeV} \lesssim E \lesssim 1\,\mathrm{EeV}, \\ E^{-2.6} & 10\,\mathrm{EeV} \lesssim E \lesssim 10^{20}\,\mathrm{eV}. \end{cases} \tag{2.6}$$

Since the pion and the muon differ only slightly in mass, the muon receives most of the energy of the pion. The kaon is considerably heavier, leading to a more equal distribution of the energy on the muon and the neutrino. Thus, the conventional neutrino flux is dominated by the contribution from kaons above $E_\nu/\cos\theta \sim 10^2\,\mathrm{GeV}$, while for muons pions remain the dominant contribution (cf. Fig. 2.2, Fig. 2.3).

The interaction probability is proportional to the density of air, which in the case of an ideal gas is inversely proportional to the temperature. The decay probability on the other hand is independent of the ambient temperature. Consequently, the critical energies $\varepsilon_i^{\mathrm{crit}}$ change with the seasonal variations of the temperature in the atmosphere.

2.2 Muons from heavy hadrons

The production of muons from heavy hadrons such as D-mesons or Λ_c-baryons is described analogously to the light mesons (cf. (2.3)). However, the critical energy $\varepsilon_i^{\mathrm{crit}}$ is of the order of a few PeV, therefore the lepton flux from heavy hadrons stems practically exclusively from the decay-dominated regime. They are commonly referred to as prompt muons and neutrinos.

Compared to prompt neutrinos, the prompt muon flux receives an additional component due to the decay of unflavored mesons such as

$$\eta \to \mu^+ + \mu^-. \tag{2.7}$$

The contributions of the various parent particles are shown in Fig. 2.2 and Fig. 2.3. The contribution of unflavored particles such as $\eta, \eta', \varrho, \omega$ is comparable to the

[1] The third term correspond to leptons from heavy hadrons, as discussed in the next section.

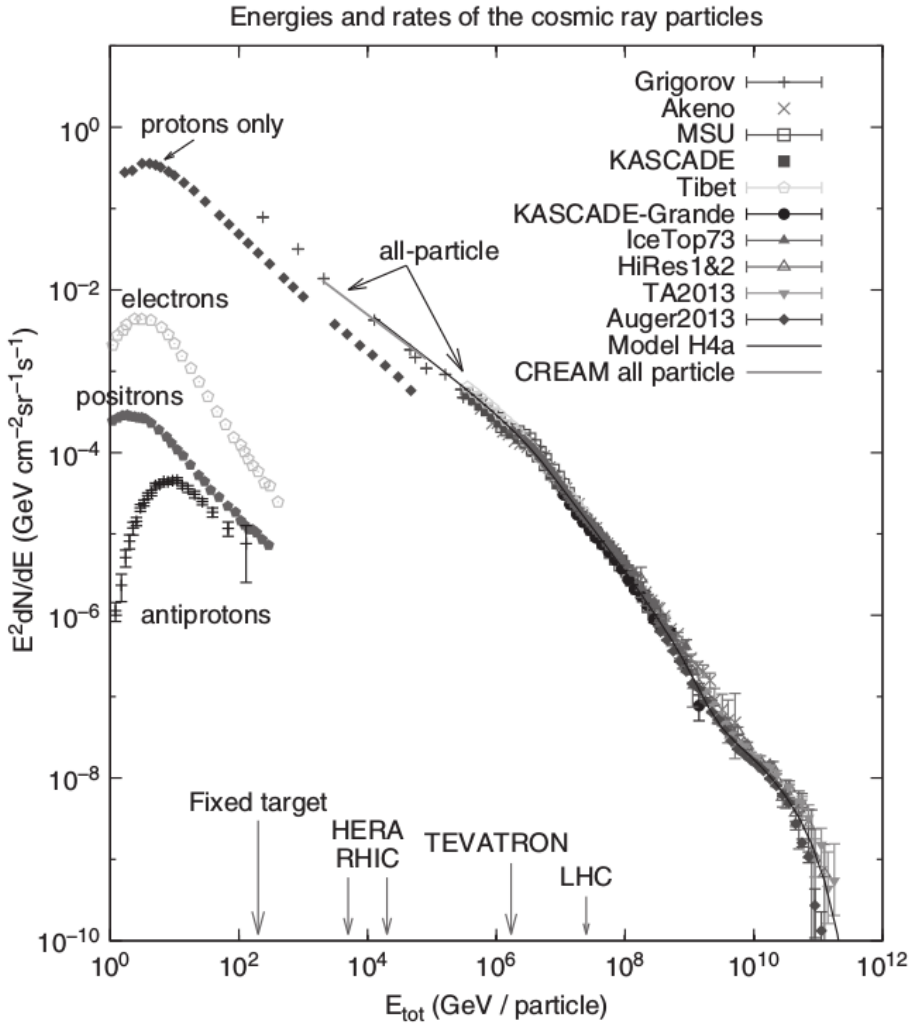

Figure 2.1: Spectrum of charged cosmic ray particles measured by various experiments [46]. The arrows at the x-axis denote the laboratory energies corresponding to various accelerator experiments.

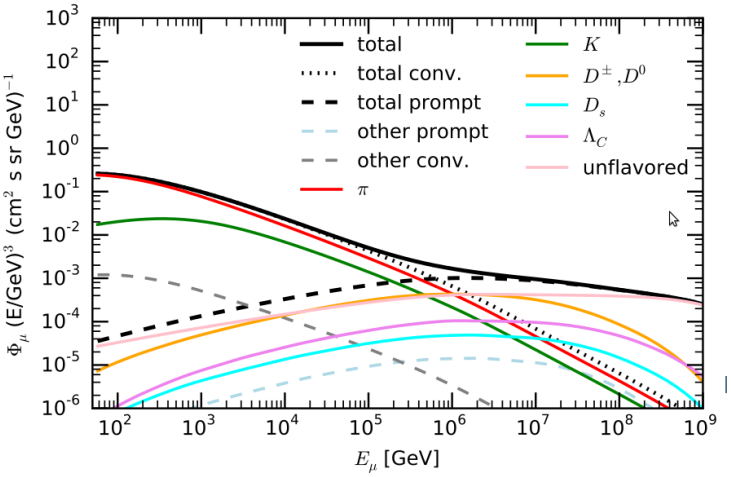

Figure 2.2: Atmospheric muon flux with partial contributions of intermediate particles [43], weighted with the third power of the muon energy. The pion component remains dominant compared to the kaon component for the conventional flux. The prompt component from unflavored meson decays is also clearly visible.

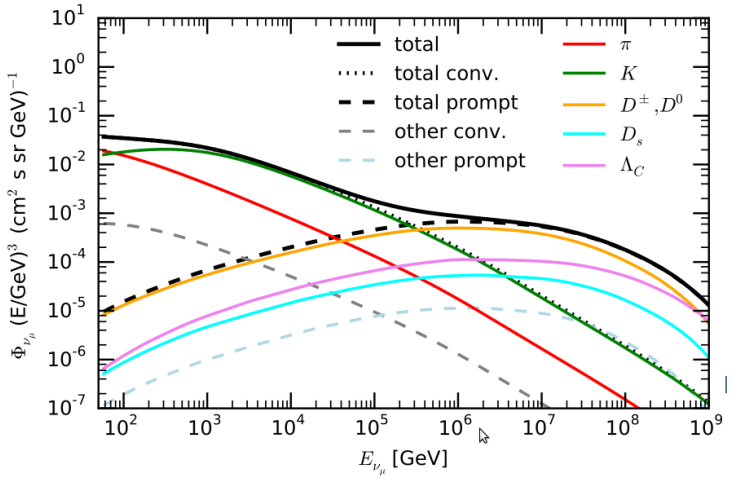

Figure 2.3: Atmospheric muon neutrino flux with partial contributions of intermediate particles [43], weighted with the third power of the muon neutrino energy. The kaon component is dominant compared to the pion component over a large part of the energy range of the conventional flux.

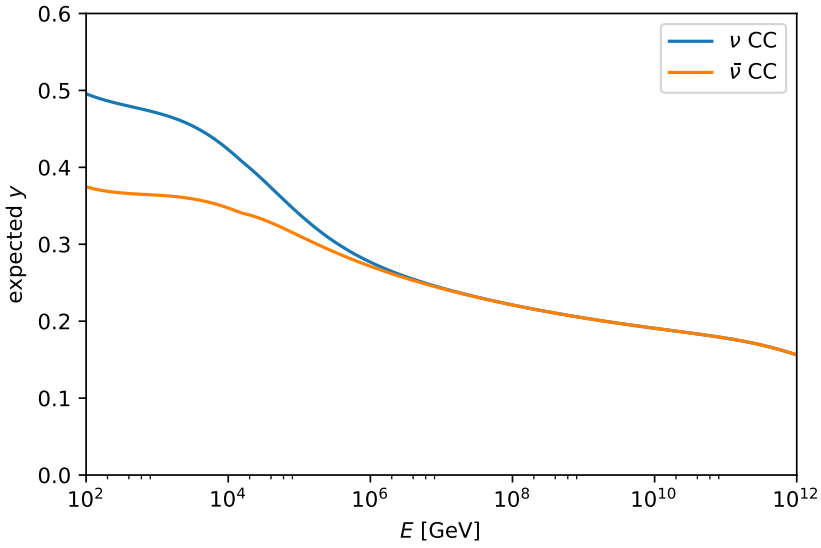

Figure 2.4: Average ratio y between neutrino energy and cascade energy in charged current neutrino and antineutrino interactions [80].

contribution of D-mesons over a large energy range and even dominates at energies above $\sim 100\,\mathrm{PeV}$.

Because the cross-section in the forward region gives the dominant contribution to the prompt flux, which is inaccessible for detectors at accelerators, the predictions for the prompt flux vary widely (e. g., [30, 42]).

Since the center-of-mass energy for the production of heavy hadrons is high, the prompt muons are often muons which carry most of the energy of the shower in which they are produced because they have to be produced early. This is in contrast to conventional muons, which are also produced at later stages of the air shower and also arrive in bundles with more or less equipartition of the energy between the muons.

2.3 Muons from neutrinos

By exchanging a W-boson with a nucleon, a muon neutrino is converted to a muon. The energy of the neutrino is divided between the hadronic cascade and the muon. The average ratio between the neutrino energy and the energy imparted to the cascade decreases with energy (cf. Fig. 2.4).

The muon direction is almost identical to the neutrino direction with a mean deviation of [46]

$$\langle\theta\rangle \approx \frac{1.5^\circ}{\sqrt{E_\nu/\mathrm{TeV}}}. \tag{2.8}$$

This small deviation together with the accuracy of the muon directional reconstruction in modern neutrino telescopes such as IceCube [4] allows to use muon

neutrinos as messenger particles in astrophysical point source investigations.

The identification of neutrino point sources will allow to solve the long-standing problem of the origin of ultra-high energy charged cosmic ray particles. Since these particles are charged, they are deflected by galactic and extragalactic magnetic fields during the propagation from their source to Earth. The sources of cosmic rays are therefore unknown. The break at about a PeV is commonly considered to denote the beginning of the end of the galactic population of cosmic rays; whether this is due to propagation effects [47], maximum attainable energy of galactic accelerators [86] or energy-dependent leakage [46] is still under debate.

Astrophysical sources which accelerate charged cosmic rays produce high-energy pions in hadronuclear and photohadronic interactions

$$p + \text{nucleus} \to \pi + X \quad (\pi = \pi^0, \pi^\pm), \tag{2.9}$$

$$p + \gamma \to \begin{cases} \pi^+ + n, \\ \pi^0 + p. \end{cases} \tag{2.10}$$

The pions in turn decay to photons and neutrinos via

$$\begin{aligned} \pi^0 &\to \gamma + \gamma, \\ \pi^+ &\to \mu^+ + \nu_\mu \\ &\hookrightarrow e^+ + \nu_e + \bar{\nu}_\mu. \end{aligned} \tag{2.11}$$

Neutrino oscillation changes the presumed source flavor distribution of $\nu_e : \nu_\mu : \nu_\tau = 1 : 2 : 0$ to equipartition $\nu_e : \nu_\mu : \nu_\tau = 1 : 1 : 1$ [73].

Since neutrinos and photons are uncharged, they are not deflected by magnetic fields and point back to their origin. However, high-energy photons can be produced not only by hadronic acceleration mechanisms, but also in leptonic sources via inverse Compton scattering of low-energy photons on electrons of high energy

$$\gamma_{\text{low energy}} + e^-_{\text{high energy}} \to \gamma_{\text{high energy}} + e^-. \tag{2.12}$$

Since the production of neutrinos in leptonic sources via [24]

$$\gamma + e^- \to \mu^+ + \mu^- + e^- \tag{2.13}$$

with subsequent decay of the muons is suppressed by the large mass of the muons, astrophysical sources producing neutrinos can be practically regarded as "smoking gun" of hadron accelerators.

The spectrum of a single source depends of course on the characteristics of the specific source. A hadronuclear model predicts a power law which roughly follows the primary proton spectrum, similar to atmospheric prompt neutrinos due to the low density of even comparatively dense astrophysical sources. The prediction of a photohadronic model naturally depends on the photon distribution; however, the general picture is a spectrum peaking at high energies (cf. Fig. 2.5, 2.6).

However, calculations of the diffuse neutrinos flux generally show a spectrum compatible with a power law $\propto E^{-\gamma}$, where $\gamma \approx 2$ (e. g. [37, 85, 109]) due to the averaging over many sources.

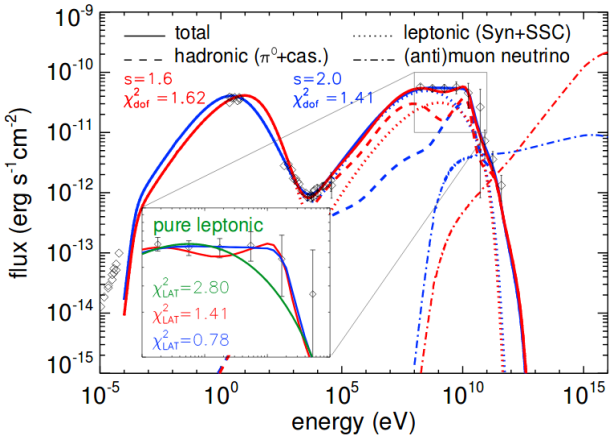

Figure 2.5: Hadronuclear model for the blazar TXS 0506+056 [76] with two assumptions on the spectral index of the power law describing the proton distribution. This model assumes independent emission zones for the neutrino emission and the photon emission.

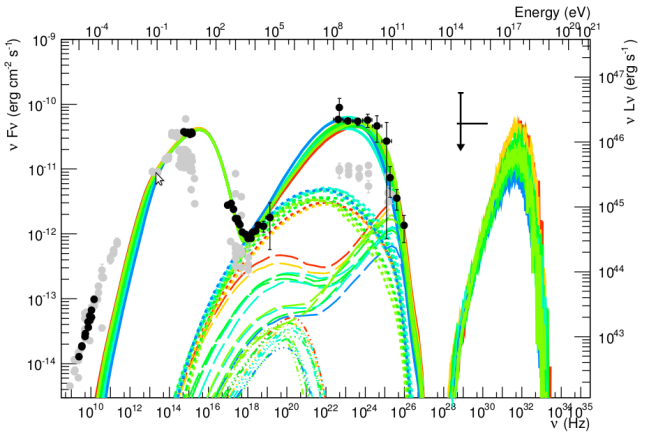

Figure 2.6: Photohadronic model for the blazar TXS 0506+056 [36]. The total flux weighted with the square of the energy (νF_ν) is shown with solid lines for photons and neutrinos, respectively, below and above 100 TeV. The dotted lines show the emission from electrons produced via $p + \gamma \rightarrow p + e^+ + e^-$, the dashed lines the emission of cascades from electron produced in pion decays and the dotted-dashed lines the proton synchrotron emission. The black dots refer to quasi-simultaneous measurements during a high-flux state, the grey dots are archival data for comparison. The colours represent increasing values of the size of the emission region.

Chapter 3

Muon interaction

The energy loss of muons is important for the simulation of the propagation of muons from their production site in the atmosphere or the surrounding ice and bedrock to the underground detector. As an example, we consider the IceCube detector (cf. Fig. 3.1), which consists of 5160 digital optical modules arranged on 86 strings frozen into a block of clear ice in a depth of 1450–2450 m at the geographic South Pole. The muons produced in air showers in the atmosphere, in the instrumented volume or the surrounding ice and rock are observed via the Cherenkov radiation of the muons and the secondary particles produced during propagation.

Muons loose energy almost exclusively by four processes, namely

- excitation, ionization and μe scattering on atomic electrons,
- bremsstrahlung,
- electron pair production,
- inelastic interaction with nuclei.

Other possible processes such as emission of Cherenkov light or muon pair production are negligible for the energy loss.

The two quantities of interest in underground detectors such as IceCube are the differential cross-section $d\sigma/dv$, where $v = (E - E')/E$ is the energy lost by the muon relative to its initial energy, and the average energy loss per distance,

$$-\left\langle \frac{dE}{dx} \right\rangle = \frac{N_A}{A} \varrho E \int v \frac{d\sigma}{dv} dv, \tag{3.1}$$

where N_A is Avogadro's constant, A is the mass number of the material and ϱ its density.[1] The average energy loss can be parametrized quasi-linearly as [15]

$$-\left\langle \frac{dE}{dx} \right\rangle \approx a(E) + b(E)E, \tag{3.2}$$

where $a(E), b(E)$ are varying at most logarithmically with energy (cf. Fig. 3.2).

[1] Instead of the distance, also the depth $X = x\varrho$ is used.

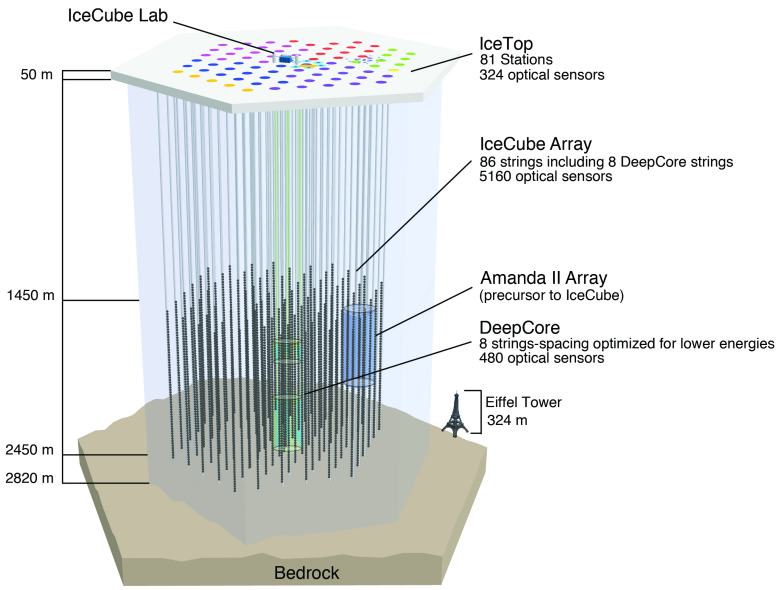

Figure 3.1: Schematic view of the IceCube neutrino observatory. Also shown are the precursor detector AMANDA and, as a scale, the Eiffel tower.

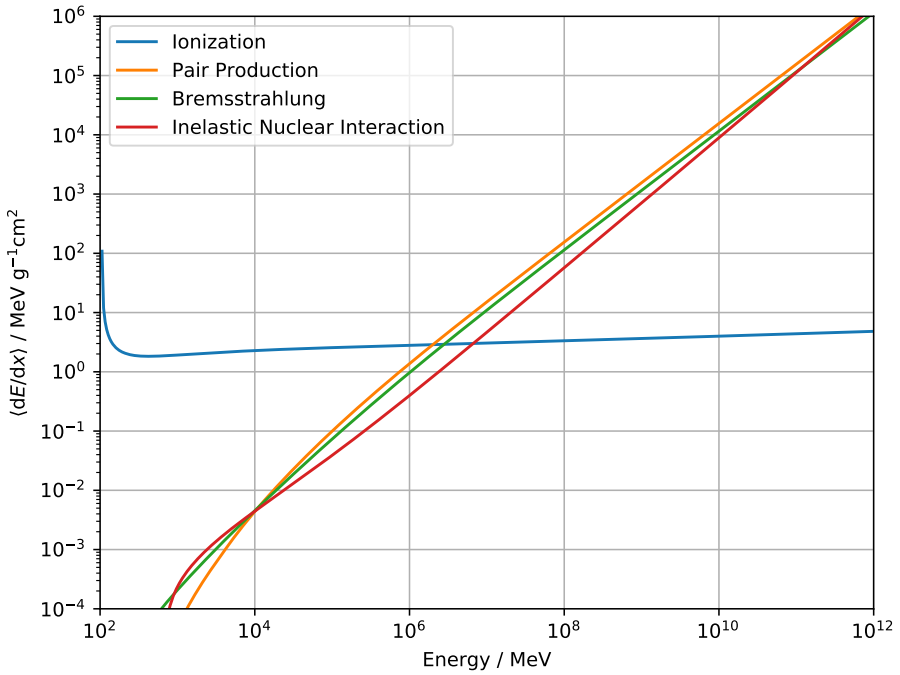

Figure 3.2: $-\langle dE/dX \rangle$ of muons in ice [98].

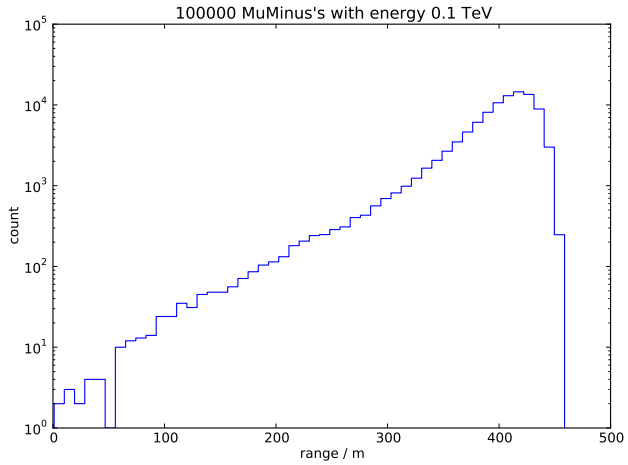

Figure 3.3: Range of monoenergetic muons of initial energy $E_\mu = 100\,\mathrm{GeV}$ in ice, calculated with the lepton propagator PROPOSAL [63]. The average range is $\langle R \rangle = (395 \pm 44)\mathrm{m}$, the range calculated on the basis of the average energy loss is $R_{\langle dE/dX \rangle} = 394\,\mathrm{m}$.

Since a muon with an energy of tens or hundreds of TeV can travel several kilometers through rock or ice, it is necessary to know the energy loss to a high precision.

Based on the quasi-linear parametrization of the average energy loss the range of muons is given by

$$R_{\langle dE/dx \rangle}(E) = \frac{1}{b} \ln\left(1 + \frac{b}{a}E\right) \tag{3.3}$$

if it is assumed that a, b are independent of energy and all energy is lost continuously. Since the energy loss is a stochastic process, the actual range fluctuates due to hard losses by mainly bremsstrahlung and inelastic nuclear interaction, with the effect of fluctuations increasing with energy. Therefore, the average range $\langle R \rangle$ becomes smaller than the range calculated on the basis of the average energy loss $R_{\langle dE/dX \rangle}$, where the ratio $\langle R \rangle / R_{\langle dE/dX \rangle}$ decreases with increasing energy (cf. Fig. 3.3, 3.4). Some muons propagate much farther than $R_{\langle dE/dX \rangle}$, but the majority loose their energy faster in large stochastic losses.

The fluctuations influence the rate of downgoing atmospheric muons and of neutrino-induced muons in opposite ways [74]. This is due to the different depths traversed and the steep spectrum of atmospheric muons. In an underground detector, the depth of rock or ice traversed by atmospheric muons is fixed for a given direction, whereas the depth of matter traversed by neutrino-induced muons is not, because the muons can originate everywhere in the surrounding matter. The rate of atmospheric muons can be written as $\int dE_\mu (dN/dE_\mu) P_{\mathrm{surv}}(E_\mu, X)$, where $P_{\mathrm{surv}}(E_\mu, X)$ is the survival probability of a muon with energy E_μ to reach a depth X. The small probability to travel larger depth than $R_{\langle dE/dX \rangle}$ is compensated for by the vastly larger flux at smaller energies, thus leading to a larger flux than expected from the average energy loss. In contrast, the neutrinos sample all depth

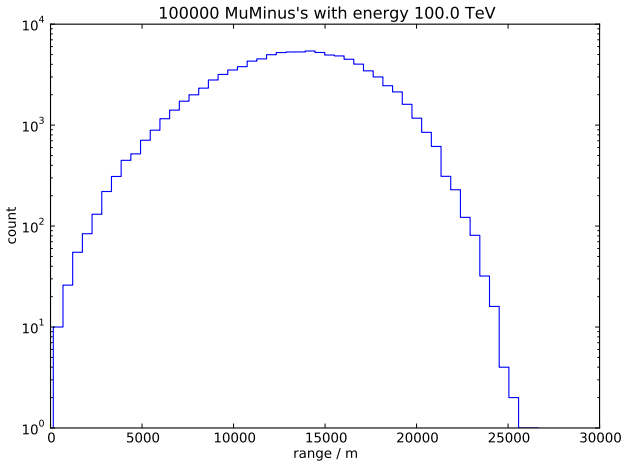

Figure 3.4: Range of monoenergetic muons of initial energy $E_\mu = 100\,\mathrm{TeV}$ in ice, calculated with the lepton propagator PROPOSAL [63]. The average range is $\langle R \rangle = (13.3 \pm 3.8)\mathrm{km}$, the range calculated on the basis of the average energy loss is $R_{\langle dE/dX \rangle} = 14.8\,\mathrm{km}$.

and $\langle R \rangle < R_{\langle dE/dX \rangle}$ decreases the flux compared to the expectation based on the average energy loss.

3.1 Ionization

$$\text{Excitation } \mu + Z \to \mu + Z^*, \tag{3.4}$$

$$\text{ionization } \mu + Z \to \mu + Z^+ + e^-, \tag{3.5}$$

$$\text{and } \mu e \text{ scattering } \mu + e^- \to \mu + e^- \tag{3.6}$$

on atomic electrons are the dominant energy loss processes for muons up to energies below about 1 TeV in water or ice. The contribution of these processes to the average energy loss makes up most of the quasi-constant coefficient $a(E)$ in the quasi-linear parametrization (3.2).

The first treatment of ionization was given by [19], the first treatment of e^--e^- scattering by [23]. Later, corrections were introduced to account for the influence of the density of the medium [101]. Also radiative corrections to the μe scattering, including bremsstrahlung by the atomic electron, were calculated [59].

Ionization differs from the other processes discussed in this section in that its contribution to the energy loss increases only logarithmically with increasing energy. Therefore it dominates the energy loss of low-energy muons. The threshold at which radiative processes become dominant depends on the material. In water, it is at about 1 TeV.

The number of μe scattering interactions per distance differential in the lost

energy ν is given by [48]

$$\begin{aligned}\frac{d^2N}{d\nu\, dX} &= \frac{1}{2}Kz^2\frac{Z}{A}\frac{1}{\beta^2}\frac{1}{\nu^2}\left[1-\beta^2\frac{\nu}{\nu_{\max}}+\frac{1}{2}\left(\frac{\nu}{E+\mu}\right)^2\right]\\ &\quad\times\left\{1+\frac{\alpha}{2\pi}[a(2b+c)-b^2]\right\},\\ a &= \ln\left(1+\frac{2\nu}{m_e}\right), b=\ln\frac{1-\nu/\nu_{\max}}{1-\nu/E}, c=\ln\frac{2m_eE(E-\nu)}{\mu^2\nu},\\ \nu_{\max} &= \frac{2m_e(E^2-\mu^2)}{m_e^2+\mu^2+2m_eE},\end{aligned} \tag{3.7}$$

where K is the ionization constant, Z is the nuclear charge of the medium, z the charge of the particle propagating through the medium, μ its mass, β its velocity in units of light speed and A the atomic mass of the medium.

Integrating this expression between $\nu_{\min}$ and $\nu_{\max}$ and adding the contribution of ionization and excitation, the average energy loss is given by

$$\begin{aligned}-\frac{dE}{dX} &= K\frac{Z}{A\beta^2}\left[\frac{1}{2}\ln\left(\frac{2m_e\beta^2\gamma^2\nu_{\text{upper}}}{I(Z)^2}\right)-\frac{\beta^2}{2}\left(1+\frac{\nu_{\text{upper}}}{\nu_{\max}}\right)\right.\\ &\quad\left.+\frac{1}{2}\left(\frac{\nu_{\text{upper}}}{2E(1+1/\gamma)}\right)^2-\frac{\delta}{2}\right].\end{aligned} \tag{3.8}$$

where

$$\begin{aligned}\nu_{\min} &= \frac{1}{2m_e}\left(\frac{I(Z)}{\beta\gamma}\right)^2,\\ \nu_{\max} &= \frac{2m_e(\gamma^2-1)}{1+2\gamma m_e/\mu+(m_e/\mu)^2},\\ \nu_{\text{upper}} &= \min(\nu_{\text{cut}},\nu_{\max}).\end{aligned}$$

Here, $I(Z)$ is the mean excitation energy, $\nu_{\text{cut}} = Ev_{\text{cut}}$ or $\nu_{\text{cut}} = e_{\text{cut}}$ refers to the cutoff at small energy losses explained in 3.6 and δ refers to the density correction [101]

$$\delta = \begin{cases}\delta_0 10^{2(X-X_0)} & X < X_0,\\ c_1X+c+a(X_1-X)^m & X_0 \leqslant X < X_1,\\ c_1x+c & X_1 \leqslant X.\end{cases} \tag{3.9}$$

where $X = \log_{10}(\beta\gamma)$, and $\delta_0, X_0, c_1, c, a, X_1$ are material constants (cf. [49]).

3.2 Bremsstrahlung

$$\mu + Z \to \mu + Z + \gamma \tag{3.10}$$

Bremsstrahlung has a slightly smaller contribution to the energy loss of muons than pair production, but is almost as important at very high energies. The differential cross section is harder ($d\sigma/dv \sim v^{-1}$) so that bremsstrahlung is mainly responsible for hard energy losses of muons in the detector. In contrast to the finite integrand of energy loss $v\, d\sigma/dv$ the lowest order cross section diverges for

$v \to 0$ due to the v^{-1} behavior of the cross section and the vanishing mass of the photon.

The first calculation of the bremsstrahlung cross section of electrons on a Coulomb center was carried out by Bethe and Heitler [21]. Already in this paper results were given also for complete screening of the nucleus by the atomic electrons in the Thomas-Fermi model. The results of this paper can be written in the form

$$d\sigma = 4Z^2\alpha \left(r_e \frac{m_e}{\mu}\right)^2 \frac{dv}{v} \left[(2 - 2v + v^2)\Phi_1 - \frac{2}{3}(1 - v)\Phi_2\right], \tag{3.11}$$

where r_e is the classical electron radius, m_e and μ are the rest mass of the electron and the initial lepton and the screening functions $\Phi_{1,2}$ depend only on the minimum momentum transfer

$$\delta = \frac{\mu^2 v}{2E(1 - v)}$$

and are given for relativistic particles by

$$\Phi_1 = \Phi_2 = \ln \frac{\mu}{\delta} - \frac{1}{2}$$

in the absence of screening. In the case of complete screening

$$\Phi_1 - \Phi_2 = \frac{1}{6}, \quad \Phi_1 = \ln\left(\frac{\mu}{m} B Z^{-1/3}\right),$$

where $B \approx 183$ is the radiation logarithm. Its exact value depends on the spatial charge distribution of the atomic electrons. Since the minimum momentum transfer decreases $\sim \mu^2/E$, the spectrum of bremsstrahlung photons is dominated by the complete screening regime at very high energies.

The first correct account for the influence of both atomic and nuclear formfactors was carried out in [87]. The formfactors are the Fourier transform of the charge distribution[2] of the atomic electrons and the nucleus, respectively,

$$F_{e,n}(q) = \frac{4\pi}{q} \int_0^\infty r \varrho_{e,n}(r) \sin qr \, dr \, . \tag{3.12}$$

The cross section is proportional to the structure function [40]

$$W_2(q^2, \nu) = -Z^2 \delta(\nu)[F_n(q) - F_e(q)]^2 \tag{3.13}$$

for the elastic interaction with an infinitely heavy nucleus, screened by atomic electrons. q is the momentum and ν the energy transferred to the nucleus. In this case, the functions $\Phi_i(\delta)$ are given for highly relativistic muons by [31]

$$\Phi_1(\delta) = \int_\delta^\infty \left[q^2 \ln x - \delta^2(y - 1)\right] [F_n(q) - F_e(q)]^2 \frac{dq}{q^3}, \tag{3.14}$$

[2]The charge distribution is assumed to be normalized such that $\int \varrho_{e,n} dV = 1$.

B	Model
183.0	Thomas-Fermi [58]
184.15	Thomas-Fermi-Molière [105]
189	Thomas-Fermi-Tietz [87]
202.4	Hydrogen atom
151.9—179.8	Hartree-Fock [60] (depends on Z)

Table 3.1: Different values of the numerical value in the radiation logarithm $L_{\mathrm{rad}} = \ln[(\mu/m_e)BZ^{-1/3}]$.

$$\Phi_2(\delta) = 6\mu^2 \int_\delta^\infty \left(1 - \frac{1}{y} - \ln x - \frac{\delta^2}{\mu^2}\ln y\right)[F_n(q) - F_e(q)]^2 \frac{dq}{q^3}, \tag{3.15}$$

$$\begin{aligned} \ln x &= \frac{1}{4\sqrt{\zeta(1+\zeta)}} \\ &\quad \times \ln \frac{1 + 4\zeta + 4\sqrt{\zeta(1+\zeta)} - \sqrt{\zeta/(1+\zeta)}}{\sqrt{1 - 8\zeta/y + 16\zeta(1+\zeta)/y^2} + 4\sqrt{\zeta(1+\zeta)}/y - \sqrt{\zeta/(1+\zeta)}}, \\ y &= \frac{q}{\delta}, \quad \zeta = \frac{q^2}{4\mu^2}. \end{aligned} \tag{3.16}$$

In the case of the hydrogen atom, the atomic form factor is known analytically as the Fourier transform of the squared modulus of the ground state electron wave function (e. g. [60])

$$F_e^{\mathrm{H}}(q) = \left[1 + \left(\frac{a_{\mathrm{Bohr}} q}{2}\right)^2\right]^{-2},$$

where $a_{\mathrm{Bohr}} = r_e/\alpha^2$ is the Bohr radius of the hydrogen atom. For heavier atoms, the atomic formfactor can be parametrized based on approximations such as the Thomas-Fermi model [105] or the Hartree-Fock model [60]. Based on the chosen approximation, the numerical value in the argument of the logarithm in the function Φ_1 in the complete screening limit, the so-called radiation logarithm, assumes different values (cf. Tab. 3.1).

The effect of the atomic formfactor is an effective cutoff of low transferred momenta. The nuclear formfactor leads to a cutoff of high transferred momenta. Since the regions where the formfactors differ substantially from 1 are very different, it is possible to consider them separately via

$$[F_n(q^2) - F_e(q^2)]^2 \approx [1 - F_e(q^2)]^2 - [1 - F_n(q^2)]^2. \tag{3.17}$$

The correction to Φ_i due to the finite nucleus can therefore be expressed as

$$\Phi_i = \Phi_i^0 - \Delta_i, \tag{3.18}$$

where Φ_i^0 contains the effect of the atomic formfactor and Δ_i the effect of the nuclear formfactor.

The interpolation of Φ_i^0 between the limiting cases of absence of screening and complete screening can be carried out in the approximation $\Phi = \Phi_1 \approx \Phi_2$ with

the function [87]

$$\Phi = \ln \frac{BZ^{-1/3}\mu/m_e}{1 + B\sqrt{e}Z^{-1/3}\delta/m_e}. \tag{3.19}$$

The difference between Φ_1, Φ_2 in the complete screening limit leads to an uncertainty of $\lesssim 3\%$ for electrons and $\lesssim 1.6\%$ for muons[3].

Another way is the use of the atomic formfactor suggested by [97]

$$F_e = \frac{1}{1 + b^2 q^2}, \quad b = \frac{BZ^{-1/3}}{m_e\sqrt{e}}. \tag{3.20}$$

This leads to the expressions [105]

$$\begin{aligned}
\Phi_1(\delta) &= \frac{1}{2}\left(1 + \ln\frac{\mu^2 b^2}{1 + b^2\delta^2}\right) - b\delta \arctan\frac{1}{b\delta}, \\
\Phi_2(\delta) &= \frac{1}{2}\left(\frac{2}{3} + \ln\frac{\mu^2 b^2}{1 + b^2\delta^2}\right) + 2b^2\delta^2\left(1 - b\delta\arctan\frac{1}{b\delta} + \frac{3}{4}\ln\frac{b^2\delta^2}{1 + b^2\delta^2}\right).
\end{aligned} \tag{3.21}$$

The results of numerical calculations based on the Thomas-Fermi model are described better by the function of (3.19); however, for hydrogen the function by (3.21) describes the results better, provided that the correct value of the radiation logarithm is used.

The results of numerical calculations by [87] based on the data in [41] for the nuclear formfactor corrections are parametrized by

$$\mathcal{A}_1 = \mathcal{A}_2 = \ln(1.5Z^{1/3}). \tag{3.22}$$

Later calculations by [10] based on the formfactor parametrization in [105]

$$F_n(q) = \left(1 + \frac{a^2 q^2}{12}\right)^{-2}, \quad a = (0.58 + 0.82A^{1/3})5.07\,\mathrm{GeV}^{-1}, \tag{3.23}$$

are parametrized by the expressions[4]

$$\begin{aligned}
\mathcal{A}_1 &= \ln\frac{\mu}{q_c} + \frac{\varrho}{2}\ln\frac{\varrho + 1}{\varrho - 1}, \\
\mathcal{A}_2 &= \ln\frac{\mu}{q_c} + \frac{1}{4}(3\varrho - \varrho^3)\ln\frac{\varrho + 1}{\varrho - 1} + \frac{2\mu^2}{q_c^2}, \\
\varrho &= \sqrt{1 + \frac{4\mu^2}{q_c^2}}, \quad q_c = 1.9 m_\mu Z^{-1/3}.
\end{aligned} \tag{3.24}$$

which for heavy nuclei ($Z \geq 10$) leads to

$$\mathcal{A}_1 - \mathcal{A}_2 \approx \frac{1}{6}, \quad \mathcal{A}_1 \approx \ln\frac{\mu}{q_c} + 1 \approx \ln(1.43Z^{1/3}). \tag{3.25}$$

[3] In the case of muons, the nuclear formfactor corrections to Φ_1, Φ_2 cancel the difference in the complete screening limit. However, the cancelling terms lead to a difference of the opposite sign in the absence of screening, see below.

[4] Here the muon mass m_μ occurs as a convenient scaling, since the inverse radius of the nucleus and the muon mass are of the same order of magnitude in units with $\hbar = c = 1$.

Therefore, in the complete screening limit for heavy nuclei, the difference between $\Phi_{1,2}$ is compensated by the difference of $\mathcal{A}_{1,2}$ in the case of muons. Calculations by [58] based on nuclear measurement data in [41] can be parametrized by

$$\mathcal{A}_2 \approx \mathcal{A}_1 = \ln(1.54A^{0.27}). \tag{3.26}$$

Both [58, 87] base their calculations on the data of [41], while [10, 11] base their calculation on [105]. A comparison of the nuclear corrections calculated based on these form factors with the parametrizations is seen in Fig. 3.5. The parametrizations of [58, 87] are only compared to $\mathcal{A}_1$, because they use the approximation $\Phi_1 \approx \Phi_2$. The nuclear formfactor correction decreases the muon bremsstrahlung cross section by 10–15% compared to bremsstrahlung on a point-like nucleus. The parametrization by [10, 11] describes well the nuclear formfactor correction for the heavy nuclei that were at the focus of their work; the parametrization by [58] describes the nuclear formfactor correction for all nuclei.

Apart from these elastic interactions there are contributions from inelastic interactions with the atom. Under the assumption that the wavefunction of the nucleus is a nonantisymmetrized product of individual proton wavefunctions, the inelastic nuclear formfactor is given due to completeness relations by [10]

$$F_n^{\text{inel}}(q) = \frac{1}{Z}[1 - F_n^2(q)], \quad Z \neq 1, \tag{3.27}$$

such that the contribution of the excitation of nuclear levels is given by $\mathcal{A}_i^{\text{inel}} = \mathcal{A}_i/Z$. Obviously, this model cannot be used for hydrogen, as there are no nuclear levels to be excited. The inelastic nuclear formfactor correction is important for light and medium nuclei, because for heavy nuclei the factor $1/Z$ is small.

The inelastic atomic formfactor describes the contribution of atomic electrons as target. When the recoil of the electron is neglected, the contribution is described by Φ_i^0/Z (cf. (3.21)) with b replaced by $c = B'/(Z^{2/3}\sqrt{e}m)$, where B' is the constant in the inelastic radiation logarithm $L'_{\text{rad}} = \ln(B'Z^{-2/3}\mu/m_e)$; in the Thomas-Fermi-Molière approximation, $B' = 1194$ [10, 105], while a numerical solution by [59] obtained $B' = 1429$. In [59] the bremsstrahlung on atomic electrons was calculated without neglect of recoil; in this case two sets of Feynman diagrams contribute to the cross section, the e-diagrams with photon emission by the electron, and the μ-diagrams with photon emission by the muon (cf. Fig. 3.6). The e-diagrams constitute radiative corrections to the ionization cross section, since the cross section $d\sigma_e \propto 1/\omega^2$ analogous to the form of the μe scattering cross section[5]. The μ-diagrams are a correction to the bremsstrahlung cross section. The results of [59] can be approximated by

$$\begin{aligned} d\sigma_\mu &= \alpha Z \left(\frac{2m_e r_e}{\mu}\right)^2 \frac{dv}{v}\left(\frac{4}{3}(1-v)+v^2\right)\Phi^{\text{in}}(\delta), \\ \Phi^{\text{in}}(\delta) &= \ln\frac{\mu/\delta}{\mu\delta/m_e^2+\sqrt{e}} - \ln\left(1+\frac{m_e}{\delta B' Z^{-2/3}\sqrt{e}}\right). \end{aligned} \tag{3.28}$$

Here, B' is the inelastic radiation logarithm.

[5] The contribution of the e-diagrams is given in the ionization cross section (3.7).

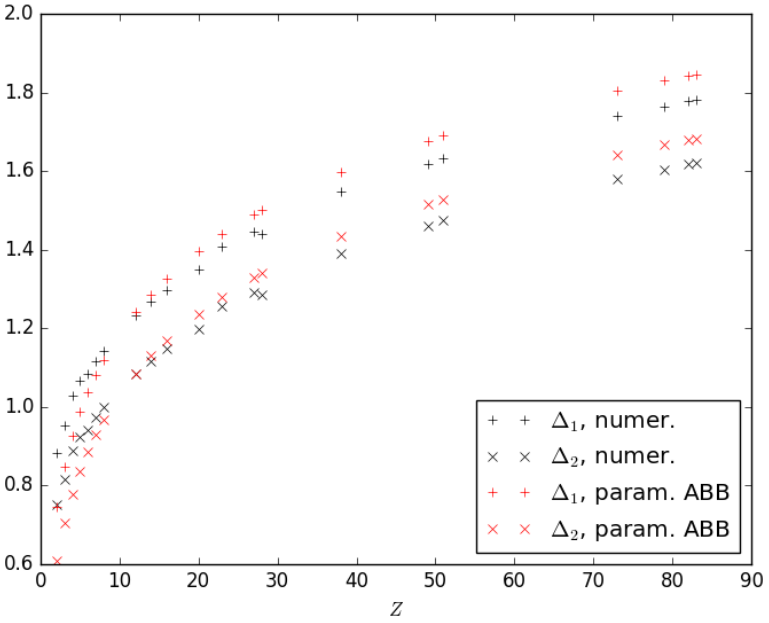

(a) Comparison of numerical results for $\Delta_{1,2}$ based on the nuclear form factor of [105] with the parametrization of [10, 11].[a]

[a] According to [10, 11], the effect of the inelastic nuclear formfactor (see below) is taken into account. According to my own calculations, this is not the case, since the parametrization fits much better the results without the inelastic nuclear formfactor.

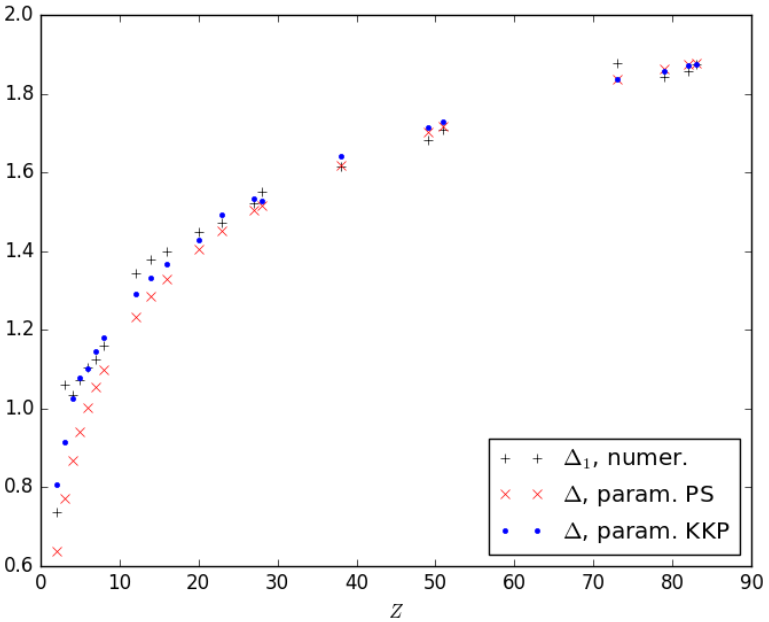

(b) Comparison of numerical results for Δ_1 based on the nuclear form factor of [41] with the parametrizations of [87] and [58].

Figure 3.5: Comparison of numerical results and different analytical parametrizations of $\Delta_{1,2}$. The mass number A corresponding to the charge number Z is chosen based on the most common isotope.

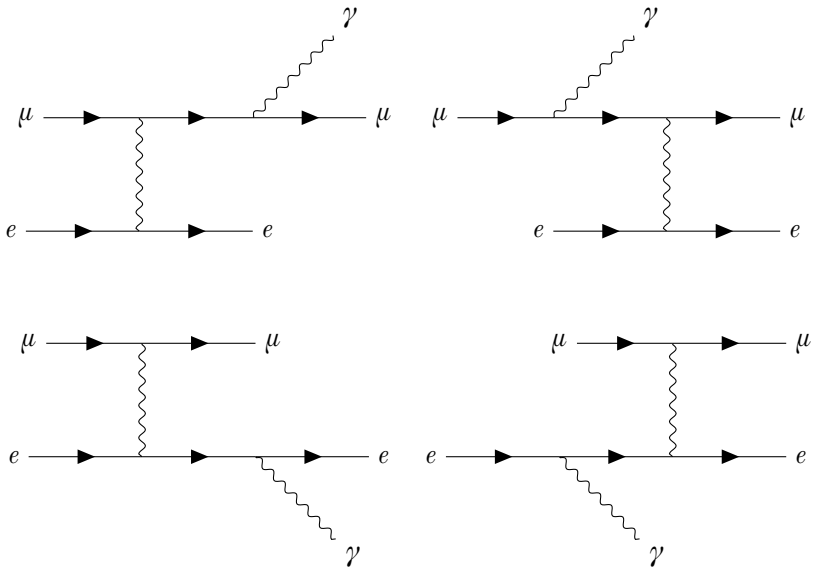

Figure 3.6: Feynman diagrams of muon bremsstrahlung on atomic electrons. The upper diagrams are the μ-diagrams, the lower the e-diagrams.

3.3 Pair production

The direct production of electron-positron pairs by muons

$$\mu + Z \to \mu + Z + e^+ + e^- \tag{3.29}$$

is the dominant energy loss process for muons at high energies. The cross section is described by two groups of Feynman diagrams, the e-diagrams and the μ-diagrams (cf. Fig. 3.7).

The main contribution to the cross section is due to the e-diagrams. The μ-diagrams are of importance only for hard energy losses, since the cross section goes as $d\sigma/dv \sim v^{-3}$ for the e-diagrams and as $d\sigma/dv \sim v^{-2}$ for the μ-diagrams for $v \gg m_e/\mu$. For $v \lesssim m_e/\mu$ the cross section due to the e-diagrams is much flatter, so that this region is responsible for the main contribution to the energy loss.

The production of an electron-positron pair by a charged particle was first calculated by [91] for a Coulomb center. Later [55] carried out calculations for the Coulomb center in the absence of screening and the case of full screening. The expressions obtained here were used in [66] to obtain an expression valid for every degree of screening. It was also pointed out that the finite extent of the nucleus influences the cross section [67]. The last important step was the calculation of the contribution of atomic electrons as target for pair production [56]. The contribution of inelastic nuclear excitations was shown to be negligible for pair production [34].

The cross section of electron pair production taking into account all the above-

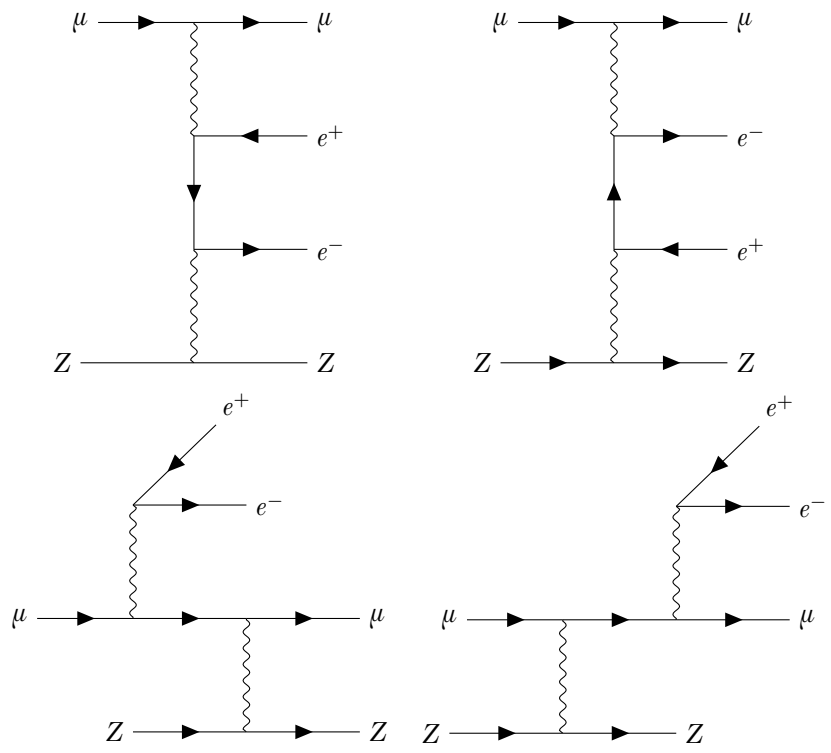

Figure 3.7: Feynman diagrams for direct pair production. The upper diagrams are the e-diagrams, the lower the μ-diagrams.

mentioned corrections can be parametrized as

$$\begin{aligned}\frac{d^2\sigma}{dv\ d\varrho} &= \frac{2}{3\pi}Z(Z+\zeta)(\alpha r_e)^2\frac{1-v}{v}\left[C_eL_e+\frac{m_e^2}{\mu^2}C_\mu L_\mu\right],\\ v &= \frac{\varepsilon_+ + \varepsilon_-}{E}, \varrho = \frac{\varepsilon_+ - \varepsilon_-}{\varepsilon_+ + \varepsilon_-},\end{aligned} \tag{3.30}$$

where $\varepsilon_\pm$ denotes the electron (positron) energy and

$$C_e = \left[(2+\varrho^2)(1+\beta)+\xi(3+\varrho^2)\right]\ln\left(1+\frac{1}{\xi}\right)+\frac{1-\varrho^2-\beta}{1+\xi}-(3+\varrho^2), \tag{3.31}$$

$$L_e = \ln\frac{BZ^{-1/3}\sqrt{(1+\xi)(1+Y_e)}}{1+\frac{2m_e\sqrt{eBZ^{-1/3}(1+\xi)(1+Y_e)}}{Ev(1-\varrho^2)}}-\frac{1}{2}\ln\left[1+\left(\frac{3m_e}{2\mu}Z^{1/3}\right)^2(1+\xi)(1+Y_e)\right], \tag{3.32}$$

$$\begin{aligned}C_\mu = &\left[(1+\varrho^2)\left(1+\frac{3}{2}\beta\right)-\frac{1}{\xi}(1+2\beta)(1-\varrho^2)\right]\ln(1+\xi)\\ &+\frac{\xi(1-\varrho^2-\beta)}{1+\xi}+(1+2\beta)(1-\varrho^2),\end{aligned} \tag{3.33}$$

$$L_\mu = \ln\frac{\frac{2}{3}\frac{\mu}{m_e}BZ^{-2/3}}{1+\frac{2m_e\sqrt{eBZ^{-1/3}(1+\xi)(1+Y_\mu)}}{Ev(1-\varrho^2)}}, \tag{3.34}$$

$$Y_e = \frac{5-\varrho^2+4\beta(1+\varrho^2)}{2(1+3\beta)\ln(3+1/\xi)-\varrho^2-2\beta(2-\varrho^2)}, \tag{3.35}$$

$$Y_\mu = \frac{4+\varrho^2+3\beta(1+\varrho^2)}{(1+\varrho^2)(3/2+2\beta)\ln(3+\xi)+1-\frac{3}{2}\varrho^2}, \tag{3.36}$$

$$\beta = \frac{v^2}{2(1-v)},\quad \xi = \left(\frac{\mu v}{2m_e}\right)^2\frac{1-\varrho^2}{1-v}, \tag{3.37}$$

$$\zeta = \frac{0.073\ln\frac{E/\mu}{1+\gamma_1 Z^{2/3}E/\mu}-0.26}{0.058\ln\frac{E/\mu}{1+\gamma_2 Z^{1/3}E/\mu}-0.14}, \tag{3.38}$$

$$\gamma_1 = 1.95\times10^{-5},\quad \gamma_2 = 5.3\times10^{-5}\text{ for } Z\neq1, \tag{3.39}$$

$$\gamma_1 = 4.4\times10^{-5},\quad \gamma_2 = 4.8\times10^{-5}\text{ for } Z=1. \tag{3.40}$$

The functions $L_{e,\mu}$ correspond to $\Phi_1 \approx \Phi_2$ in the bremsstrahlung cross section; however, due to the additional degrees of freedom of the muonic part of the e-diagrams and the electronic part in the μ-diagrams $L_{e,\mu}, C_{e,\mu}$ arise after an additional integration.

3.4 Landau-Pomeranchuk-Migdal effect and Ter-Mikaelian effect

The cross sections in this chapter have been calculated for the interaction with one isolated atom. This is a good approximation if the volume in which the interaction

takes place contains only one atom. The linear dimension of this volume is given in the case of bremsstrahlung by the formation length following from the uncertainty relation

$$\ell \sim \frac{\hbar}{\delta}, \tag{3.41}$$

where δ denotes the minimum momentum transfer. Since $\delta = \mu^2 v/[2E(1-v)]$, the formation length can be larger than the interatomic distance for very high energies or for very small momentum transfers. If the formation length is larger than the interatomic distance, the bremsstrahlung process is suppressed because the coherence of the wavefunctions of the photon and the radiating lepton are disturbed. The effect of Coulomb scattering on the wavefunction of the lepton is called Landau-Pomeranchuk-Migdal (LPM) effect [72, 81], the effect of Compton scattering by surrounding electrons on the wavefunction of the photon is called Ter-Mikaelian (TM) effect [103]. If the scattering angle due to multiple Coulomb scattering θ_s is greater than the typical angle of the bremsstrahlung photon $\theta_{\mathrm{br}} \sim \mu/E$, the bremsstrahlung process is suppressed. The average scattering angle due to multiple Coulomb scattering while traversing a distance ℓ is given by

$$\langle \theta_s^2 \rangle = \left(\frac{\mu\sqrt{4\pi/\alpha}}{E} \right)^2 \frac{\ell}{X_0}, \tag{3.42}$$

where X_0 is the medium-dependent radiation length, i.e. the distance over which the lepton looses $1/e$ of its energy.

The LPM effect also has an influence on the pair production cross section [90, 104]; however, the effect is very small, since the energy of the lower-energy electron is the dominant factor for the determining factor. The average energy loss is noticeably changed due to the LPM effect only at extremely high energies $\gtrsim 10^{24}\,\mathrm{eV}$ (cf. Fig. 3.8). Therefore the following discussion is limited to the bremsstrahlung cross section.

Both effects affect the production of secondaries with low v; in the case of the bremsstrahlung cross section, the infrared divergent behaviour $d\sigma/dv \propto 1/v$ changes to $d\sigma/dv \propto 1/\sqrt{v}$ in the region affected by the LPM effect and $d\sigma/dv \propto v$ in the region where the TM effect is important [62]. The calculation of the LPM effect on the bremsstrahlung cross section has been carried out using a quasi-classical method [13, 90]. The calculation leads to an indefinite numerical factor $\ln(\theta_2/\theta_1)$ arising from a small-angle approximation. The value of this factor is determined by the assumption that the cross section in the regime where the LPM effect is unimportant coincides with the cross section under the usual assumption of interaction with a single isolated atom. The final result can be expressed by the substitution

$$\left[\frac{4}{3}(1-v)+v^2\right] \Phi(\delta) \to \frac{\xi(s)}{3}\left\{v^2 G(s) + 2[1+(1-v)^2]\varphi(s)\right\} \tag{3.43}$$

or analogously

$$\Phi_1(\delta) \to \frac{\xi(s)}{3}[G(s)+2\varphi(s)]\Phi_1(\delta) \tag{3.44}$$

$$\Phi_2(\delta) \to \frac{2}{3}\xi(s)G(s)\Phi_2(\delta). \tag{3.45}$$

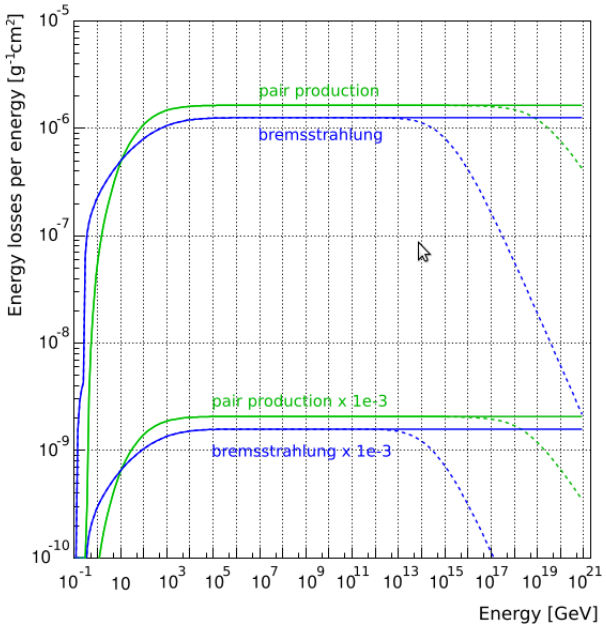

Figure 3.8: Average energy loss of muons due to pair production and bremsstrahlung with and without the LPM and TM effect [63] in ice and Fréjus rock (cf. C; the latter is scaled by 10^{-3} for better visibility).

Adopting the scheme of [100], the functions $\xi(s), G(s), \varphi(s)$ are given by

$$\varphi(s) = \begin{cases} 1 - \exp\left(-6s[1 + (3-\pi)s] + \frac{s^3}{0.623 + 0.796s + 0.658s^2}\right) & s < 1.549\,54, \\ 1 - 0.012s^{-4} & s \geqslant 1.549\,54, \end{cases} \tag{3.46}$$

$$\psi(s) = 1 - \exp\left(-4s - \frac{8s^2}{1 + 3.936s + 4.97s^2 - 0.05s^3 + 7.50s^4}\right), \tag{3.47}$$

$$G(s) = \begin{cases} 3\psi(s) - 2\varphi(s) & s < 0.710\,390, \\ \frac{36s^2}{36s^2+1} & 0.710\,390 \leqslant s < 0.904\,912, \\ 1 - 0.022s^{-4} & s \geqslant 0.904\,912, \end{cases} \tag{3.48}$$

$$\xi(s) \approx \xi(s') = \begin{cases} 2 & s' < s_1, \\ 1 + h - \frac{0.08(1-h)[1-(1-h)^2]}{\ln(s_1)} & s_1 \leq s' < 1, \\ 1 & s' \geqslant 1, \end{cases} \tag{3.49}$$

where

$$s = \frac{s'}{\sqrt{\xi(s')}}, \tag{3.50}$$

$$s_1 = \sqrt{2}\frac{Z^{1/3} D_n}{B}\frac{m_e}{\mu}, \tag{3.51}$$

$$s' = \sqrt{\frac{E_{\mathrm{LPM}}}{E}\frac{v}{8(1-v)}}, \tag{3.52}$$

$$h = \frac{\ln s'}{\ln s_1}, \tag{3.53}$$

$$E_{\mathrm{LPM}} = \frac{\alpha(\mu c^2)^2 X_0}{4\pi\hbar c}. \tag{3.54}$$

The TM effect operates in a part of the regime where the LPM effect is important. Its effect can be described by the substitutions

$$\begin{aligned} \xi(s) &\to \xi(\Gamma s), \\ \varphi(s) &\to \frac{\varphi(\Gamma s)}{\Gamma}, \\ G(s) &\to \frac{\psi(\Gamma s)}{\Gamma^2}, \end{aligned} \tag{3.55}$$

where

$$\Gamma = 1 + \left(\frac{\hbar\omega_p}{\mu v}\right)^2, \tag{3.56}$$

with the plasma frequency $\omega_p = \sqrt{4\pi n Z e^2/m}$. $n = (N_A/A)\varrho$ denotes the electron density.

3.5 Nuclear interaction

$$\mu + A \to \mu + X \tag{3.57}$$

The inelastic interaction with nuclei is a subdominant process for the energy loss of muons. It is also responsible for hard energy losses. The contribution to the average energy loss is about 10%. Since this process is dominated by small momentum transfers, phenomenological models based on Regge theory or generalized vector meson dominance are applied. Perturbative QCD is only applicable to losses with a large transferred momentum, which present a correction to the non-perturbative main contribution.

The calculations of this effect are carried out in two directions. One direction views the inelastic nuclear interaction as a generalization of the photonuclear interaction

$$\gamma + N \to X, \tag{3.58}$$

the other approach views inelastic interaction as a generalization of elastic scattering, which can be described by the structure functions introduced in [40] in the context of Regge theory.

In both cases, it follows from kinematical considerations, that the minimum transferred energy is given by

$$v_{\min} E = m_\pi + \frac{m_\pi^2}{2m_N}, \tag{3.59}$$

where m_π, m_N are the masses of the pion and the nucleon.

3.5.1 Calculations based on photonuclear interaction

A widely employed parametrization based on the photonuclear interaction was presented by [22] and later improved in [32, 33]

$$\begin{aligned}\frac{d\sigma}{dv} &= \frac{\alpha}{2\pi} A\sigma_{\gamma N}(\nu) v \\ &\times \left\{ \frac{3}{4} G(x) \left[\varkappa \ln\left(1+\frac{m_1^2}{t}\right) - \frac{\varkappa m_1^2}{m_1^2+t} - \frac{2\mu^2}{t} + \frac{4\mu^2}{m_1^2} \ln\left(1+\frac{m_1^2}{t}\right) \right] \right. \\ &+ \frac{1}{4} \left[\left(\varkappa + \frac{2\mu^2}{m_2^2}\right) \ln\left(1+\frac{m_2^2}{t}\right) - \frac{2\mu^2}{t} \right] \\ &\left. + \frac{\mu^2}{2t} \left[\frac{3}{4} G(x) \frac{m_1^2-4t}{m_1^2+t} + \frac{1}{4} \frac{m_2^2}{t} \ln\left(1+\frac{t}{m_2^2}\right) \right] \right\},\end{aligned} \tag{3.60}$$

where $t = Q^2_{\min} = \mu^2 v^2/(1-v)$, $\varkappa = 1-2/v+2/v^2$, $\nu = vE$, $m_1^2 = 0.54\,\mathrm{GeV}^2$, $m_2^2 = 1.8\,\mathrm{GeV}^2$ and

$$\begin{aligned} G(x) &= \frac{3}{x^3}\left(\frac{x^2}{2} - 1 + e^{-x}(1+x)\right) && Z \neq 1, \\ &= 1 && Z = 1; \\ x &\simeq 0.002\,82 A^{1/3} \sigma_{\gamma N}(\nu). \end{aligned}$$

$G(x)$ describes the shadowing of the nucleons.

This calculation is based on the generalized vector meson dominance, which describes the interaction of photons with nucleons by fluctuations into vector mesons such as ρ, ω, φ, ψ, ϒ and their excited states ρ′, ρ″, ..., ω′, ω″, ..., etc. $\sigma_{\gamma N}(\nu)$ is the absorption cross section of a photon by a nucleon, for which several parametrizations of lab data are widely used, e. g. the parametrization of [22]

$$\sigma_{\gamma N}(\nu) = \left[114.3 + 1.647 \ln^2\left(0.0213 \frac{\nu}{\mathrm{GeV}}\right)\right] \mu\mathrm{b}, \tag{3.61}$$

the parametrization of [65]

$$\sigma_{\gamma N}(\nu) = \left(96.1 + \frac{82}{\sqrt{\nu/\mathrm{GeV}}}\right) \mu\mathrm{b}, \qquad \nu \leqslant 17\,\mathrm{GeV}, \tag{3.62}$$

$$\sigma_{\gamma N}(\nu) = \left[114.3 + 1.647 \ln^2\left(0.0213 \frac{\nu}{\mathrm{GeV}}\right)\right] \mu\mathrm{b}, \quad 17\,\mathrm{GeV} \leq \nu \leq 200\,\mathrm{GeV}, \tag{3.63}$$

$$\sigma_{\gamma N}(\nu) = \left(49.2 + 11.1 \ln\frac{\nu}{\mathrm{GeV}} + \frac{151.8}{\sqrt{\nu/\mathrm{GeV}}}\right) \mu\mathrm{b}, \qquad \nu \geqslant 200\,\mathrm{GeV}, \tag{3.64}$$

the parametrization of [93, 94], which uses an interpolation of the measured values of the HERA detector below 200 GeV and coincides with (3.64) above this value; and the parametrization of [27]

$$\sigma_{\gamma N}(\nu) = (63.5 s^{0.097} + 145 s^{-0.5}) \mu\mathrm{b}, \tag{3.65}$$

where $s = 2m_N\nu/\mathrm{GeV}$.

3.5.2 Calculations based on Regge theory

The Regge theory is an effective theory for hadronic interactions. Its basis is the experimentally established Chew-Frautschi relation [38] between the mass squared m^2 of a meson and its spin J

$$m^2(J) \approx aJ + m_0^2 \tag{3.66}$$

which is extended into the complex spin plane to describe scattering processes by the exchange of a quasiparticle with non-integer spin called reggeon. An additional quasiparticle is necessary to describe cross section data at high energy which is called pomeron. Using this theory the scattering data of the electron-proton collider HERA can be parametrized by [6, 7]

$$\frac{d\sigma}{dv\ dQ^2} = \frac{4\pi\alpha^2}{Q^4}\frac{F_2}{v}\left[1 - v - \frac{Mxv}{2E} + \left(1 - \frac{2\mu^2}{Q^2}\right)\frac{v^2}{2}\frac{1 + 4M^2x^2/Q^2}{1+R}\right] \tag{3.67}$$

with

$$x = \frac{Q^2}{2MEv}, \tag{3.68}$$

$$F_2^p(x,Q^2) = \frac{Q^2}{Q^2 + m_0^2}(F_2^P + F_2^R), \tag{3.69}$$

$$F_2^i(x,Q^2) = c_i(t)x_i^{a_i(t)}(1-x)^{b_i(t)}, \quad i = P, R, \tag{3.70}$$

$$t = \ln\frac{\ln\frac{Q^2+Q_0^2}{\Lambda^2}}{\ln\frac{Q_0^2}{\Lambda^2}}, \tag{3.71}$$

$$x_i = \frac{Q^2 + m_i^2}{Q^2 + m_i^2 + W^2 - M^2}, \tag{3.72}$$

$$W^2 = M^2 + 2MEv - Q^2. \tag{3.73}$$

Here, a_R, b_R, c_R, and b_P increase with Q^2 as

$$f(t) = f_1 + f_2 t^{f_3}, \tag{3.74}$$

and a_P, c_P decrease with Q^2 as

$$g(t) = g_1 + (g_1 - g_2)\left[\frac{1}{1+t^{g_3}} - 1\right]. \tag{3.75}$$

This leads to 23 free parameters which have to be constrained by a fit to experimental data. The parametrization of [6] is used by default in the lepton propagator PROPOSAL. It does not correctly describe the behaviour in the resonance region (cf. Fig. 3.9).

3.6 Propagation algorithm

After this discussion of the processes contributing to the energy loss of muons, the simulation of muon propagation is described. The stochastic nature of the energy deposition in muon interactions necessitates a Monte-Carlo simulation of

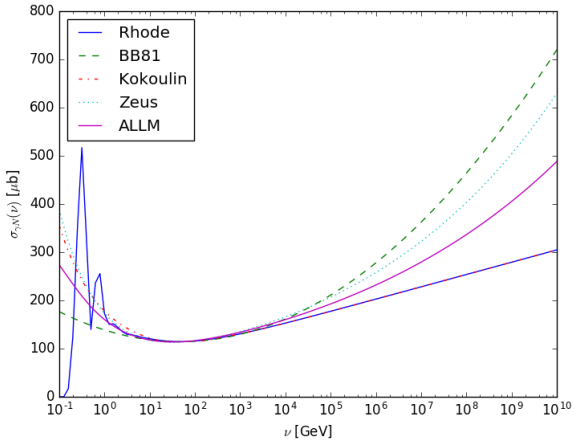

Figure 3.9: Comparison of the different parametrizations of the photonuclear cross section.

the propagation of muons (cf. [39, 63, 64, 70, 74, 99]). The simulation of all energy losses, however, is impossible due to the infrared divergence of the bremsstrahlung cross section. Due to this physical reason and also to reduce the computational cost of muon propagation, the losses are separated into hard losses treated stochastically, and soft losses treated continuously. This artificial division can happen either at a specified energy e_{cut} or at a specified relative energy loss v_{cut}. These cutoff parameters are chosen sufficiently small to ensure that their size does not influence the results. The following equations are written for a relative cut v_{cut}; the corresponding equations for an absolute cut e_{cut} follow analogously.

The probability for a particle of energy $E(x)$ to undergo a stochastic hard loss over a distance dx is given by

$$dP(x) = \frac{dN}{dx}(E(x))\bigg|_{\text{hard}} dx, \tag{3.76}$$

where

$$\frac{dN}{dx}\bigg|_{\text{hard}} = \sum_k \frac{N_A}{A}\varrho \int_{v_{\text{cut}}}^{v_{\text{max}}} \frac{d\sigma_k}{dv} \tag{3.77}$$

is the integrated number of interactions per distance for all processes. The probability for a particle to experience no hard stochastic losses over a distance $[x_i, x_f]$, which shall be divided into infinitesimal partial distances dx, and to loose energy

stochastically between x_f and $x_f + dx$, is therefore given by

$$\begin{aligned}
&(1 - dP(E(x_i))) \cdots (1 - dP(E(x_{f-1}))) \cdot dP(E(x_f)) \\
&\approx \exp(-dP(E(x_i))) \cdots \exp(-dP(E(x_{f-1}))) \cdot dP(E(x_f)) \\
&\overset{dx\to 0}{\longrightarrow} \exp\left(- \int_{E(x_i)}^{E(x_f)} dP(E(x)) \right) dP(E(x_f)) \\
&= d\left[-\exp\left(\int_{E(x_i)}^{E(x_f)} \frac{\frac{dN}{dx}(E)\big|_{\text{hard}}}{-\frac{dE}{dx}\big|_{\text{soft}}} dE \right) \right] \\
&\equiv d(-\xi), \quad \xi \in (0, 1].
\end{aligned} \tag{3.78}$$

Here, ξ represents a random variable, and

$$-\frac{dE}{dx}\bigg|_{\text{soft}} = \frac{N_A}{A} \varrho E \sum_k \int_0^{v_{\text{cut}}} v \frac{d\sigma_k}{dv} dv \tag{3.79}$$

is the soft energy loss per distance. The energy E_f at the next stochastic loss is therefore determined by

$$-\ln \xi = \int_{E_i}^{E_f} \frac{\frac{dN}{dx}\big|_{\text{hard}}(E)}{-\frac{dE}{dx}\big|_{\text{soft}}(E)}. \tag{3.80}$$

A solution to this equation exists under the condition

$$\xi > \xi_0 \equiv \exp\left(\int_{E_i}^{e_{\text{low}}} \frac{\frac{dN}{dx}\big|_{\text{hard}}(E)}{-\frac{dE}{dx}\big|_{\text{soft}}(E)} dE \right), \tag{3.81}$$

where e_{low} is a lower limit on the energy below which the particle is no longer propagated. The most conservative value is the particle mass, which is used by default in [63].

The effect of v_{cut} or e_{cut} on the distribution of initially monoenergetic muons E_i after propagation is the occurrence of a peak near $E_i(1-v_{\text{cut}})$ or $E_i - e_{\text{cut}}$. This can be alleviated by using a sufficiently small $v_{\text{cut}}, e_{\text{cut}}$, leading to large running times. An alternative approach is the continuous randomization [39], which smears out the lost energy according to a Gaussian distribution with mean $\varDelta E = E_i - E_f$ and variance

$$\langle (\varDelta(\varDelta E))^2 \rangle = -\int_0^{e_{\text{cut}}} \frac{dE}{-\frac{dE}{dx}\big|_{\text{soft}}} E_i^2 \left(\int_0^{e_{\text{cut}}/E_i} v^2 \left. \frac{dN}{dx} \right|_{\text{hard}} dv \right). \tag{3.82}$$

where $e = vE$.

The size of the stochastic loss and the process by which it happens are determined by the ratio between the total hard cross section and the differential cross section.

3.7 Improved parametrizations of the bremsstrahlung and pair production cross section

3.7.1 Improved bremsstrahlung cross section

Based on the calculations reviewed in section 3.2, we propose the following parametrization of the bremsstrahlung cross section, which preserves the difference between $\Phi_{1,2}, \Delta_{1,2}$

$$v\frac{d\sigma}{dv} = 4Z^2\alpha\left(r_e\frac{m_e}{\mu}\right)^2\left[(2-2v+v^2)\Phi_1 - \frac{2}{3}(1-v)\Phi_2\right] \tag{3.83}$$

$$\Phi_1 = \Phi_1^0 - \Delta_1 \tag{3.84}$$

$$\Phi_2 = \Phi_2^0 - \Delta_2 \tag{3.85}$$

where for hydrogen $\Phi_{1,2}^0$ is given by (3.21) and for heavier nuclei

$$\Phi_1^0 = \ln\frac{BZ^{-1/3}\mu/m_e}{1+BZ^{-1/3}\sqrt{e}\delta/m_e}, \tag{3.86}$$

$$\Phi_2^0 = \ln\frac{BZ^{-1/3}e^{-1/6}\mu/m_e}{1+BZ^{-1/3}e^{1/3}\delta/m_e}. \tag{3.87}$$

This parametrization is exact in both the complete screening limit and in the absence of screening by construction. The nuclear corrections $\Delta_{1,2}$ are given by (3.24) with $q_c = \mu e/D_n$. Here, B is to be taken from [60] and $D_n = 1.54A^{0.27}$.

Adding the contribution of atomic electrons and the inelastic nuclear form factor, we obtain

$$\begin{aligned}\frac{d\sigma}{dv} = 4Z^2\alpha\left(r_e\frac{m_e}{\mu}\right)^2\frac{1}{v}\Bigg\{&\left[(2-2v+v^2)\Phi_1(\delta) - \frac{2}{3}(1-v)\Phi_2(\delta)\right]\\ &+ \frac{1}{Z}s_{\text{atomic}}(v,\delta)\Bigg\},\end{aligned} \tag{3.88}$$

where

$$\Phi_1(\delta) = \ln\frac{\frac{\mu}{m_e}BZ^{-1/3}}{1+BZ^{-1/3}\sqrt{e}\delta/m_e} - \Delta_1\left(1-\frac{1}{Z}\right), \tag{3.89}$$

$$\Phi_2(\delta) = \ln\frac{\frac{\mu}{m_e}BZ^{-1/3}e^{-1/6}}{1+BZ^{-1/3}e^{1/3}\delta/m_e} - \Delta_2\left(1-\frac{1}{Z}\right), \tag{3.90}$$

$$\Delta_1 = \ln\frac{\mu}{q_c} + \frac{\varrho}{2}\ln\frac{\varrho+1}{\varrho-1}, \tag{3.91}$$

$$\Delta_2 = \ln\frac{\mu}{q_c} + \frac{3\varrho-\varrho^3}{4}\ln\frac{\varrho+1}{\varrho-1} + \frac{2\mu^2}{q_c^2}, \tag{3.92}$$

$$\varrho = \sqrt{1+\frac{4\mu^2}{q_c^2}}, q_c = m_\mu e/D_n, \tag{3.93}$$

$$s_{\text{atomic}}(\delta) = \left[\frac{4}{3}(1-v)+v^2\right]\left[\ln\frac{\mu/\delta}{\mu\delta/m_e^2+\sqrt{e}} - \ln\left(1+\frac{m_e}{\delta B' Z^{-2/3}\sqrt{e}}\right)\right]. \tag{3.94}$$

The difference between $\Phi_{1,2}$ appears in different limiting cases depending on the mass μ of the primary particle. For muons, the difference occurs in the absence of screening, which dominates at low energies and for very hard losses, because the difference between $\Phi^0_{1,2}$ in the complete screening limit is counteracted by the difference between $\mathcal{A}_{1,2}$. The difference between $\mathcal{A}_{1,2}$ is not lifted in the absence of screening, however. A comparison of the average bremsstrahlung energy loss and of the differential cross section is shown in Fig. 3.10.

For electrons, the difference shows up in the complete screening limit. For electrons, however, a further correction due to higher-order corrections is important (see chapter 6).

3.7.2 Improved pair production cross section

The parametrization in (3.30) is based on the interpolation between complete and no screening by [88] and the calculations for the nuclear formfactor correction by [87], thus using the approximation $\Phi_1 \approx \Phi_2$, where $\Phi_{1,2}$ are functions analogous to the functions in the bremsstrahlung cross section. This approximation entails an uncertainty of $\sim 3\%$ [61].

Based on the results from [55], where the cross section is calculated without this approximation for the limiting cases of complete screening and no screening, we can derive an expression for the cross section without using this approximation in an analogous procedure to [66, 67]. Analogously to the new bremsstrahlung cross section, $\Phi_{1,2}$ are interpolated separately. In contrast to the bremsstrahlung cross section, there are additional terms not contained in the main logarithm (see $\mathcal{A}^{N,S}_{e,\mu}$ below), which arise from the additional integration. In [66], this term was taken into account as

$$\frac{|\mathcal{A}^N_{e,\mu}|}{C_{e,\mu}} = \ln(1 + Y_{e,\mu}), \tag{3.95}$$

where $Y_{e,\mu}$ approximately describe the more complex actual function (cf. Fig. 3.11 for a comparison for the e-diagrams).

The function Φ_e is given in the absence of screening and the case of complete screening by

$$\Phi^N_e = C_e \ln \frac{Ev(1-\varrho^2)}{2m\sqrt{e}\sqrt{1+\xi}} - \frac{1}{2}|\mathcal{A}^N_e|, \tag{3.96}$$

$$\Phi^S_e = C_e \ln(BZ^{-1/3}\sqrt{1+\xi}) + \frac{1}{2}\mathcal{A}^S_e, \tag{3.97}$$

where

$$\begin{aligned} |\mathcal{A}^N_e| = {} & [(2+\varrho^2)(1+\beta) + \xi(3+\varrho^2)]\,\mathrm{Li}_2\,\frac{1}{1+\xi} - (2+\varrho^2)\xi \ln\left(1+\frac{1}{\xi}\right) \\ & - \frac{\xi+\varrho^2+\beta}{1+\xi}, \end{aligned} \tag{3.98}$$

$$\begin{aligned} \mathcal{A}^S_e = {} & |\mathcal{A}^N_e| - \frac{1}{6}\left\{[(1-\varrho^2)(1+\beta) + \xi(3-\varrho^2)] \ln\left(1+\frac{1}{\xi}\right)\right. \\ & \left. + \frac{1+2\beta+\varrho^2+\xi(3-\varrho^2)}{1+\xi}\right\}. \end{aligned} \tag{3.99}$$

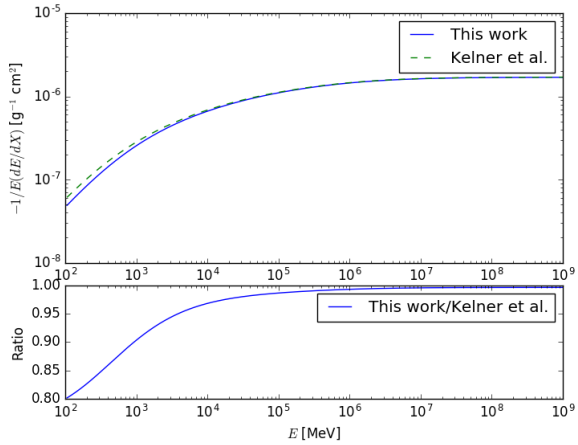

(a) Average bremsstrahlung energy loss.

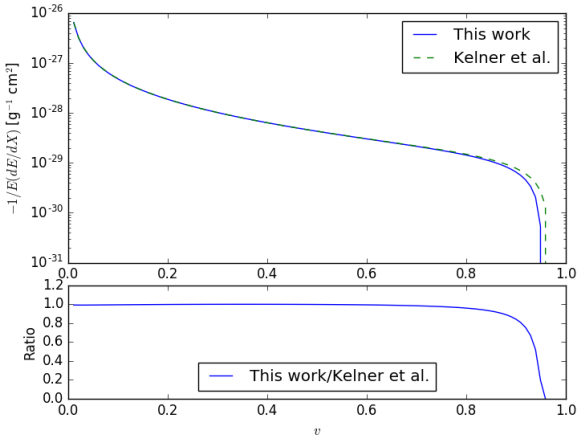

(b) Differential cross section at 10 GeV muon energy.

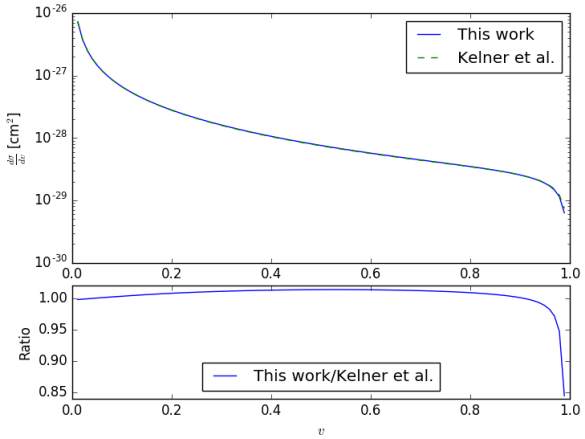

(c) Differential cross section at 100 GeV muon energy.

Figure 3.10: Comparison of the average bremsstrahlung energy loss and the differential cross section at 10 GeV and 100 GeV between the improved parametrization presented here and the parametrization of [58] for a material with $Z = 11, A = 22$.

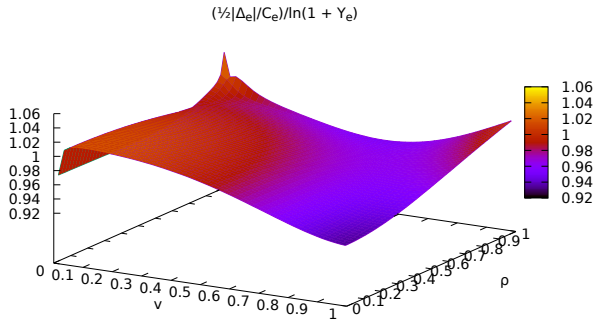

Figure 3.11: Ratio of the non-logarithmic term in the pair production cross section to its parametrization of [66] for the e-diagrams.

Here and in the following, $\mathrm{Li}_2(x)$ is the dilogarithm, defined as

$$\mathrm{Li}_2(x) = -\operatorname{Re}\int_0^x \frac{\ln(1-t)}{t}\,dt. \tag{3.100}$$

The functions $|\mathit{\Delta}_e^N|, \mathit{\Delta}_e^S$ are equal except for the terms arising from the difference $L_1 - L_2 = 1/6$ in the complete screening limit, such that the coefficient of Φ_2 is given by $6(\mathit{\Delta}_e^N - \mathit{\Delta}_e^S)$. We therefore have the conditions for the coefficients $C_{1,2}$ of $\Phi_{1,2}$

$$C_1^e + C_2^e = C_e, \tag{3.101}$$

$$C_1^e \mathit{\Delta}_1^e + C_2^e \mathit{\Delta}_2^e = |\mathit{\Delta}_e^N|, \tag{3.102}$$

$$C_1^e \mathit{\Delta}_1^e + C_2^e \left(\mathit{\Delta}_2^e - \frac{1}{6}\right) = \mathit{\Delta}_e^S \tag{3.103}$$

where $\mathit{\Delta}_{1,2}^e$ denote the terms not proportional to the main logarithm arising from $\Phi_{1,2}$, respectively.

Thus, the cross section for the e-diagrams using an analytical interpolation

for $\Phi_{1,2}$ analogous to [66, 87] is given by

$$\begin{aligned}
\frac{d\sigma}{dv\ d\varrho} &= \frac{2}{3\pi}(Z\alpha r_e)^2 \frac{1-v}{v}\left\{C_1^e L_1^e + C_2^e L_2^e\right\},\\
L_1^e &= \ln\frac{BZ^{-1/3}\sqrt{(1+\xi)X_e}}{X_e + \frac{2m_e\sqrt{e}BZ^{-1/3}(1+\xi)}{Ev(1-\varrho^2)}},\\
L_2^e &= \ln\frac{BZ^{-1/3}e^{-1/6}\sqrt{(1+\xi)X_e}}{X_e + \frac{2m_e e^{1/3}BZ^{-1/3}(1+\xi)}{Ev(1-\varrho^2)}},\\
X_e &= \exp\left(-\frac{|\mathcal{A}_e^N|}{B_e}\right),\\
C_2^e &= [(1-\varrho^2)(1+\beta)+\xi(3-\varrho^2)]\ln\left(1+\frac{1}{\xi}\right)\\
&\quad + 2\frac{1-\beta-\varrho^2}{1+\xi} - (3-\varrho^2),\\
C_1^e &= C_e - C_2^e,
\end{aligned} \tag{3.104}$$

without the nuclear formfactor correction and the contribution of atomic electrons.

For the μ-diagrams, it follows analogously from

$$\begin{aligned}
|\mathcal{A}_\mu^N| &= \left[(1+\varrho^2)\left(1+\frac{3}{2}\beta\right) - \frac{1}{\xi}(1+2\beta)(1-\varrho^2)\right]\mathrm{Li}_2\left(\frac{\xi}{1+\xi}\right)\\
&\quad + \left(1+\frac{3}{2}\beta\right)\frac{1-\varrho^2}{\xi}\ln(1+\xi)\\
&\quad + \left[1-\varrho^2-\frac{\beta}{2}(1+\varrho^2)+\frac{1-\varrho^2}{2\xi}\beta\right]\frac{\xi}{1+\xi},
\end{aligned} \tag{3.105}$$

$$\begin{aligned}
\mathcal{A}_\mu^S &= |\mathcal{A}_\mu^N| - \frac{1}{6}\left\{1-\beta-(1+\beta)\varrho^2 - 2\frac{1-\beta-\varrho^2}{1+\xi}\right.\\
&\quad \left. + [(1-\beta)(1-\varrho^2)-\xi(1+\varrho^2)]\frac{\ln(1+\xi)}{\xi}\right\}
\end{aligned} \tag{3.106}$$

that the corresponding expression for the μ-diagrams is given by

$$\begin{aligned}
\frac{d\sigma}{dv\ d\varrho} &= \frac{2}{3\pi}\left(Z\alpha r_e \frac{m_e}{\mu}\right)^2 \frac{1-v}{v}\left\{C_1^\mu L_1^\mu + C_2^\mu L_2^\mu\right\},\\
L_1^\mu &= \ln\frac{B\frac{\mu}{m_e}Z^{-1/3}\sqrt{(1+1/\xi)X_\mu}}{X_\mu + \frac{2m_e\sqrt{e}BZ^{-1/3}(1+\xi)}{Ev(1-\varrho^2)}},\\
L_2^\mu &= \ln\frac{\frac{\mu}{m_e}BZ^{-1/3}e^{-1/6}\sqrt{(1+1/\xi)X_\mu}}{X_\mu + \frac{2m_e e^{1/3}BZ^{-1/3}(1+\xi)}{Ev(1-\varrho^2)}},\\
X_\mu &= \exp\left(-\frac{|\Delta_\mu^N|}{C_\mu}\right),\\
C_2^\mu &= [(1-\beta)(1-\varrho^2) - \xi(1+\varrho^2)]\frac{\ln(1+\xi)}{\xi} - 2\frac{1-\beta-\varrho^2}{1+\xi}\\
&\quad + 1 - \beta - (1+\beta)\varrho^2,\\
C_1^\mu &= C_\mu - C_2^\mu,
\end{aligned} \tag{3.107}$$

The correction for atomic electrons can be obtained by the substitution $Z^2 \to Z(Z+\xi)$ as above [56]. The newer more accurate calculations for the nuclear formfactor correction by [58] can be incorporated by replacing $L_{1,2}^e, L_{1,2}^\mu$ by the expressions

$$\begin{aligned}
L_1^e &= \ln\frac{BZ^{-1/3}\sqrt{(1+\xi)X_e}}{X_e + \frac{2m_e\sqrt{e}BZ^{-1/3}(1+\xi)}{Ev(1-\varrho^2)}}\\
&\quad - \frac{1}{2}\ln\left[1 + \left(\frac{m_e}{\mu}D_n\right)^2 (1+\xi)/X_e\right],
\end{aligned} \tag{3.108}$$

$$\begin{aligned}
L_2^e &= \ln\frac{BZ^{-1/3}e^{-1/6}\sqrt{(1+\xi)X_e}}{X_e + \frac{2m_e e^{1/3}BZ^{-1/3}(1+\xi)}{Ev(1-\varrho^2)}}\\
&\quad - \frac{1}{2}\ln\left[1 + \left(\frac{m_e}{\mu}D_n\right)^2 e^{-1/3}(1+\xi)/X_e\right],
\end{aligned} \tag{3.109}$$

$$L_1^\mu = \ln\frac{X_\mu\frac{\mu}{m_e}BZ^{-1/3}/D_n}{X_\mu + \frac{2m_e\sqrt{e}BZ^{-1/3}(1+\xi)}{Ev(1-\varrho^2)}}, \tag{3.110}$$

$$L_2^\mu = \ln\frac{X_\mu\frac{\mu}{m_e}BZ^{-1/3}/D_n}{X_\mu + \frac{2m_e e^{1/3}BZ^{-1/3}(1+\xi)}{Ev(1-\varrho^2)}}, \tag{3.111}$$

$$D_n = 1.54A^{0.27}, \tag{3.112}$$

analogous to the procedure in [67]. The cross section differential in v and the average energy loss are shown in Fig. 3.12.

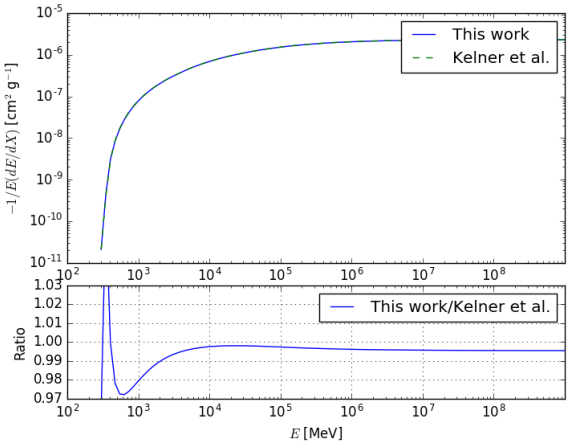

(a) Average pair production energy loss.

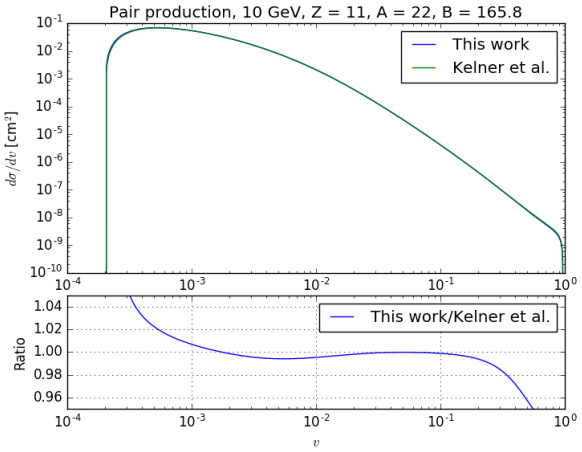

(b) Differential cross section at 10 GeV muon energy.

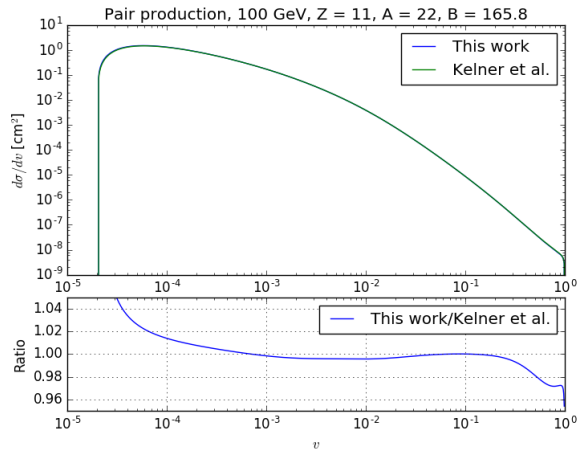

(c) Differential cross section at 100 GeV muon energy.

Figure 3.12: Comparison of the average pair production energy loss and the differential cross section at 10 GeV and 100 GeV between the improved parametrization presented here and the parametrization of [58] for a material with $Z = 11, A = 22$.

3.8 Other muon energy loss processes

3.8.1 Muon pair production

Besides the production of an electron-positron pair, at sufficiently high energy the production of a muon-antimuon pair is also a possible process

$$\mu Z \to \mu\mu^+\mu^- Z. \tag{3.113}$$

This process was considered in [57]. The energy loss is smaller than the one for electron pair production by approximately $m_e^2/m_\mu^2 \sim 10^{-4}$, and therefore irrelevant for the energy loss of the muon. However, the conversion of a single muon into a bundle of three muons can be interesting for densely instrumented detectors [71], as it results in a narrow bundle.

3.8.2 Muon energy loss and the giant dipole resonance

The giant dipole resonance (GDR) is a resonance of nuclei with a resonance energy and integrated cross section of [79]

$$\nu_{\mathrm{GDR}} \approx (40A^{-1/3} + 7.5)\mathrm{MeV}, \tag{3.114}$$

$$\int \sigma(\nu)\, d\nu \;\approx \frac{(A-Z)Z}{A} 60\,\mathrm{MeV\,mb}. \tag{3.115}$$

The energy transferred to the nucleus is rather small, but the cross section associated with the process is large. Therefore it is interesting to assess the energy loss due to the giant dipole resonance. Using the method of equivalent photons (cf. chapter 4), we obtain

$$\begin{aligned} -\left\langle \frac{dE}{dx} \right\rangle &= \frac{N_\mathrm{A}}{A}\varrho \int n(\nu)\nu\sigma(\nu)\, d\nu \\ &= \frac{2\alpha}{\pi}\frac{N_\mathrm{A}}{A}\varrho \int \nu \ln\frac{E_\mu}{\nu}\sigma(\nu)\frac{d\nu}{\nu} \\ &\approx \nu_{\mathrm{GDR}}\frac{2\alpha}{\pi}\frac{N_\mathrm{A}}{A}\varrho \ln\frac{E_\mu}{\nu_{\mathrm{GDR}}} \int \sigma(\nu)\, d\nu\ . \end{aligned} \tag{3.116}$$

For very large volume neutrino telescopes in ice or water, the most abundant nucleus is ^{16}O. If we use the values above, we obtain

$$-\left\langle \frac{dE}{dx} \right\rangle \approx 4.2 \times 10^{-5}\,\mathrm{MeV\,cm^2\,g^{-1}}\varrho \ln\frac{E}{\nu_{\mathrm{GDR}}},$$

which corresponds to $\sim 10^{-4}$ of the ionization loss and rises only logarithmically with energy. This process can therefore be neglected.

3.8.3 Muon interaction via exchange of a W boson

The weak interaction process

$$\mu N \to \nu_\mu X, \tag{3.117}$$

where N is an initial nucleon and X is a hadronic final state, is similar to the neutrino charged current interaction. Compared to other processes, it is strongly

suppressed; however, the signature of a high-energy muon stopping in the detector with a hadronic cascade is similar to the so-called "lollipop" signature expected for high-energy tau events.[6]

The cross section of charged current muon interaction follows by crossing symmetry from the neutrino charged current interaction cross section as

$$d\sigma(\mu N \to \nu_\mu X) = \frac{1}{2} d\sigma(\nu_\mu N \to \mu X). \tag{3.118}$$

The factor $1/2$ follows from the averaging over the initial polarization of the muon, which can be left- and righthanded in contrast to the neutrino.

Using the fit of [26] for the total charged current neutrino nucleon cross section at high energies

$$\begin{aligned}\sigma_{\mathrm{CC}} = &-2.097 \times 10^{-32} + 4.703 \times 10^{-33} \ln E_\nu - 3.666 \times 10^{-34} \ln^2 E_\nu \\ &+ 1.010 \times 10^{-35} \ln^3 E_\nu,\end{aligned} \tag{3.119}$$

where E_ν is in GeV and σ_{CC} in cm^2, we can estimate the rate of tau- and muon-induced lollipop events as (cf. [25])

$$R_\mu = 2\pi N_A \varrho V_{\mathrm{eff}} \int_{E_{\mu,\min}}^{\infty} \frac{1}{2} \sigma_{\mathrm{CC}} \Phi_\mu(E_0)\, dE_\mu\, d\cos\theta, \tag{3.120}$$

(3.121)

where V_{eff} is the effective volume of the detector, $\Phi_\mu(E)$ the flux of atmospheric muons and $E_0 = e^{bx}E + a/b(e^b - 1)$ the energy of the muon before propagation over a distance $x = d/\cos\theta$ for a detector at a depth of d underground. Taking $V_{\mathrm{eff}} = 0.9\,\mathrm{km}^3$, $d = 1550\,\mathrm{m}$ and $\varrho = 0.918\,\mathrm{g\,cm}^{-3}$, roughly corresponding to the IceCube detector, and [2]

$$\Phi_\mu(E) = 1.06 \times 10^{-10}\,\mathrm{s}^{-1}\,\mathrm{cm}^{-2}\,\mathrm{TeV}^{-1}\,\mathrm{sr}^{-1} \left(\frac{E}{10\,\mathrm{TeV}}\right)^{-3.78}, \tag{3.122}$$

we obtain a rate of about $2 \times 10^{-2}\,\mathrm{yr}^{-1}$.

To assess the importance of this process as background to tau neutrino searches via the lollipop channel, we estimate the rates of actual tau-induced lollipop events [16]

$$R_\tau = 2\pi \frac{N_A}{A} \varrho A_{\mathrm{eff}} \int_{E_{\nu,\min}}^{\infty} \sigma_{\mathrm{CC}} \Phi_{\nu_\tau}(E_\nu)(L - x_{\min})[e^{x_{\min}/R_\tau((1-y)E_\nu)}]_{y=\langle y\rangle} dE_\nu, \tag{3.123}$$

[6] Tau leptons have a very short livetime in the rest frame of $290.3 \times 10^{-15}\,\mathrm{s}$ and therefore decay fast. Due to their higher mass, the average energy loss of tau leptons is smaller than for muons of the same energy. The rough scaling of the average energy loss of a lepton with mass m is $\propto m^{-2}$ for bremsstrahlung, $\propto m^{-1}$ for pair production and inelastic nuclear interaction and $\propto m^0$ for ionization [92]. The energy of a muon with the same average energy loss as a tau lepton with a given energy is therefore a factor 6 to 11 lower [33] since inelastic nuclear interaction dominates the energy loss at tau energies above 100 TeV.

where $R_\tau(E_\tau) = c\tau(E_\tau/m_\tau) \approx E_\tau 50\,\mathrm{m/PeV}$ is the range of tau leptons, L the length of the detector and y the inelasticity of the neutrino interaction, approximated by the mean value $\langle y \rangle \approx 0.25$. The minimum length x_{min} the τ lepton has to travel before decay has been assumed as 100 m. Due to neutrino absorption by the earth, only downgoing events are considered. Using $A_{\mathrm{eff}} \approx 1\,\mathrm{km}^2, L \approx 1\,\mathrm{km}$ and the neutrino flux per flavor [3]

$$\Phi_\nu(E) = 0.66 \times 10^{-18}\,\mathrm{cm}^{-2}\,\mathrm{s}^{-1}\,\mathrm{Gev}{-}1\,\mathrm{sr}^{-1} \left(\frac{E}{100\,\mathrm{TeV}}\right)^{-1.91}, \qquad (3.124)$$

a rate of about $0.3\,\mathrm{yr}^{-1}$ is obtained. Therefore, a measurement of the ν_τ flux via the lollipop channel is possibly contaminated by muons at the 10% level. Both estimates are very optimistic, assume a 100% efficient event selection and make simple approximations. A more detailed calculation of the event rate would require a detailed simulation of the detector. This process might be interesting for future detectors with even larger volume.

Chapter 4

The Weizsäcker-Williams method

The Weizsäcker-Williams method, also called method of equivalent photons, is an approximate method in quantum electrodynamics, which is based on the observation of Fermi [44] that the electric field of a fast moving nucleus is similar to a flux of real photons. Independently, Weizsäcker and Williams investigated this problem in the context of classical electrodynamics [106, 107] for a point charge. This allows to express the bremsstrahlung cross section through the Compton cross section and a flux of photons equivalent to the field of the nucleus.

The interaction of muons with atoms has to take into account the atomic and nuclear form factor. In this chapter, the equivalent photon flux for an extended nucleus is calculated, analogous to the treatment of a point nucleus in [17]. This photon flux will be used in the following chapter to calculate the radiative corrections to the bremsstrahlung energy loss and cross section.

Consider the two processes (a) and (b) in Fig. 4.1. If the momentum transfer squared $|k^2|$ in diagram (b) is small, it is possible to express process (b) by process (a). The particle with momentum p is assumed to have mass M, energy ε and to move ultrarelativistically ($\varepsilon \gg M$) in the rest system of the particle with momentum q and mass m. If $m \neq M$, it is assumed that$m < M$.

The amplitude of process (a) can be expressed in the form

$$M_{fi}^{(r)} = -e(e^{\mu} J_{\mu}) \tag{4.1}$$

with e^{μ} the 4-vector of polarization and J^{μ} the transition current describing the interaction in the circle. The amplitude of process (b) is accordingly

$$M_{fi} = \frac{Ze^2}{k^2}(j^{\mu} J_{\mu}) \tag{4.2}$$

with j^{μ} the transition current of particle M and Ze its charge. The current J_{μ} is a function of $k = Q - q$ where $k^2 = 0$ in (a) and $k^2 \neq 0$ in (b). In the case $|k^2| \ll m^2$ we can approximate the current J in (b) also by its value at $k^2 = 0$, since J_{μ} is necessarily a function which assumes a finite limiting value at $k^2 = 0$ because process (a) is also possible.

Compared to the initial momentum $|\mathbf{p}| \approx \varepsilon$ the change of momentum $\mathbf{k} = \mathbf{p} - \mathbf{p}'$ at emission of a virtual photon is small, so that its motion is quasiclassical. We

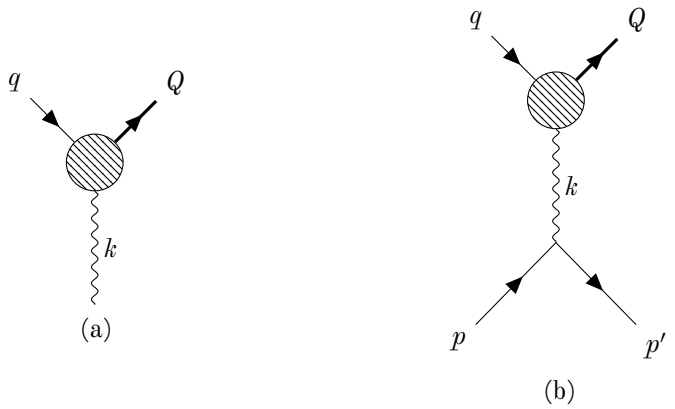

Figure 4.1: Process with (a) a real photon, $k^2 = 0$, and (b) a virtual photon, $k^2 < 0$. Q can refer to a system of several particles.

can therefore neglect its spin so that

$$j_\mu = p_\mu + p'_\mu \approx 2p_\mu. \tag{4.3}$$

Gauge invariance requires $jk = 0$ and therefore

$$0 = \varepsilon\omega - p_x k_x \Leftrightarrow \omega = v k_x, \tag{4.4}$$

where the x-axis has been chosen in the direction of motion of particle M, $v = p_x/\varepsilon$ is the velocity of particle M and ω the energy of the photon. This leads to

$$-k^2 = -\omega^2 + k_x^2 + \mathbf{k}_\perp^2 \approx \omega^2(1 - v^2) + \mathbf{k}_\perp^2, \tag{4.5}$$

and the condition $|k^2| \ll m^2$ is equivalent to $\mathbf{k}_\perp^2 \ll m^2$ and the condition $\omega \ll m/\sqrt{1 - v^2} = m\varepsilon/M$, which is much weaker due to the assumption that $\varepsilon \gg M$. Since the current J_μ is also gauge-invariant, $Jk = 0$ and we obtain

$$J_0 = \frac{J_x}{v} + \frac{\mathbf{J}_\perp \mathbf{k}_\perp}{\omega}, \tag{4.6}$$

so that the scalar product jJ is given by the expression

$$\begin{aligned} jJ &\approx 2pJ = 2(J_0\varepsilon - J_x p_x) \\ &= 2\varepsilon(J_0 - J_x v) = 2\varepsilon\left(\frac{J_x}{v} + \frac{\mathbf{J}_\perp \mathbf{k}_\perp}{\omega} - J_x v\right) \\ &= 2\frac{\varepsilon}{\omega}\left(\mathbf{k}_\perp \mathbf{J}_\perp + \frac{1 - v^2}{v}\omega J_x\right) \\ &\approx 2\frac{\varepsilon}{\omega}\left(\mathbf{k}_\perp \mathbf{J}_\perp + \frac{\omega M^2}{\varepsilon^2} J_x\right). \end{aligned} \tag{4.7}$$

We now evaluate the scalar product Je. This is simplified by using the polarization vector in Coulomb gauge $ek = -\mathbf{e}\mathbf{k} = 0$, leading to $e_x \approx -\mathbf{e}_\perp \mathbf{k}_\perp/\omega$, and therefore

$$Je = -\mathbf{e}_\perp\left(\mathbf{J}_\perp - \frac{\mathbf{k}_\perp}{\omega} J_x\right). \tag{4.8}$$

Comparing the expressions (4.7) and (4.8), we observe that they are proportional to each other if the second term in parentheses can be neglected. The current J is connected to the upper part of the diagram, and the components $J_x, \mathbf{J}_\perp$ have to be considered as quantities of comparable magnitude. Therefore, the region of validity of this approximation is given by $|\mathbf{k}_\perp| \ll \omega$ and $\omega \ll |\mathbf{k}_\perp|\varepsilon^2/M^2$; these do not contradict the earlier established conditions for $\omega, \mathbf{k}_\perp$.

Considering that in (4.8) the photon is polarized in the $x, \mathbf{k}$-plane such that $\mathbf{e}_\perp \parallel \mathbf{k}_\perp$, and that under the above conditions $\mathbf{e}_\perp^2 \approx e^2 = 1$, we now obtain

$$M_{fi} = M_{fi}^{(r)} \frac{Ze}{-k^2} \frac{2\varepsilon}{\omega} |\mathbf{k}_\perp|, \tag{4.9}$$

subject to the conditions

$$\begin{aligned} |\mathbf{k}_\perp| &\ll \omega \ll m\gamma, \\ \frac{\omega}{\gamma^2} &\ll |\mathbf{k}_\perp| \ll m, \\ \gamma = \frac{\varepsilon}{M} &= \frac{1}{\sqrt{1-v^2}}. \end{aligned} \tag{4.10}$$

This relation between the amplitudes leads to the desired relation between the cross section of processes (a) and (b). In the rest system of m we have according to the usual formulæ

$$d\sigma_r = |M_{fi}^{(r)}|^2 (2\pi)^4 \delta^4(P_f - P_i) \frac{1}{4m\omega} \, d\varrho_Q \, , \tag{4.11}$$

$$d\sigma = |M_{fi}|^2 (2\pi)^4 \delta^4(P_f - P_i) \frac{1}{4m\varepsilon} \frac{d^3p'}{2\varepsilon(2\pi)^3} \, d\varrho_Q \, , \tag{4.12}$$

where $d\varrho_Q$ denotes the statistical weight of the particles Q. We obtain

$$d\sigma = d\sigma_r \, n(\mathbf{k}) \, d^3p' \, , \tag{4.13}$$

where

$$n(\mathbf{k}) = \frac{Z^2 e^2}{4\pi^3} \frac{\mathbf{k}_\perp^2}{\omega(\mathbf{k}_\perp^2 + \omega^2/\gamma^2)^2}. \tag{4.14}$$

The factor $n(\mathbf{k})$ can be interpreted as density of equivalent photons in $\mathbf{k}$-space for the production of the same system of particles Q as in $d\sigma_r$ with $\mathbf{p}'$ in the interval d^3p' . The integration over d^3p' is equivalent to integration over $d^3k = d\omega \; d^2k_\perp$. The $\mathbf{k}_\perp$-integration corresponds to the averaging over the polarization direction of the photon k such that

$$d\sigma = n(\omega) \, d\omega \; d\sigma_r \tag{4.15}$$

where

$$n(\omega) = \int n(\mathbf{k}) 2\pi k_\perp \, dk_\perp = \frac{2Z^2\alpha}{\pi\omega} \int \frac{k_\perp^3 \, dk_\perp}{(k_\perp^2 + \omega^2/\gamma^2)^2}. \tag{4.16}$$

This integral diverges logarithmically for $k_\perp \to \infty$ and has to be regularized. We can set the upper limit of integration to $k_\perp \sim m$, the upper limit of the inequality in (4.10), if not only the argument of the resulting logarithm is big compared

to 1, but also the logarithm itself, leading to logarithmic accuracy. The spectral distribution is therefore given by

$$n(\omega)\,d\omega \;= \frac{2}{\pi} Z^2 \alpha \frac{d\omega}{\omega} \ln \frac{\gamma m}{\omega}. \tag{4.17}$$

This derivation was carried out for an ultrarelativistically moving point charge. If we neglect the spin but take into account the extended charge distribution, as is appropriate for fast moving atoms and nuclei, the current j_μ is multiplied by the form factor $F(k^2) = F_n(k^2) - F_e(k^2)$. In this case the spectral distribution of equivalent photons is given by

$$n(\omega)\,d\omega \;= \frac{2Z^2\alpha}{\pi\omega} \int \frac{k_\perp^3}{(\mathbf{k}_\perp^2 + \omega^2/\gamma^2)^2} |F(k_\perp^2 + \omega^2/\gamma^2)|^2 \, dk_\perp \,. \tag{4.18}$$

In this work the charge distribution of the nucleus and of the atomic electrons are described by a Gaussian and an exponential distribution, respectively, resulting in the form factors [50]

$$F_{\mathrm{n}}(q^2) = \exp\left[-\frac{q^2 R_{\mathrm{n}}^2}{6}\right], \tag{4.19}$$

$$F_{\mathrm{a}}(q^2) = \left[1 + \frac{q^2 R_{\mathrm{a}}^2}{12}\right]^{-2} \tag{4.20}$$

with R the Rms-radius of the charge distribution. The atomic and nuclear radius can be parametrised for light and medium nuclei as [35]

$$R_{\mathrm{n}} = 1.27 A^{0.27}\mathrm{fm}, \tag{4.21}$$

$$R_{\mathrm{a}} = \frac{183 Z^{-1/3}}{2.718 m_{\mathrm{e}}} \tag{4.22}$$

with Z the nucleus charge and A its mass number, and for hydrogen

$$R_{\mathrm{p}} = 0.85\,\mathrm{fm}. \tag{4.23}$$

With the above formfactors, the calculation of the pseudophoton flux integral gives

$$\begin{aligned} n(\omega)\,d\omega \;= \frac{\alpha Z^2}{\pi} \Bigg[& \frac{1}{(bz+1)^2}\left(-\frac{17}{6} - 4b^2z^2 - 7bz\right) \\ & -2\exp\left(\frac{a}{b}\right)(az - 2bz + a/b - 1)\,\mathrm{Ei}(1, a(z+1/b)) \\ & -(2az + 4bz + 2)\,\mathrm{Ei}(1, az) + (2az+1)\,\mathrm{Ei}(1, 2az) \\ & + (4bz+1)\ln\left(1 + \frac{1}{bz}\right) - e^{-2az} + 4e^{-az}\Bigg] \frac{d\omega}{\omega}, \end{aligned} \tag{4.24}$$

where $\mathrm{Ei}(1,x) = \int_x^\infty e^{-t}/t\,dt$ is the exponential integral, $z = \omega^2/\gamma^2$, $a = R_{\mathrm{n}}^2/6$, $b = R_{\mathrm{a}}^2/12$.

Chapter 5

Radiative corrections

5.1 Radiative corrections to the average bremsstrahlung energy loss of high-energy muons

Previous calculations took into account the modification of the Coulomb interaction with the nucleus by elastic and inelastic nuclear form factors, the contribution of atomic electrons as target for muon bremsstrahlung and the inelastic interaction with the target nucleus. This section[1] discusses the correction of the energy loss through virtual and real radiative corrections. Since this correction is small compared to the main contribution, we restrict our treatment of the nucleus to elastic atomic and nuclear form factors.

In the calculation of radiative corrections in QED, processes with virtual photons can give rise to logarithmically divergent integrals; to obtain a finite result, it is necessary to add the cross section for the emission of an additional photon with energy $\omega < \omega_{\min}$ which cancels this divergence. Usually $\omega_{\min}$ is identified with the finite energy resolution of the detector and assumed to be small compared to the mass of the radiating particle, such that the approximation of classical currents can be used. The contribution of harder photons indistinguishable from a single photon is then evaluated numerically according to the conditions of the experiment (see e. g. [12]). In the problem of muon propagation, however, the particle may traverse several kilometers of material before the energy losses can be seen by the detector. Therefore the cross section has to be integrated over all kinematically allowed states of the additional photon. So the energy loss depends only on the primary energy of the muon.

Unless stated otherwise, all equations are presented in a system of units where $\hbar = c = m_\mu = 1$.

5.1.1 Method

This calculation uses a modified Weizsäcker-Williams method [106, 107], which approximates the effect of a nucleus by a spectrum of equivalent photons. This method allows to express the bremsstrahlung cross section $d\sigma_{\mathrm{B}}$ through the Compton cross section $d\sigma_{\mathrm{C}}$ convolved with the equivalent photon flux. Using

[1] The results of these calculations were published in [95].

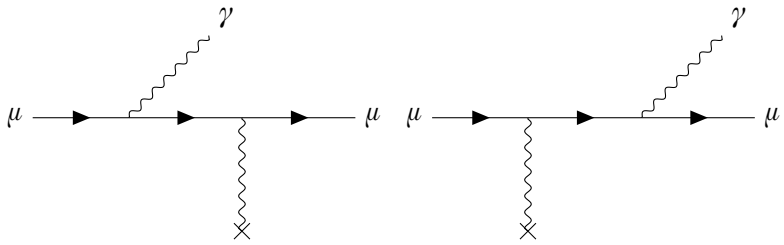

Figure 5.1: Tree level diagrams for muon bremsstrahlung.

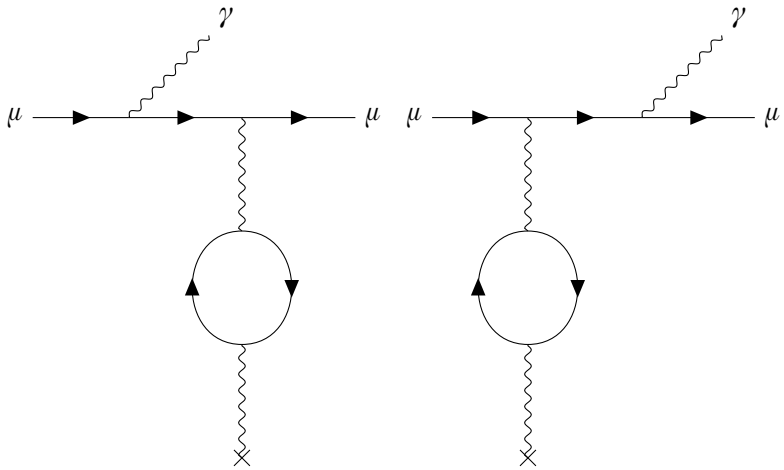

Figure 5.2: Vacuum polarization diagrams for muon bremsstrahlung on atoms.

the radiative corrections to the Compton effect in [28], the radiative corrections to the bremsstrahlung spectrum were first calculated in the soft-photon approximation in [82] for an unscreened or completely screened nucleus. The diagrams taken into account are shown in[2] Fig. 5.1, 5.2, 5.3, 5.4, 5.5, 5.6.

Energy loss

Considering the collision of a fast muon with an atom, we introduce two systems of reference: the laboratory system K_Z in which the atom is at rest and the muon has a Lorentz factor $\gamma \gg 1$, and the system K_μ in which the muon is at rest and the atom has a Lorentz factor of γ.

It is convenient to calculate the energy loss in the frame K_μ. In K_Z the average energy loss per unit length caused by bremsstrahlung is given by

$$-\left\langle \frac{dE}{dx} \right\rangle = NE\Sigma, \quad \Sigma = \frac{1}{E}\int (E - E')\, d\sigma_{\mathrm{B}} \,. \tag{5.1}$$

where E (E') is the initial (final) muon energy, N is the number density of target atoms per unit volume. The quantity Σ can be rewritten in a relativistically

[2]These are all diagrams contributing at next-to-leading order, except diagrams with two photons exchanged to the nucleus, which will be considered in the following chapter in Coulomb corrections. Self-energy and vacuum polarization diagrams on the outer legs vanish identically due to the use of on-shell renormalization, as is customary in quantum electrodynamics.

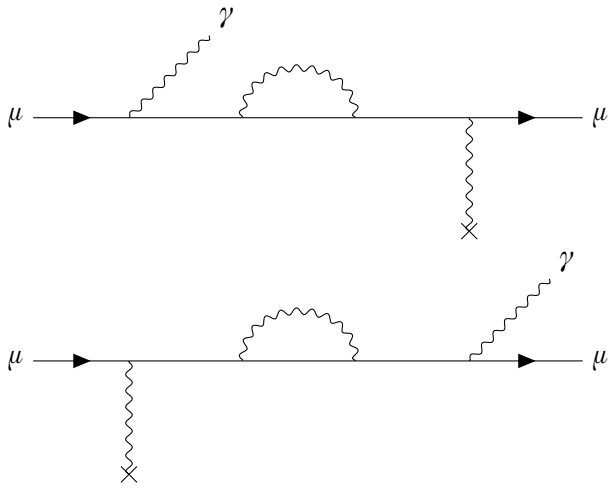

Figure 5.3: Fermion self energy diagrams for muon bremsstrahlung on atoms.

invariant form as

$$\Sigma = \frac{1}{(up)} \int ((up) - (up')) \, d\sigma_{\mathrm{B}} \, , \tag{5.2}$$

where u is the 4-velocity of the atom and p, p' are the initial and final 4-momenta of the muon respectively, $(up) = u^0 p^0 - \mathbf{up}$ is the scalar product of 4-vectors. Using the Weizsäcker-Williams method it is possible to rewrite this as

$$\Sigma = \int \frac{(up) - (up')}{(up)} \, d\sigma_{\mathrm{C}} \, n(\omega) d\omega, \tag{5.3}$$

where ω is the energy of the equivalent photon. In this equation we will calculate the integrand in the K_μ frame. For Compton scattering the energy-momentum conservation gives $(u, p - p') = (u, q' - q)$, where q (q') is the initial (final) photon 4-momentum. In the frame K_μ we have $(uq)/\gamma = \omega(1 - \beta) \approx \omega/(2\gamma^2)$, where ω is the initial photon energy and ω' the final photon energy. Since $\omega \sim \gamma$, the ratio $(uq)/\gamma \sim 1/\gamma$ is negligible. The other term is

$$\frac{(uq')}{\gamma} = \omega'(1 - \beta \cos\theta) \approx \frac{1}{2}\omega'(\theta^2 + 1/\gamma^2). \tag{5.4}$$

In Compton scattering $\theta \lesssim 1/\sqrt{\gamma}$ [17] and the second term in parentheses is negligible. Therefore we obtain for the first case

$$1 - \frac{(up')}{(up)} \approx 1 - \frac{\omega'}{\omega}. \tag{5.5}$$

Similarly for double Compton scattering we have

$$1 - \frac{(up')}{(up)} \approx \omega_1(1 - \cos\theta_1) + \omega_2(1 - \cos\theta_2), \tag{5.6}$$

where $\omega_{1,2}, \theta_{1,2}$ are the energies and angles of the final photons.

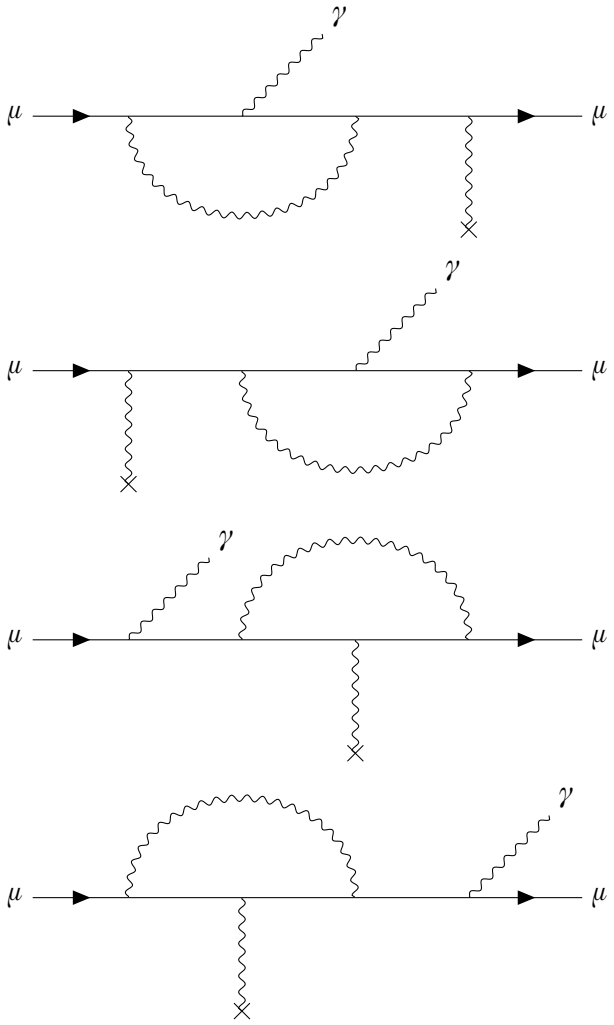

Figure 5.4: Vertex correction diagrams for muon bremsstrahlung on atoms.

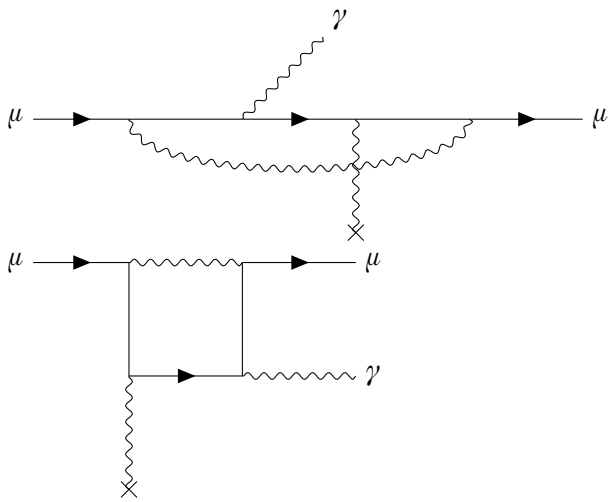

Figure 5.5: Four-point function diagrams for muon bremsstrahlung on atoms.

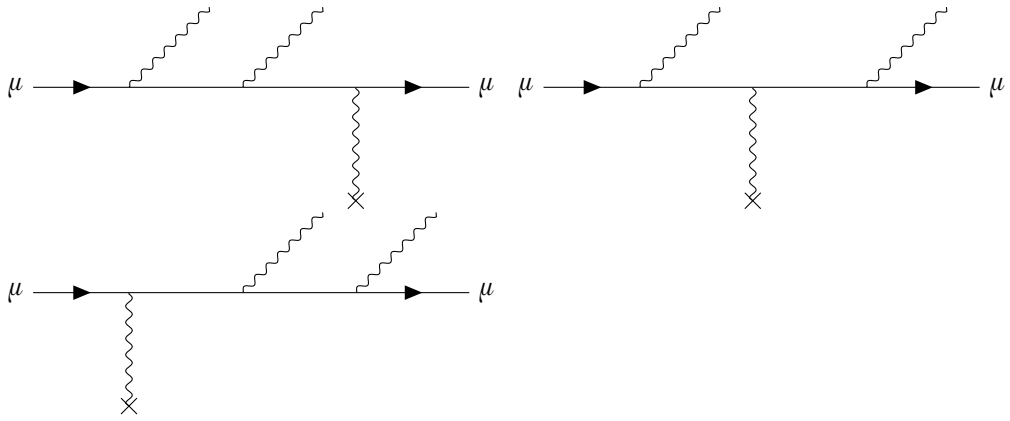

Figure 5.6: Double bremsstrahlung diagrams for muon bremsstrahlung on atoms.

Corrections to energy loss

The contribution to the energy loss of a pseudophoton with energy ω in the rest system of the charged projectile can be conveniently expressed by the angles and energies of the final particles in this system as

$$\Sigma_{\text{virt}} = \int \left(1 - \frac{\omega'}{\omega}\right) d\sigma(\omega, \omega') \tag{5.7}$$

for virtual radiative corrections, where $d\sigma(\omega, \omega')$ is the differential cross section for Compton scattering and the scattering angle θ is determined by conservation laws; and

$$\Sigma_{\text{real}} = \int [\omega_1(1 - \cos\theta_1) + \omega_2(1 - \cos\theta_2)] d\sigma(\omega, \omega_1, \omega_2, \theta_1, \theta_2) \tag{5.8}$$

for the double bremsstrahlung contribution, where $d\sigma(\omega, \omega_1, \omega_2, \theta_1, \theta_2)$ is the differential cross section for double Compton scattering, dependent on the initial and final photon energies ω and ω_1, ω_2 and the scattering angles θ_1, θ_2; the azimuthal angle between the two photons is determined by conservation laws. All quantities refer to the rest system of the muon. This formulation improves the numerical stability compared to using the angles in the lab frame, because the cross section is strongly peaked in the forward direction, while this peak is much broader in the rest frame.

In addition, the contribution from vacuum polarization was calculated directly. The loop correction to the virtual photon coupled to the atom can be interpreted as a factor modifying the form factor of the atom.

5.1.2 Results

The radiative corrections to the Compton cross section by virtual photons can be written as [28]

$$d\sigma_{\text{C, vir}} = -\frac{\alpha r_\mu^2}{2\pi} \left(\frac{\tau}{\varkappa}\right)^2 \text{Re}\, U_{\text{C, vir}} d\Omega \tag{5.9}$$

with

$$\begin{aligned}
U_{\text{C, vir}} &= P(\varkappa, \tau) + P(\tau, \varkappa), \\
P(\varkappa, \tau) &= \left(1 - \frac{2y}{\tanh 2y}\right) \ln\frac{\lambda}{\mu} \cdot U_{\text{C}} - \frac{2y}{\tanh 2y}[2h(y) - h(2y)]U_{\text{C}} \\
&\quad + \left[-4\frac{y \sinh 2y}{\varkappa\tau}(2 - \cosh 2y)\frac{2y}{\tanh y}\right] h(y) + \ln\varkappa \left\{ \frac{4y}{\tanh 2y} \left[\frac{4}{\varkappa\tau}\cosh^2 y \right.\right. \\
&\quad \left. + \frac{\varkappa - 6}{2\tau\cosh 2y} + \frac{4}{\varkappa^2} - \frac{1}{\varkappa} - \frac{\tau}{2\varkappa} - \frac{\varkappa}{\tau} - 1\right] \\
&\quad + \frac{3\tau}{2\varkappa^2} + \frac{3\tau}{2\varkappa} + \frac{3}{\tau} + 1 - \frac{7}{\varkappa\tau} + \frac{8}{\varkappa} - \frac{8}{\varkappa^2} + \frac{2\varkappa - \tau^2 - \varkappa^2\tau}{2\varkappa^2\tau(\varkappa - 1)} \\
&\quad \left. - \frac{1}{2\tau}\frac{2\varkappa^2 + \tau}{(\varkappa - 1)^2}\right\} + \frac{y^2}{\sinh^2 y}\left[\frac{2}{\varkappa} - \frac{7}{4}\varkappa - \frac{3}{4}\frac{\tau^2}{\varkappa}\right] \\
&\quad - 4y\tanh y\left(\frac{1}{2} - \frac{1}{\varkappa}\right) + 4\left(\frac{1}{\varkappa} + \frac{1}{\tau}\right)^2
\end{aligned}$$

$$
\begin{aligned}
&- \frac{12}{\varkappa} - \frac{3\varkappa}{2\tau} - \frac{2\varkappa}{\tau^2} + \frac{1}{\varkappa - 1}\left(\frac{\varkappa}{\tau} + \frac{1}{2}\right) \\
&+ G_0(\varkappa)\left[\frac{\varkappa^2}{\tau} + \frac{\tau}{\varkappa^2} + \frac{\varkappa}{\tau} + \varkappa + \frac{\tau}{2} + \frac{2}{\varkappa} - \frac{3}{\tau} - 1\right] \\
&+ \text{terms antisymmetric in } \varkappa, \tau, \\
U_{\mathrm{C}} &= 4\left(\frac{1}{\varkappa} + \frac{1}{\tau}\right)^2 - 4\left(\frac{1}{\varkappa} + \frac{1}{\tau}\right) - \frac{\varkappa}{\tau} - \frac{\tau}{\varkappa}
\end{aligned}
$$

with

$$
4\sinh^2 y = \varkappa + \tau, \tag{5.10}
$$

$$
\begin{aligned}
h(y) &= \frac{1}{y}\int_0^y \frac{u\,du}{\tanh u} \\
&= \ln(2\sinh y) - \frac{y}{2} + \frac{1}{2y}\left(\frac{\pi^2}{6} - \mathrm{Li}_2(e^{-2y})\right),
\end{aligned} \tag{5.11}
$$

$$
\begin{aligned}
G_0(\varkappa) &= -\frac{2}{\varkappa}\int_{1-\varkappa}^{1} \frac{\ln(1-u)}{u}\,du \\
&= \frac{2}{\varkappa}\left[-\mathrm{Li}_2(1-\varkappa) + \frac{\pi^2}{6}\right] \text{ for } \varkappa > 1, \\
&= \frac{2}{\varkappa}\left[\mathrm{Li}_2\left(\frac{1}{1-\varkappa}\right) + \frac{1}{2}\ln^2(1-\varkappa) - \frac{\pi^2}{6}\right] \text{ for } \varkappa < 1.
\end{aligned} \tag{5.12}
$$

This expression can be represented in the form

$$
P = P_0 + P_1 \ln\lambda \tag{5.13}
$$

where λ is the fictitious photon mass necessary to regularize the infrared divergences which cancels out in the final result. The functions P_0 and P_1 depend only on the initial and final photon energies ω, ω'. Then the virtual radiative corrections to the differential Compton cross section are given by

$$
d\sigma_{\mathrm{corr}} = -\alpha r_\mu^2 (P_0 + P_1 \ln\lambda)\frac{d\omega'}{\omega^2} \tag{5.14}
$$

and we obtain

$$
\sigma_{\mathrm{corr}} = -\frac{\alpha r_\mu^2}{\omega^2}\int_{\omega_*}^{\omega} (P_0 + P_1 \ln\lambda)\,d\omega' \tag{5.15}
$$

for the total cross section, where $\omega_* = \omega/(1+2\omega)$ and $r_\mu = r_e(m_e/m_\mu)$ is the classical muon radius. To determine the correction to the average energy loss we have to calculate the integral

$$
\Sigma_{\mathrm{corr}} = \Sigma_{\mathrm{virt}} + \Sigma_{\mathrm{real}} = -\frac{1}{\omega^2}\int_{\omega_*}^{\omega} (P_0 + P_1 \ln\lambda)\left(1 - \frac{\omega'}{\omega}\right)\,d\omega'\,. \tag{5.16}
$$

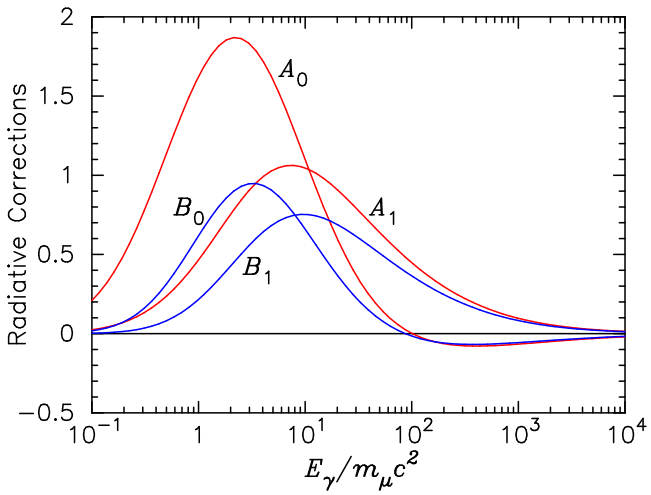

Figure 5.7: Numerical results of the integration over angles and energies for the contribution of the pseudophoton with energy E_γ for the functions defined in (5.17), (5.18).

The results can be expressed through the following functions:

$$A_i = -\frac{1}{\omega^2}\int_{\omega_*}^{\omega} P_i\, d\omega' \tag{5.17}$$

$$B_i = -\frac{1}{\omega^2}\int_{\omega_*}^{\omega} P_i \left(1-\frac{\omega'}{\omega}\right) d\omega' \,, \tag{5.18}$$

$$i = 0, 1.$$

The graphs of the functions $A_{0,1}, B_{0,1}$ which only depend on ω are shown in Fig. 5.7.

For the calculation of the integral (5.6) we used the cross section from [78]. The cross section differential in the photon energies is given by

$$d\sigma_{\rm D} \;= \frac{Z^2\alpha^2 r_\mu^2}{4\pi^2}\Phi(\delta)\frac{\varepsilon_2\omega_1\omega_2\, d\omega_1\;\; d\omega_2}{\varepsilon_1^5}\frac{X}{{f_3}^2}\, d\cos\theta_1'\;\; d\cos\theta_2'\;\; d\varphi \,, \tag{5.19}$$

where θ_1', θ_2' are the scattering angles of the two photons, φ is the angle between these momenta and

$$\begin{aligned} X = {} & 2(ab-c)[(a+b)(x+2)-(ab-c)-8]-2x(a^2+b^2)-8c \\ & + \frac{4x}{AB}[(A+B)(x+1)-(aA+bB)(2+z(1-x)/x) \\ & + x^2(1-z)+2z]-2\varrho[ab+c(1-x)], \end{aligned} \tag{5.20}$$

with the abbreviations

$$a = \sum_i \frac{1}{\varkappa_i}, \qquad b = \sum_i \frac{1}{\varkappa_i'}, \qquad c = \sum_i \frac{1}{\varkappa_i\varkappa_i'}, \tag{5.21}$$

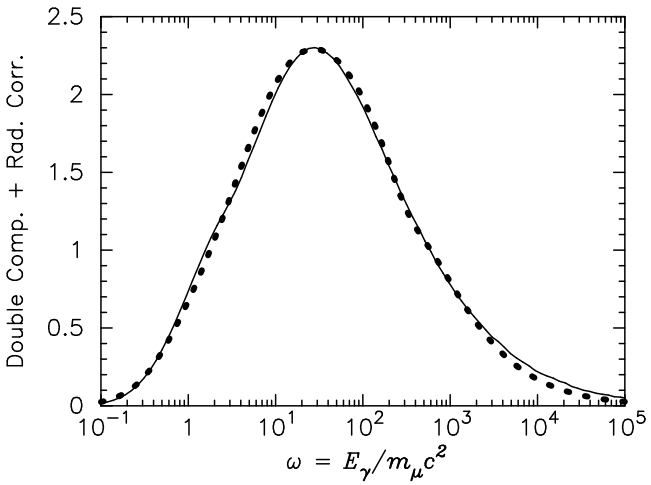

Figure 5.8: Comparison of the numerical results (solid line) and the analytical parametrisation (5.27) (dots).

$$x = \sum_i \varkappa_i = \sum_i \varkappa'_i, \qquad z = \sum_i \varkappa_i \varkappa'_i, \tag{5.22}$$

$$A = \prod_i \varkappa_i, \qquad B = \prod_i \varkappa'_i, \qquad \varrho = \sum_i \left(\frac{\varkappa_i}{\varkappa'_i} + \frac{\varkappa'_i}{\varkappa_i} \right). \tag{5.23}$$

The quantities $\varkappa'_i, \varkappa_i$ denote the scalar products

$$\varkappa_i = pq_i, \tag{5.24}$$

$$\varkappa'_i = p'q_i, \tag{5.25}$$

denoting by q_0 the initial photon and by $q_{1,2}$ the final photons.

The integral diverges as $\omega_{1,2} \to 0$, so we integrated over the region $\omega_{1,2} > \omega_{\min}$. Let us denote the result of this integration as $\alpha r_\mu^2 \gamma X(\omega, \omega_{\min})$. The sum

$$f(\omega) \equiv X(\omega, \omega_{\min}) + B_0(\omega) + B_1(\omega) \ln(2\omega_{\min}) \tag{5.26}$$

in the limit $\omega_{\min} \to 0$ does not depend on $\omega_{\min}$. Numerical calculations for $\omega_{\min} = 10^{-4}$ and $\omega_{\min} = 10^{-5}$ give practically the same result (here we use the known relation $\lambda = 2\omega_{\min}$). For the convenience of further calculations we have obtained the following approximate formula:

$$f(\omega) = 405\omega \left[1 - \frac{(0.006\omega)^2}{16 + (0.006\omega)^4} \right] \frac{\ln(1 + 0.00654\omega)}{1 + 4\ln^2(\omega + 1) + \omega^2}, \tag{5.27}$$

The comparison between the numerical results and this approximation is shown in Fig. 5.8.

By numerical integration over the product of the pseudophoton flux and this function the energy loss is obtained. It can be approximated by the function

$$-\frac{1}{E} \left\langle \frac{dE}{dx} \right\rangle = Z^2 \alpha^2 N r_\mu^2 c_1 \ln \frac{R_a/(R_n c_2)}{1 + R_a/(R_n c_2) \cdot c_3/\gamma} \tag{5.28}$$

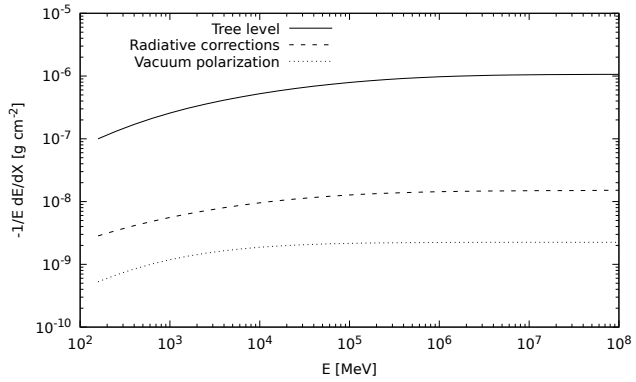

Figure 5.9: Average energy loss for oxygen ($Z = 8, A = 16$).

with

$$c_1 = 8.303, \tag{5.29}$$

$$c_2 = 0.999, \tag{5.30}$$

$$c_3 = 4.099 + 6.335 Z^{1/3}. \tag{5.31}$$

An additional contribution is due to vacuum polarization, which cannot be calculated using the equivalent photon method. This contribution corresponds to modifying the tree level expression with a factor [9]

$$\Pi(q^2) = \frac{\alpha}{\pi}\left[\frac{1}{9} - \left(1 - \frac{\xi^2}{3}\right)\left(1 - \frac{\xi}{2}\ln\frac{\xi+1}{\xi-1}\right)\right], \tag{5.32}$$

where $\xi = \sqrt{1 + 4m_e^2/q^2}$ in the case of virtual electrons and analogously with $m_e \to m_\mu$ for muons. However, the vacuum polarization vanishes for real photons after renormalization and increases with increasing momentum; because the bremsstrahlung cross section is dominated by low momentum transfers, this contribution is small. The correction due to vacuum polarization to the average energy loss is about an order of magnitude smaller than the correction of other radiative corrections (cf. Fig. 5.9).

Ratio to the main contribution

When the main contribution to the bremsstrahlung energy loss is calculated in the modified Weizsäcker-Williams method with the above form factors, the ratio between the radiative correction and the main contribution is independent of Z and A and can be approximated by

$$-\frac{1}{E}\left\langle\frac{dE}{dx}\right\rangle_{\text{rad}} = -\frac{1}{E}\left\langle\frac{dE}{dx}\right\rangle_{0}\alpha\delta(\gamma) \tag{5.33}$$

with

$$\delta(\gamma) = 2.66\frac{\xi-1}{\xi+1}, \quad \xi = 0.0406\sqrt{\gamma} + 3.39 \tag{5.34}$$

for light and medium nuclei and

$$\delta(\gamma) = 2.77\frac{\xi - 1}{\xi + 1}, \quad \xi = 0.02\sqrt{\gamma} + 5.32. \tag{5.35}$$

for hydrogen.

5.2 Radiative corrections to the differential bremsstrahlung cross section

The average energy loss calculated in the previous section is important for calculations of underground muon flux, but to correctly account for the fluctuations around the average energy loss it is necessary to use the differential cross section. For this task, it is necessary to change the method used above. The minimum momentum transfer, which was approximated as $\omega_{\text{eq}}/\gamma$ in the energy loss calculation, in this case has to be replaced by the more exact expression $\delta = \mu^2\omega/2\varepsilon_1\varepsilon_2$. where ω is the final photon energy and $\varepsilon_{1,2}$ denote the initial and final muon energy. Also, the energies of the final photons have to be transformed to the rest system of the nucleus, so that only the scattering angles remain in the lab system.

For the single bremsstrahlung cross section, we can make use of the Compton relation[3]

$$\omega_1' = \frac{\omega_0'}{1 + \omega_0'(1 - \cos\theta_1')}, \tag{5.36}$$

which follows from energy-momentum relation, and the Lorentz transformation

$$\omega_1 = \varepsilon_1\omega_1'(1 - \beta_1\cos\theta_1') \tag{5.37}$$

where $\beta_1 \approx 1$ for $\varepsilon_1 \gg 1$. The propagator denominators $\varkappa = 2p_1q_0 = -2\omega_0'$, $\tau = -2p_1q_1 = 2\omega_1'$ and the integral over the initial equivalent photon energy $d\omega_0'$ thus become

$$\varkappa = -\frac{2\omega_1}{\varepsilon_1(1 - \cos\theta_1')}, \tag{5.38}$$

$$\tau = \frac{2\omega_1}{\varepsilon_2(1 - \cos\theta_1')}, \tag{5.39}$$

$$d\omega_0' = \frac{\varepsilon_1\, d\omega_1}{\varepsilon_2^2(1 - \cos\theta_1')}. \tag{5.40}$$

Since the differential cross section of the Compton effect in lowest order of perturbation theory is given in the rest system of the muon by

$$\begin{aligned} d\sigma_{\text{C}}\,(\omega_0', \mathbf{k}_1') &= \frac{1}{2}r_\mu^2\left(\frac{\varkappa}{\tau}\right)^2 U_{\text{C}}\, d\Omega_1'\,, \\ U_{\text{C}} &= 4\left(\frac{1}{\varkappa} + \frac{1}{\tau}\right)^2 - 4\left(\frac{1}{\varkappa} + \frac{1}{\tau}\right) - \frac{\varkappa}{\tau} - \frac{\tau}{\varkappa}, \end{aligned} \tag{5.41}$$

[3] In this section quantities in the laboratory system where the nucleus is at rest are distinguished from the quantities of the rest system of the muon by denoting the latter with a prime.

the tree level bremsstrahlung cross section is given by

$$\begin{aligned} d\sigma_{\mathrm{B}}\,(\omega_1) &= n(\omega_0')\, d\sigma_{\mathrm{C}}\,(\omega_0', \mathbf{k}_1') \\ &= \frac{Z^2\alpha r_\mu^2}{\pi}\Phi(\delta)\frac{\varepsilon_2\, d\omega_1}{\varepsilon_1\omega_1} U_{\mathrm{C}}\, d\Omega_1' \end{aligned} \tag{5.42}$$

where $\Phi(\delta)$ follows from $n(\omega_0')$ by replacing the minimum momentum transfer ω_0'/γ by the more accurate value δ, except the prefactor $Z^2\alpha/\pi$. Integrating over the angles in $d\Omega_1'$, we obtain

$$d\sigma_{\mathrm{B}}\,(\omega_1) = 4Z^2\alpha r_\mu^2 \frac{d\omega_1}{\omega_1}\Phi(\delta)\left[\frac{4}{3}\frac{\varepsilon_2}{\varepsilon_1} + \left(\frac{\omega_1}{\varepsilon_1}\right)^2\right], \tag{5.43}$$

the known expression for tree level bremsstrahlung in the approximation $\Phi_1 \approx \Phi_2$. For the virtual photon corrections we replace U_{C} by $-(\alpha/\pi)U_{\mathrm{virt}}$, where [28]

$$U_{\mathrm{virt}} = P(\varkappa, \tau) + P(\tau, \varkappa). \tag{5.44}$$

The real photon correction is calculated analogously using the double Compton cross section by [78]. Here, the scalar products $\varkappa_i, \varkappa_i'$ are expressed in the variables above by

$$\varkappa_1 = \frac{\omega_1}{\varepsilon_1(1-\cos\theta_1')}, \qquad \varkappa_1' = -f_1\frac{\omega_1}{\varepsilon_2(1-\cos\theta_1')(1-\cos\theta_2')}, \tag{5.45}$$

$$\varkappa_2 = \frac{\omega_2}{\varepsilon_1(1-\cos\theta_2')}, \qquad \varkappa_2' = -f_2\frac{\omega_2}{\varepsilon_2(1-\cos\theta_1')(1-\cos\theta_2')}, \tag{5.46}$$

$$\varkappa_3 = -f_3\frac{\varepsilon_1}{\varepsilon_2(1-\cos\theta_1')(1-\cos\theta_2')}, \quad \varkappa_3' = \frac{f_3}{(1-\cos\theta_1')(1-\cos\theta_2')}, \tag{5.47}$$

$$f_1 = \frac{\omega_2}{\varepsilon_1}(1-\cos\theta_1') + \frac{\varepsilon_1-\omega_2}{\varepsilon_1}(1-\cos\theta_2') - \frac{\omega_2(\varepsilon_1-\omega_2)}{\varepsilon_1^2}(1-\cos\theta_{12}'), \tag{5.48}$$

$$f_2 = \frac{\omega_1}{\varepsilon_1}(1-\cos\theta_2') + \frac{\varepsilon_1-\omega_1}{\varepsilon_1}(1-\cos\theta_1') - \frac{\omega_1(\varepsilon_1-\omega_1)}{\varepsilon_1^2}(1-\cos\theta_{12}'), \tag{5.49}$$

$$f_3 = \frac{\omega_1}{\varepsilon_1}(1-\cos\theta_2') + \frac{\omega_2}{\varepsilon_1}(1-\cos\theta_1') - \frac{\omega_1\omega_2}{\varepsilon_1^2}(1-\cos\theta_{12}'), \tag{5.50}$$

with $\cos\theta_{12}' = \sin\theta_1'\sin\theta_2' + \cos\theta_1'\cos\theta_2'\cos\varphi$.

The differential cross section depends on the initial energy only in the function $\Phi(\delta)$, such that the result of the integration over the scattering angles depends only on the ratios ω_i/ε_1. The numerical integration is improved by integrating over $\cos\theta_{12}'$ instead of φ since the Jacobian of this transformation leads to an integrable singularity which can be used as a weight function for the QUADPACK [89] subroutine `QAWS`. The other variables were integrated over with the cubature algorithm DCUHRE [18]. We obtain the results shown in Fig. 5.10 for the sum

of virtual and real radiative corrections differential in the energy carried away by all photons. The numerical results are described by the following parametrization with an accuracy better than 1%:

$$\left.\frac{d\sigma}{dv}\right|_{\text{rad}} = \frac{Z^2\alpha^2 r_\mu^2}{v}\Phi(\delta)f(v), \tag{5.51}$$

where

$$f(v) = \begin{cases} a_1 + b_1 v + c_1 v^2 & v < 0.02, \\ a_2 + b_2 v + c_2 v^2 + d_2 v^3 & 0.02 \leqslant v < 0.1, \\ \quad a_3 + b_3 v + c_3 v^2 + d_3 v \ln v & \\ +e_3 \ln(1-v) + f_3 \ln^2(1-v), & 0.1 \leqslant v < 0.9, \\ \quad a_4 + b_4 v + c_4 v^2 + d_4 v \ln v & \\ +e_4 \ln(1-v) + f_4 \ln^2(1-v), & v \geqslant 0.9 \end{cases} \tag{5.52}$$

with

$$a_1 = -0.003\,49, \quad b_1 = 148.84, \quad c_1 = -987.531, \tag{5.53}$$

$$a_2 = 0.1642, \quad b_2 = 132.573, \quad c_2 = -585.361, \quad d_2 = 1407.77, \tag{5.54}$$

$$a_3 = -2.8922, \quad b_3 = -19.0156, \quad c_3 = 57.698, \tag{5.55}$$

$$d_3 = -63.418, \quad e_3 = 14.1166, \quad f_3 = 1.842\,06,$$

$$a_4 = 2134.19, \quad b_4 = 581.823, \quad c_4 = -2708.85, \tag{5.56}$$

$$d_4 = 4767.07, \quad e_4 = 1.529\,18, \quad f_4 = 0.361\,933.$$

The parametrization of the correction diverges $\propto \ln^2(1-v)$ for $v \to 1$. This does contradict neither the finite result for the energy loss in the previous section nor the necessarily finite cross section integrated over v above a certain $v_{\min} > 0$ that is necessary for propagation simulations, since this is an integrable singularity. Also, for any finite muon energy, the factor $\Phi(\delta)$ cuts off the cross section at $v \approx 1 - \mu\sqrt{e}/2\varepsilon_1$.

The additional contribution of vacuum polarization can be expressed by

$$\frac{d\sigma}{dv} = 4Z^2\alpha^2 \left(r_e \frac{m_e}{\mu}\right)^2 \Phi(\delta)\left[\frac{4}{3}(1-v) + v^2\right] s_{\text{vac}}(\delta, Z), \tag{5.57}$$

where $s_{\text{vac}}(\delta, Z)$ is weakly dependent on Z and can be parametrized for muon bremsstrahlung as

$$\begin{aligned} s_{\text{vac}}(\delta, Z) &= \frac{\alpha}{\pi} b(Z) \ln(a(Z)^{1/b(Z)} + e^{c(Z)/b(Z)}\delta), \\ a(Z) &= 2.602\,88 - 0.064\,68 Z^{1/3}, \\ b(Z) &= 0.267\,183 + 0.009\,790\,99 Z^{1/3}, \\ c(Z) &= 2.055\,36 - 0.086\,075\,2 Z^{1/3}. \end{aligned} \tag{5.58}$$

The vacuum polarization acts as a modification of the form factor and therefore alters the screening functions $\Phi_{1,2}(\delta)$ by a factor which can manifestly only depend on δ.

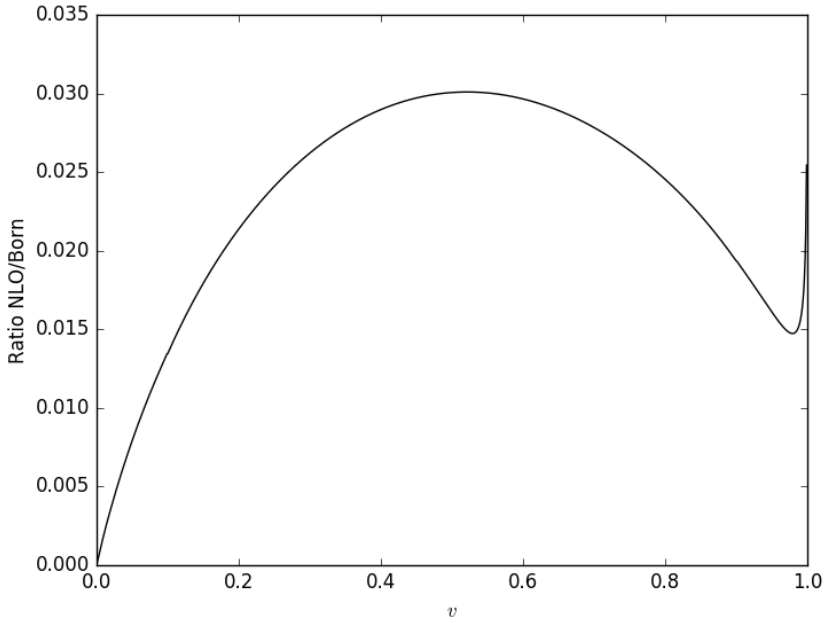

Figure 5.10: Ratio between radiative corrections and tree level bremsstrahlung cross section.

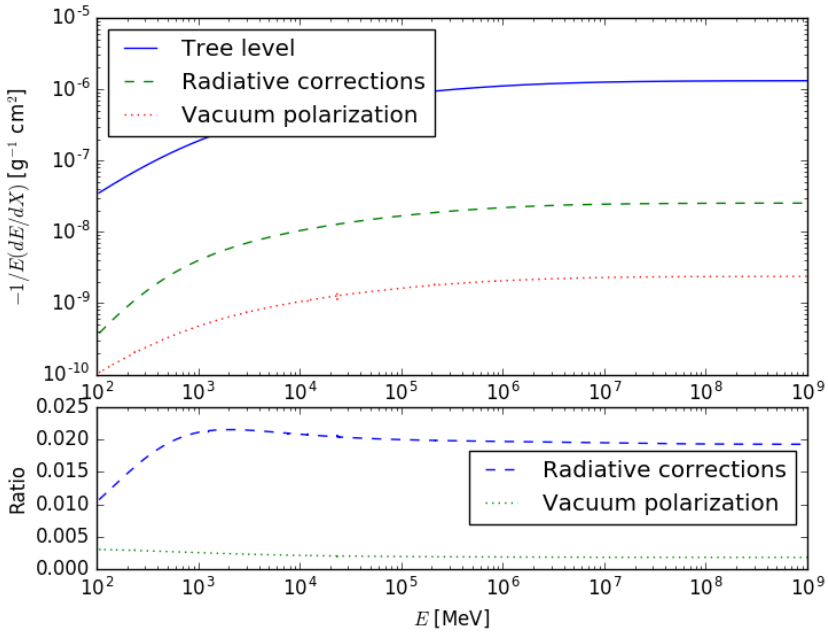

Figure 5.11: Correction to the average bremsstrahlung energy loss due to radiative corrections for a medium with $Z = 11, A = 22$.

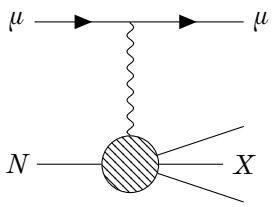

Figure 5.12: Effective Feynman diagram for inelastic nuclear interaction on tree level.

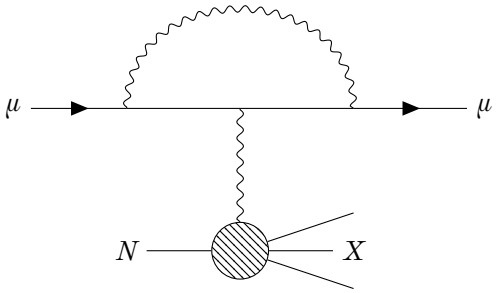

Figure 5.13: Vertex correction to inelastic nuclear interaction.

5.3 Radiative corrections to the cross section of inelastic nuclear interaction

The next-to-leading-order radiative corrections to the cross section of inelastic nuclear scattering are the one-loop corrections and the emission of a bremsstrahlung photon simultaneous to the inelastic interaction with the nucleon (cf. Fig. 5.12, 5.13, 5.14, 5.15). Depending on the energy transferred to the nucleus and the photon, it is debatable whether this should be considered a radiative correction to the nuclear interaction or a nuclear correction to bremsstrahlung [10, 58]. Low-lying nucleon resonances, which are less important for inelastic interaction because of the small deposited energy, can be important because of their big cross section as a nuclear correction to bremsstrahlung, which grows $\sim A$ and is comparable to the correction corresponding to the inelastic nuclear formfactor.

The energy of the muon before and after the interaction is denoted by $\varepsilon_{1,2}$, respectively, the energy transferred to the nucleus is denoted by $-\nu$ and the momentum transferred to the nucleus by q^2. The inelastic structure functions are assumed as [10, 22]

$$W_1(q^2,\nu) = \frac{A}{4\pi^2\alpha}\left(|\nu| - \frac{q^2}{2M}\right)\sigma_\mathrm{T}, \tag{5.59}$$

$$W_2(q^2,\nu) = \frac{A}{4\pi^2\alpha}\left(|\nu| - \frac{q^2}{2M}\right)\frac{q^2}{q^2+\nu^2}(\sigma_\mathrm{T}+\sigma_\mathrm{L}), \tag{5.60}$$

where

$$\sigma_\mathrm{T} = \sigma_{\gamma N}(|\nu| - q^2/2M)\left[0.75\frac{m_1^4}{(m_1^2+q^2)^2}G(x) + 0.25\frac{m_2^2}{m_2^2+q^2}\right], \tag{5.61}$$

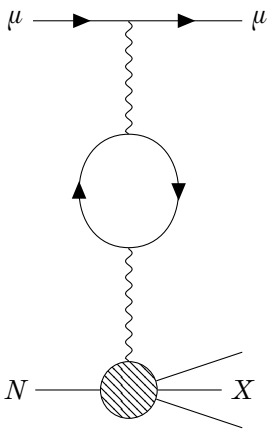

Figure 5.14: Effective Feynman diagram for inelastic nuclear interaction with vacuum polarization.

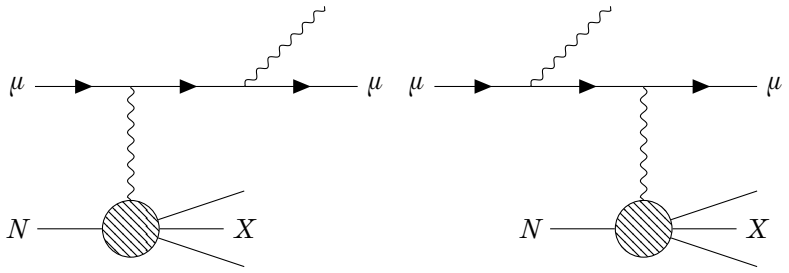

Figure 5.15: Bremsstrahlung correction to inelastic nuclear interaction.

$$\sigma_{\mathrm{L}} = \xi\sigma_{\gamma N}(|\nu| - q^2/2M)\left\{0.75\frac{m_1^2 q^2}{(m_1^2+q^2)^2}G(x) + 0.25\left[\frac{m_2^2}{q^2}\ln\left(1+\frac{q^2}{m_2^2}\right) - \frac{m_2^2}{m_2^2+q^2}\right]\right\}. \tag{5.62}$$

Here, $\sigma_{\gamma N}(E_\gamma)$ is the photonuclear cross section, M is the nucleon mass, $m_1^2 = 0.54\,\mathrm{GeV}^2$ and $m_2^2 = 1.8\,\mathrm{GeV}$ describe the effective hadronic spectrum of vector mesons of a light particle with mass m_1 and a continuum starting at mass m_2. Nucleus shadowing is accounted for by the factor $G(x)$, which is the same as in (3.60). The factor $\xi = 0.25$ is the ratio of the absorption cross section of longitudinally and transversally polarized mesons. Among the photonuclear cross sections presented in 3.5, the interpolated cross section of [93, 94] is the only one containing these resonances. It is therefore used in this section.

The expressions for the bremsstrahlung cross section change when the energy transferred to the nucleus is no longer negligible. The cross section is in this case [10] given by (3.11), where Φ_1, Φ_2 are given by

$$\Phi_1 = -\int d\nu\,\frac{dq}{q^3}W_2(q^2,\nu)\left\{q^2\ln x - \delta'^2\left(\frac{q'}{\delta'}-1\right) + 2\delta'\nu\ln\frac{q'}{\delta'}\right\}, \tag{5.63}$$

$$\Phi_2 = 6\mu^2\int d\nu\,\frac{dq}{q^3}W_2(q^2,\nu)\left\{1 - \frac{\delta'^2}{\mu^2}\ln\frac{q'}{\delta'} - \ln x - \frac{\delta'}{q'}\right\}, \tag{5.64}$$

where

$$\delta' = \frac{\mu^2(\omega-\nu)}{2\varepsilon_1\varepsilon_2},$$
$$q' = \sqrt{q^2+\nu^2}+\nu.$$

The contribution of the structure function W_1, which is negligible for elastic bremsstrahlung, leads to an additional term $(1/\varepsilon_1^2)\Phi_3$, which is added to the expression in brackets in (3.11) and is given by

$$\Phi_3 = \frac{1}{8}W_1(q^2,\nu)\left\{4(4\mu^4-q^4)\ln x - 2\mu^4\frac{\omega}{\delta'}(2\mu^2-q^2)\left(1-\frac{\delta'}{q'}\right)\left[\frac{1}{\varepsilon_1^2}+\frac{1}{\varepsilon_2^2}\right] - 2\mu^4\omega^2\left[\frac{1}{\varepsilon_1^2}+\frac{1}{\varepsilon_2^2}\right]\left[\sqrt{\frac{q'^2}{\delta'^2}8\xi\frac{q'}{\delta'}+16\xi(1+\xi)} - 1 - 4\xi + \xi\ln\frac{q'}{\delta'}\right] + 8\delta'\omega(2\mu^2-q^2)\ln\frac{q'}{\delta'}\right\}. \tag{5.65}$$

Neglecting this term does not noticeably alter the cross section differential in ω, ν for high-energy muons.

These expression are approximations based on the assumption that the energy $-\nu$ transferred to the nucleus is small compared to the energy of the muon and the photon the interaction. This only distorts the cross section at the upper kinematical limit where almost all the energy of the initial muon goes into either the photon or the nuclear interaction. Since the cutoff at this limit is rather steep, the error of using the approximation $\nu^2 \ll \omega^2$ is only small.

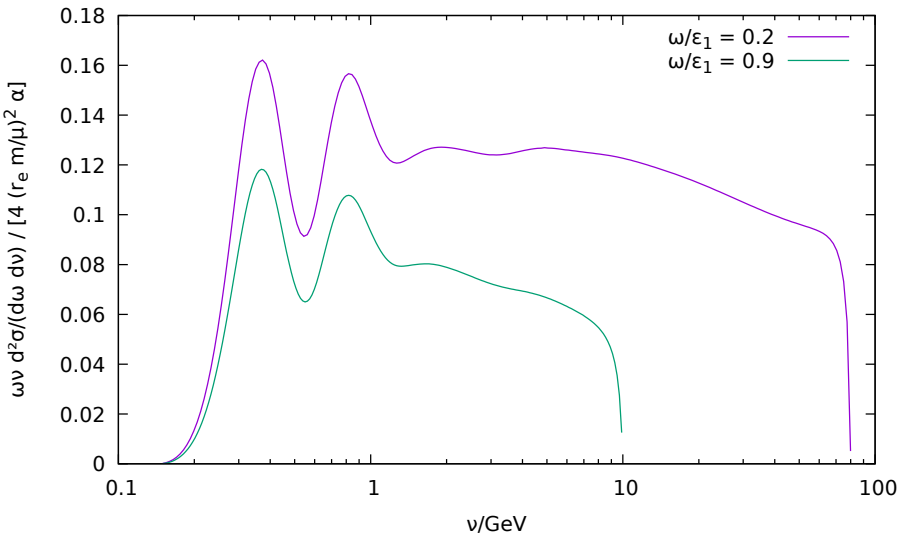

Figure 5.16: Differential cross section of bremsstrahlung with inelastic nuclear excitation for a muon of 100 GeV primary energy on a proton target without account of shadowing.

A numerical integration leads to the cross section shown in Fig. 5.16, 5.17 for selected values of ω and ε_1. The high peaks around 1 GeV correspond to resonances such as the Δ-resonance.

If we consider bremsstrahlung as radiative correction to the inelastic interaction cross section, we also have to take into account the virtual corrections due to a vertex correction. The tree-level cross section is given by[4]

$$\begin{aligned}
\frac{d\sigma}{d\nu} &= \frac{\alpha^2\pi}{2(\varepsilon_1^2-\mu^2)} \int\limits_{\mu^2\nu^2/\varepsilon_1\varepsilon_2}^{\infty} \frac{dq^2}{q^4}\left[L_{\mu\mu}W_1 - W_2 L_{44}\right], \\
L_{\mu\nu} &= \mathrm{Sp}\left\{\gamma_\mu(i\hat{p}_1-\mu)\gamma_\nu(i\hat{p}_2-\mu)\right\}, \\
L_{\mu\mu} &= \delta_{\mu\nu}L_{\mu\nu} = 8\mu^2 - 4q^2, \\
L_{44} &= \frac{P_\mu P_\nu}{M^2}L_{\mu\nu} = 2q^2 - 8\varepsilon_1\varepsilon_2.
\end{aligned} \tag{5.66}$$

which coincides within about 5% with the parametrization of [22] in (3.60). Using the renormalized expression for the vertex correction in the case of space-like

[4] In this section, for consistency with [10], the Euler metric is used.

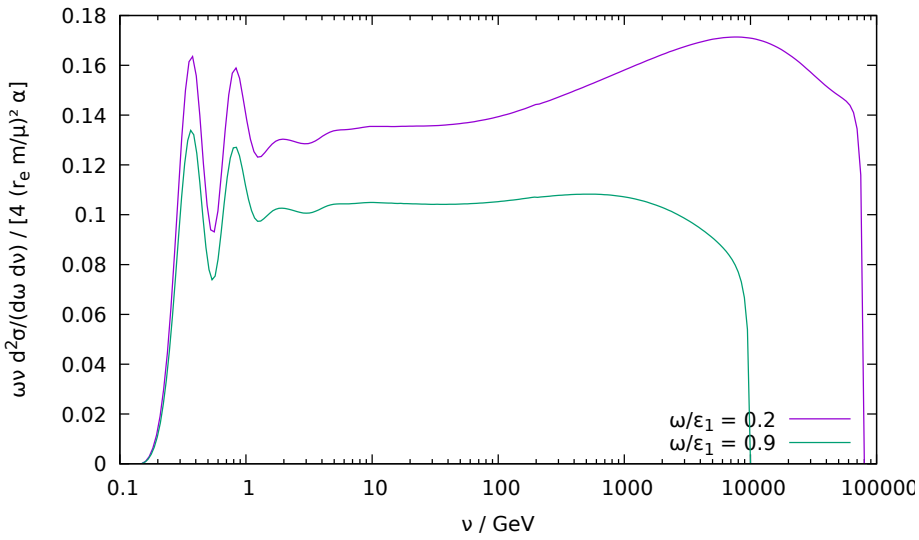

Figure 5.17: Differential cross section of bremsstrahlung with inelastic nuclear excitation for a muon of 100 TeV primary energy on a proton target without account of shadowing.

photon (see e. g. [9])

$$\begin{aligned}\mathcal{A}_\mu^{\mathrm{R}} &= \frac{\alpha}{\pi}\gamma_\mu\left\{\left(\ln\frac{\mu}{\lambda}-1\right)\left(\frac{1+a^2}{2a}\ln b+1\right)+\frac{1}{4a}\ln b\right.\\ &\quad\left.-\frac{1+a^2}{4a}\left[2\,\mathrm{Li}_2(1+b)+\ln b-\frac{\pi^2}{2}\right]\right\}\\ &\quad-\frac{i\alpha}{8\pi\mu}(\gamma_\mu\hat{q}-\hat{q}\gamma_\mu)\frac{a^2-1}{2a}\ln b,\\ &\equiv\frac{\alpha}{\pi}\left[\gamma_\mu\mathcal{A}_1+i\frac{\gamma_\mu\hat{q}-\hat{q}\gamma_\mu}{8\mu}\mathcal{A}_2\right],\end{aligned} \tag{5.67}$$

where $a=\sqrt{1+4\mu^2/q^2}$, $b=(a-1)/(a+1)$, $q^2>0$, the virtual photon correction is achieved by replacing $L_{\mu\mu}, L_{44}$ with

$$L_{44}^{\mathrm{virt}} = \frac{\alpha}{\pi}\left\{(2q^2-8\varepsilon_1\varepsilon_2)\mathcal{A}_1-8(\nu^2+q^2)\mathcal{A}_2\right\}, \tag{5.68}$$

$$L_{\mu\mu}^{\mathrm{virt}} = \frac{\alpha}{\pi}\left\{(8\mu^2-4q^2)\mathcal{A}_1+24q^2\mathcal{A}_2\right\}. \tag{5.69}$$

Vacuum polarization can be calculated analogous to the bremsstrahlung cross section. Because the minimum momentum transfer is comparable to or greater than the electron mass for $\nu/\varepsilon_1 \gtrsim m_e/\mu$, this contribution is much more important than for bremsstrahlung.

Taking all these corrections into account, we obtain the differential cross section shown in Fig. 5.18, 5.19. The average energy loss on hydrogen is shown in Fig. 5.20. The radiative corrections increase the average energy loss by about 3%.

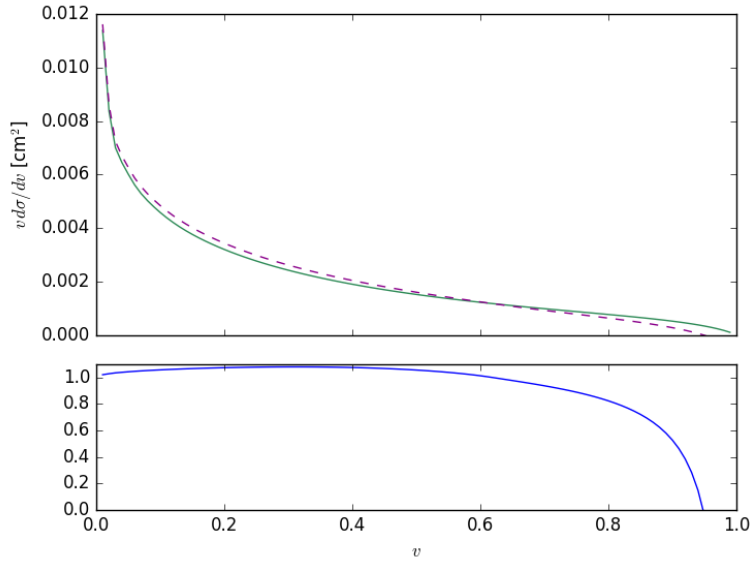

Figure 5.18: The differential cross section for inelastic nuclear interaction on tree level (solid line) and adding higher-order corrections (dashed line) for a muon energy of 100 GeV.

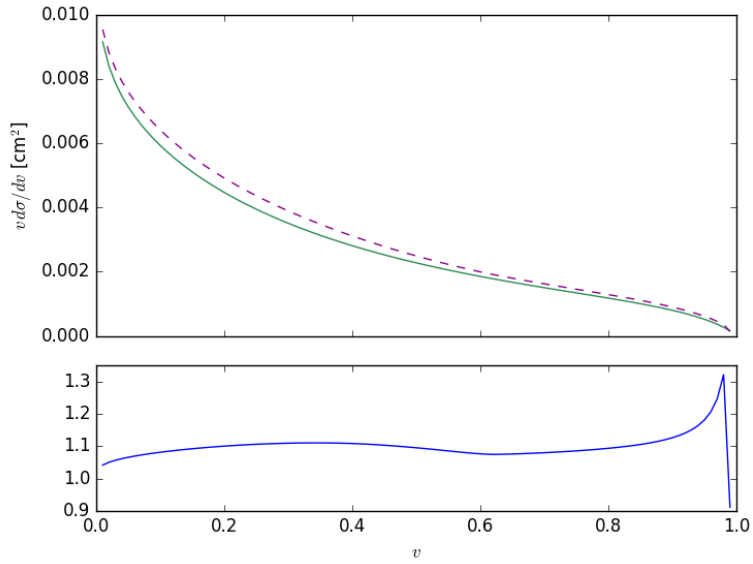

Figure 5.19: The differential cross section for inelastic nuclear interaction on tree level (solid line) and adding higher-order corrections (dashed line) for a muon energy of 100 TeV.

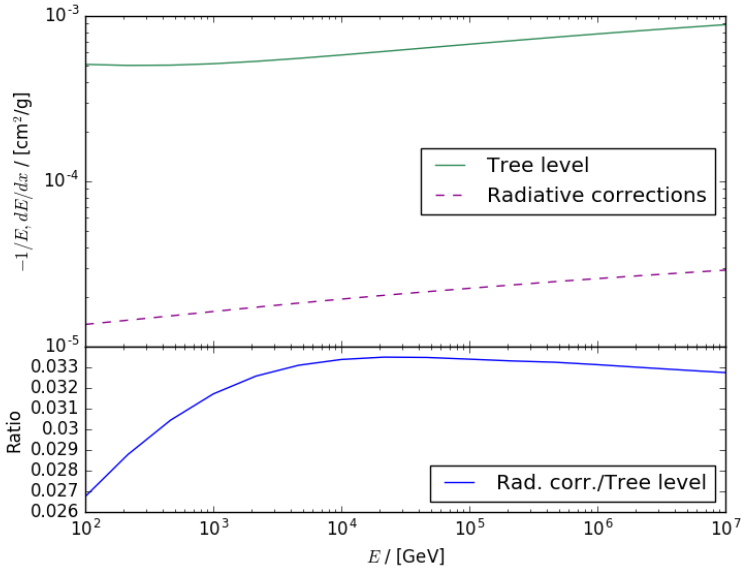

Figure 5.20: Average energy loss through inelastic nuclear interaction on hydrogen on tree level (solid line) and higher-order corrections (dashed line).

Chapter 6

Coulomb corrections

6.1 Introduction

The effect of higher-order corrections in the nuclear coupling constant $Z\alpha$, where Z is the nuclear charge and α the fine structure constant, so-called Coulomb corrections, has been considered for pair production in [53, 54] for a point-like nucleus. However, in [53], it was pointed out that the effect of a form factor can be sizeable. In this section, the corrections are calculated for a realistic nuclear charge distribution.[1] This process has been considered recently in [69] in the quasiclassical approximation, neglecting the nuclear form factor, but taking into account higher-order corrections to the interaction of the initial charged particle with the nucleus, which will be neglected in the following, because only muons are considered as initial charged particle, while in [69] emphasis was put also on ions as initial particles. Here, the correction to the spectrum of secondary particles and also the average energy loss of the muon is calculated.

The effect of Coulomb corrections on the bremsstrahlung cross section has been calculated in [20] for electrons and was shown to be large (from $\sim 1\%$ for medium nuclei such as iron to $\sim 10\%$ for heavy nuclei such as uranium). In [11] Coulomb corrections for muon bremsstrahlung on extended nuclei were calculated in the approximation of a homogeneously charged sphere for the nuclear charge density and were found to be small ($\lesssim 0.5\%$). This process was also considered more recently in [68], in whose approximation the correction for muons vanishes identically, independently of the form of the nuclear potential.

6.2 Higher order corrections in $Z\alpha$ for a point-like nucleus

The coupling to the field of the nucleus is governed by the coupling constant $\nu = Z\alpha$, which for high Z can achieve values which are not very small compared to 1, and therefore should be treated non-perturbatively. The first work on this subject was [20], where the corrections to the cross sections of bremsstrahlung and pair production by real photons were calculated using wave functions which

[1] The results of these calculations have been published in [96].

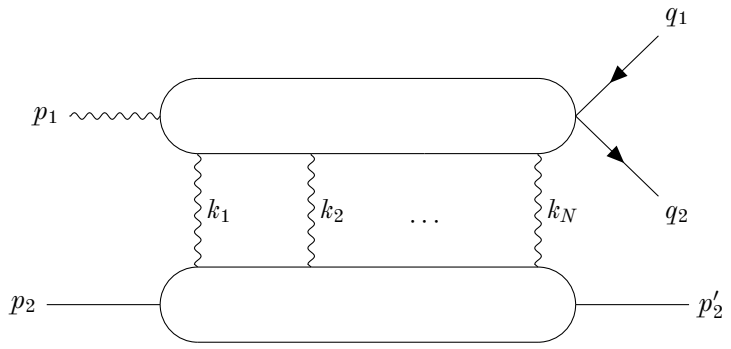

Figure 6.1: Diagram of the pair production process with N photons exchanged with the nucleus.

are approximate solutions of the Dirac equation for a Coulomb field. The final result is in the case of pair production by a real photon the expression

$$\begin{aligned} \frac{d\sigma}{dx} &= \frac{4}{3} Z^2 \alpha r_e^2 \{1 + 2[x^2 + (1-x)^2]\} \left(\ln \frac{2x(1-x)\omega}{m} - \frac{1}{2} - f(Z\alpha) \right), \\ f(\nu) &= \nu^2 \sum_{n=1}^{\infty} \frac{1}{n(n^2+\nu^2)}, \end{aligned} \tag{6.1}$$

where $x = \varepsilon_+/\omega$ is the ratio of the initial photon energy ω and the positron energy ε_+. It is very difficult to extend this treatment to a more realistic description of the nucleus as the wave functions would have to be determined for the given potential. The term $\ln[2x(1-x)\omega/m] - \frac{1}{2}$ arising from the leading order calculation is called the main logarithm in the following[2], the term $f(Z\alpha)$ arising from higher-order corrections in the coupling to the nuclear field is called Coulomb correction.

In [53], this result was obtained again in a much simpler way by resummation of the perturbation series. Moreover, the approach in [53] allows for the inclusion of realistic atomic and nuclear form factors. In [14] this approach was applied to the problem of electron-positron photoproduction in the field of a screened nucleus. In [54], the results of [53] were used to calculate the Coulomb correction to the pair production cross section by high-energy muons on a pointlike nucleus. First, the calculations of [53] are briefly reviewed and then this treatment is extended to calculate the corrections for a screened extended nucleus which allows also to determine the Coulomb correction to muon bremsstrahlung.

The main contribution to the cross section arises from small scattering angles, therefore the momenta (cf. Fig. 6.1) are expressed in Sudakov variables [102]

$$\begin{aligned} k_i &= \alpha_i \tilde{p}_1 + \beta_i \tilde{p}_2 + k_{i\perp}, \\ q_i &= x_i \tilde{p}_1 + y_i \tilde{p}_2 + q_{i\perp}, \end{aligned} \tag{6.2}$$

where $\tilde{p}_1 = p_1 + (Q^2/s)p_2$, $\tilde{p}_2 = p_2 - (m^2/s)p_1$ are almost light-like vectors, $Q^2 = -p_2^2$ is the virtuality of the photon and $s = 2p_1p_2 \gg Q^2, m^2$ is the center of momentum energy. As a simplification, the mass of the nucleus and of the produced lepton are set equal $p_2^2 = q_1^2 = q_2^2 = m^2$. The mass of the nucleus does

[2] For an atomic field different from the Coulomb case, the main logarithm changes also.

not enter the final result, where its mass is considered infinite. Denoting again by x the fraction of the energy of the initial photon ω which is transferred to the antilepton,

$$x_1 = x, \qquad x_2 = 1 - x,$$
$$y_1 = \frac{m^2 + \mathbf{q}_1^2}{xs}, \qquad y_2 = \frac{m^2 + \mathbf{q}_2^2}{(1-x)s}$$

with $\mathbf{q}_i^2 = -q_{i\perp}^2$. The amplitude for the diagram with N exchanged photons is given in the impact representation [75] by

$$\mathscr{M}_N = \frac{8\pi^2 s(-i)^{N-1}}{N!} \int \prod_{i=1}^{N} \left(\frac{d^2\mathbf{k}_i}{(2\pi)^2 \mathbf{k}_i^2} \right) \delta \left(\sum_{j=1}^{N} \mathbf{k}_j - \mathbf{q}_1 - \mathbf{q}_2 \right) J_{\gamma\to\ell\bar{\ell}}^N J_A^N. \quad (6.3)$$

The impact factors are given by

$$J_{\gamma\to\ell\bar{\ell}}^N = \int \prod_{i=1}^{N-1} \left(\frac{d(\beta_i s)}{2\pi i} \right) (iA)_{\mu_1\ldots\mu_N} \frac{\tilde{p}_2^{\mu_1} \cdots \tilde{p}_2^{\mu_N}}{s^N}, \quad (6.4)$$

$$J_A^N = \int \prod_{i=1}^{N-1} \left(\frac{d(\alpha_i s)}{2\pi i} \right) (iB)_{\mu_1\ldots\mu_N} \frac{\tilde{p}_1^{\mu_1} \cdots \tilde{p}_1^{\mu_N}}{s^N}. \quad (6.5)$$

where $(iA)_{\mu_1\ldots\mu_N}$ is the amplitude corresponding to the upper part of the diagram in Fig. 6.1 and $(iB)_{\mu_1\ldots\mu_N}$ to the lower part.

For an infinitely heavy point nucleus, the impact factor is given by

$$J_A^N = i(-1)^N (eZ)^N. \quad (6.6)$$

Accounting for an extended nucleus can be either carried out by modifying the impact factor or equivalently by modifying the Coulomb propagator $1/\mathbf{k}_i^2$ in (6.3).

The impact factors for the lepton part of the diagram can be determined by a recurrence relation. The impact factor for one exchanged photon is given by

$$J_{\gamma\to\ell\bar{\ell}}^1(\mathbf{q}_1, \mathbf{q}_2) = ie^2 \bar{u}_1 [m\hat{\mathbf{e}} S^1 - 2x(\mathbf{T}^1 \mathbf{e}) - \hat{\mathbf{T}}^1 \hat{\mathbf{e}}] \frac{\hat{\tilde{p}}_2}{s} u_2 \quad (6.7)$$

for a transversely polarized photon with polarization vector $\mathbf{e}$ and for a longitudinally polarized photon by

$$J_{\gamma\to\ell\bar{\ell}}^1(\mathbf{q}_1, \mathbf{q}_2) = -ie^2 \sqrt{Q^2} x(1-x) S^1(\mathbf{q}_1, \mathbf{q}_2) \bar{u}_1 \frac{\hat{\tilde{p}}_2}{s} u_2, \quad (6.8)$$

where

$$S^1 \equiv S^1(\mathbf{q}_1, \mathbf{q}_2) = \frac{1}{\mu^2 + \mathbf{q}_1^2} - \frac{1}{\mu^2 + \mathbf{q}_2^2}, \quad (6.9)$$

$$\mathbf{T}^1 \equiv \mathbf{T}^1(\mathbf{q}_1, \mathbf{q}_2) = \frac{\mathbf{q}_1}{\mu^2 + \mathbf{q}_1^2} + \frac{\mathbf{q}_2}{\mu^2 + \mathbf{q}_2^2}, \quad (6.10)$$

$$\mu^2 = m^2 + Q^2 x(1-x). \quad (6.11)$$

The scalar S^N and vector $\mathbf{T}^N$ structures are related by the recurrence relations

$$S^N(\mathbf{q}_1,\mathbf{q}_2,\mathbf{k}_N) = S^{N-1}(\mathbf{q}_1,\mathbf{q}_2-\mathbf{k}_N) - S^{N-1}(\mathbf{q}_1-\mathbf{k}_N,\mathbf{q}_2), \tag{6.12}$$

$$\mathbf{T}^N(\mathbf{q}_1,\mathbf{q}_2,\mathbf{k}_N) = \mathbf{T}^{N-1}(\mathbf{q}_1,\mathbf{q}_2-\mathbf{k}_N) - \mathbf{T}^{N-1}(\mathbf{q}_1-\mathbf{k}_N,\mathbf{q}_2), \tag{6.13}$$

because due to Bose symmetry the N-th t-channel photon can be considered as the last one attached to the lepton line, from which the relations follow immediately [52]. The dependence on the other t-channel photon momenta $\mathbf{k}_1,\dots\mathbf{k}_{N-1}$ is omitted for clarity. The integral over the t-channel momenta

$$J_e^N(\mathbf{q}_1,\mathbf{q}_2) = \int \prod_{i=1}^{N} \frac{d^2\mathbf{k}_i}{\mathbf{k}_i^2} F(\mathbf{k}_i)\delta\left(\sum_{j=1}^{N}\mathbf{k}_j - \mathbf{q}\right) S^N \tag{6.14}$$

with the formfactor $F(\mathbf{k})$ can be recast using the recurrence relations as

$$J_S^N(\mathbf{q}_1,\mathbf{q}_2) = \int \frac{d^2\mathbf{k}}{\mathbf{k}^2} F(\mathbf{k})[J_S^{N-1}(\mathbf{q}_1,\mathbf{q}_2-\mathbf{k}) - J_S^{N-1}(\mathbf{q}_1-\mathbf{k},\mathbf{q}_2)] \tag{6.15}$$

such that for the Fourier transform of $J_S^N(\mathbf{q}_1,\mathbf{q}_2)$

$$j_S^N(\mathbf{r}_1,\mathbf{r}_2) = \frac{1}{(2\pi)^2}\int e^{i\mathbf{q}_1\mathbf{r}_1+\mathbf{q}_2\mathbf{r}_2} J_S^N(\mathbf{q}_1,\mathbf{q}_2)\, d^2\mathbf{q}_1\ d^2\mathbf{q}_2 \tag{6.16}$$

the recurrence relation assumes the form

$$\begin{aligned} j_S^N(\mathbf{r}_1,\mathbf{r}_2) &= j_S^{N-1}(\mathbf{r}_1,\mathbf{r}_2)\pi\varphi(\mathbf{r}_1,\mathbf{r}_2) \\ \varphi(\mathbf{r}_1,\mathbf{r}_2) &= \frac{1}{\pi}\int \frac{d^2\mathbf{k}}{\mathbf{k}^2}(e^{i\mathbf{k}\mathbf{r}_2} - e^{i\mathbf{k}\mathbf{r}_1}). \end{aligned} \tag{6.17}$$

Using the Fourier transform of J_S^1

$$j_S^1(\mathbf{r}_1,\mathbf{r}_2) = \frac{1}{2}K_0(\mu|\mathbf{r}_1-\mathbf{r}_2|)\varphi(\mathbf{r}_1,\mathbf{r}_2), \tag{6.18}$$

the total impact factor to all orders, inverting the Fourier transform, is given by

$$\begin{aligned} J_S(\mathbf{q}_1,\mathbf{q}_2) = \frac{i}{(2\pi)^2 2\nu}\int d^2\mathbf{r}_1\ d^2\mathbf{r}_2\ e^{-i\mathbf{q}_1\mathbf{r}_1 - i\mathbf{q}_2\mathbf{r}_2} \\ \times K_0(\mu|\mathbf{r}_1-\mathbf{r}_2|)[e^{-i\nu\varphi(\mathbf{r}_1,\mathbf{r}_2)}-1], \end{aligned} \tag{6.19}$$

and analogously for the vector structure by

$$\begin{aligned} \mathbf{J}_T(\mathbf{q}_1,\mathbf{q}_2) = \frac{-1}{(2\pi)^2 2\nu}\int d^2\mathbf{r}_1\ d^2\mathbf{r}_2\ e^{-i\mathbf{q}_1\mathbf{r}_1 - i\mathbf{q}_2\mathbf{r}_2} \\ \times \frac{\mu(\mathbf{r}_1-\mathbf{r}_2)}{|\mathbf{r}_1-\mathbf{r}_2|}K_1(\mu|\mathbf{r}_1-\mathbf{r}_2|)[e^{-i\nu\varphi(\mathbf{r}_1,\mathbf{r}_2)}-1]. \end{aligned} \tag{6.20}$$

Here $K_\nu(z)$ is the modified Bessel function. To obtain the amplitude out of the impact factor, according to [108] the impact factor is multiplied by a universal phase factor and the amplitude is given by

$$\begin{aligned} \mathscr{M} = 8\pi e\nu s\left(\frac{x}{1-x}\right)^{-i\nu}\bar{u}_1\{m\hat{\mathbf{e}}J_S(\mathbf{q}_1,\mathbf{q}_2) \\ - 2x[\mathbf{J}_T(\mathbf{q}_1,\mathbf{q}_2)\mathbf{e}] - \hat{\mathbf{J}}_T(\mathbf{q}_1,\mathbf{q}_2)\hat{\mathbf{e}}\}\frac{\hat{\bar{p}}_2}{s}u_2 \end{aligned} \tag{6.21}$$

for a transversely polarized incident photon and by

$$\mathscr{M} = -16\pi e\nu s \left(\frac{x}{1-x}\right)^{-i\nu} \sqrt{Q^2} x(1-x)\bar{u}_1 J_S(\mathbf{q}_1, \mathbf{q}_2)\frac{\hat{\bar{p}}_2}{s}u_2 \tag{6.22}$$

for a longitudinally polarized incident photon.

The total cross section is obtained by integration over the transversal momenta $\mathbf{q}_1, \mathbf{q}_2$ and the energy fraction x as

$$d\sigma = \frac{2\nu^2\alpha}{\pi^2}\{m^2|J_S|^2 + |\mathbf{J}_T|^2[x^2 + (1-x)^2]\}\, dx\ d^2\mathbf{q}_1\ d^2\mathbf{q}_2 \tag{6.23}$$

for the transversely polarized photon, summed over all polarization states. To obtain the Coulomb correction to the Born cross section, the Born approximation cross section has to be subtracted. Therefore the correction $d\sigma_2$, for $d\sigma = d\sigma_1 + d\sigma_2$ with $d\sigma_1$ the Born approximation cross section, is given for the transversely and longitudinally polarized photon by

$$\frac{d\sigma_2^T}{dx} = \frac{2\alpha\nu^2}{\pi^2}\{m^2 A_1 + [x^2 + (1-x)^2]A_2\}, \tag{6.24}$$

$$\frac{d\sigma_2^S}{dx} = \frac{2\alpha\nu^2}{\pi^2} 4Q^2x^2(1-x)^2 A_1, \tag{6.25}$$

respectively, where

$$A_1 = \int d^2\mathbf{q}_1\ d^2\mathbf{q}_2\ (|J_S|^2 - |J_S^1|^2), \tag{6.26}$$

$$A_2 = \int d^2\mathbf{q}_1\ d^2\mathbf{q}_2\ (|\mathbf{J}_T|^2 - |\mathbf{J}_T^1|^2). \tag{6.27}$$

6.3 Higher-order corrections for an extended screened nucleus

In the calculation of corrections in a Coulomb field, the expressions for A_1, A_2 contain terms which diverge and have to be regularized, which leads to not well-defined expressions when attempting a numerical integration. As pointed out by [14], the divergences are removed when screening is taken into account.

Using the form factor [105]

$$\begin{aligned} F(k) &= F_n(k) - F_e(k), \\ F_n(k) &= \left(1 + \frac{a^2k^2}{12}\right)^{-2}, \qquad a = (0.58 + 0.82A^{1/3})5.07\ \mathrm{GeV}^{-1} \\ F_e(k) &= \frac{1}{1+b^2k^2}, \qquad b = \frac{184.15Z^{-1/3}}{m_e\sqrt{e}}, \end{aligned}$$

φ is given by

$$\begin{aligned} \varphi(\mathbf{r}_1, \mathbf{r}_2) &= \frac{1}{\pi}\int \frac{d^2\mathbf{k}}{\mathbf{k}^2} F(|\mathbf{k}|)(e^{i\mathbf{k}\mathbf{r}_2} - e^{i\mathbf{k}\mathbf{r}_1}) \\ &= 2[K_0(\mathcal{A}_e r_2) - K_0(\mathcal{A}_e r_1)] + 2[K_0(\mathcal{A}_n r_1) - K_0(\mathcal{A}_n r_2)] \\ &\quad + \mathcal{A}_n r_1 K_1(\mathcal{A}_n r_1) - \mathcal{A}_n r_2 K_1(\mathcal{A}_n r_2), \\ \mathcal{A}_e &= \frac{1}{b}, \quad \mathcal{A}_n = \frac{\sqrt{12}}{a}. \end{aligned} \tag{6.28}$$

The quantities A_1, A_2 are given by the expressions

$$A_1 = \frac{\pi}{2\nu^2\mu^4}\int_0^\infty dx \int_0^\infty dR \int_0^{2\pi} d\theta\, x^3 {K_0}^2(x)\{2 - 2\cos(\nu\varphi_{12}) - \nu^2\varphi_{12}^2\}, \quad (6.29)$$

$$A_2 = \frac{\pi}{2\nu^2\mu^2}\int_0^\infty dx \int_0^\infty dR \int_0^{2\pi} d\theta\, x^3 {K_1}^2(x)\{2 - 2\cos(\nu\varphi_{12}) - \nu^2\varphi_{12}^2\}, \quad (6.30)$$

$$\varphi_{12} = \varphi\left(\frac{xR}{\mu}, \frac{x\sqrt{R^2+1-2R\cos\theta}}{\mu}\right). \quad (6.31)$$

In the case of a Coulomb field, $\varphi = \ln(\mathbf{r}_1^2/\mathbf{r}_2^2)$ and A_1, A_2 assume the values

$$\begin{aligned} A_1^{\mathrm{C}} &= -\frac{2\pi^2}{3\mu^4} f(\nu), \\ A_2^{\mathrm{C}} &= -\frac{4\pi^2}{3\mu^2} f(\nu), \\ f(\nu) &= \frac{1}{2}\{\Psi(1-i\nu) + \Psi(1+i\nu) - 2\Psi(1)\} \\ &= \nu^2 \sum_{n=1}^{\infty} \frac{1}{n(n^2+\nu^2)}. \end{aligned}$$

When realistic form factors are employed, it is no longer possible to evaluate the Coulomb corrections in closed form. The numerical results can be approximated by

$$A_1 = A_1^{\mathrm{C}} g_1(\mu/\mathrm{MeV}, \nu), \quad A_2 = A_2^{\mathrm{C}} g_2(\mu/\mathrm{MeV}, \nu), \quad (6.32)$$

$$g_i(x,\nu) = \frac{a_i(\nu) + b_i(\nu)x}{1 + c_i(\nu)x + d_i(\nu)x^2}, \quad (6.33)$$

where a_i, b_i, c_i, d_i are approximately cubic polynomials for $Z > 5$

$$\begin{aligned} a_1(\nu) &= 1.0026 - 2.2789\times10^{-2}\nu + 2.9437\times10^{-2}\nu^2 - 4.1536\times10^{-2}\nu^3, \\ b_1(\nu) &= 1.9465\times10^{-2} - 7.7063\times10^{-2}\nu + 1.9979\times10^{-1}\nu^2 - 1.4107\times10^{-1}\nu^3, \\ c_1(\nu) &= 3.6785\times10^{-2} + 5.4466\times10^{-2}\nu - 9.2971\times10^{-2}\nu^2 + 2.7357\times10^{-2}\nu^3, \\ d_1(\nu) &= 9.9382\times10^{-4} + 2.4601\times10^{-3}\nu + 2.6733\times10^{-3}\nu^2 - 2.8198\times10^{-3}\nu^3; \\ a_2(\nu) &= 1.0046 - 1.9267\times10^{-2}\nu + 4.5255\times10^{-2}\nu^2 - 5.1603\times10^{-2}\nu^3, \\ b_2(\nu) &= 8.8223\times10^{-3} - 5.2931\times10^{-2}\nu + 1.4854\times10^{-1}\nu^2 - 1.0764\times10^{-1}\nu^3, \\ c_2(\nu) &= 3.7141\times10^{-2} + 1.2897\times10^{-1}\nu - 2.2677\times10^{-1}\nu^2 + 1.0776\times10^{-1}\nu^3, \\ d_2(\nu) &= 7.1144\times10^{-4} + 1.7710\times10^{-3}\nu + 5.0240\times10^{-3}\nu^2 - 4.5527\times10^{-3}\nu^3. \end{aligned}$$

Since the correction is small for low Z, it is possible to use this parametrization for all Z.

This Coulomb correction for the virtual photon pair production can be used to calculate several cross sections. Setting $Q^2 = 0, \mu^2 = m^2$, one obtains the

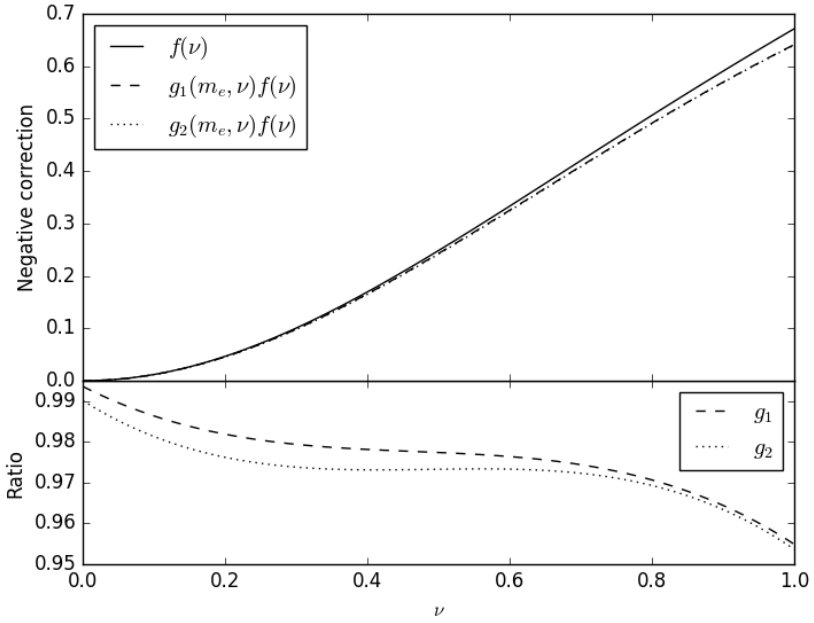

Figure 6.2: Correction to the main logarithm of bremsstrahlung and photoproduction for electrons due to Coulomb corrections for a Coulomb field and a screened nucleus. Shown are the correction $f(\nu)$ for a Coulomb field (solid line) and the corrections which account for the screened nucleus $g_1(m_e,\nu)f(\nu)$ (dashed line), $g_2(m_e,\nu)f(\nu)$ (dotted line).

corrections for real photoproduction of particles with mass m on a screened extended nucleus. The numerical examples show that for electrons, the result of [20] is reproduced with a small correction for heavy nuclei (see Fig. 6.2), while for muons the correction due to multiphoton exchange is very small (see Fig. 6.3). Since the main logarithm assumes the value $\ln[BZ^{-1/3}(m_\mu/m_e)] - \ln(1.54A^{0.27})$ with $B \simeq 183$ [58] in the full-screening limit, the correction to the energy loss spectrum due to Coulomb corrections is negligible with very high accuracy

$$\max_Z \frac{f(\nu)g_{1,2}(m_\mu,\nu)}{\ln\left(B\frac{m_\mu}{m_e}Z^{-1/3}\right) - \ln(1.54A^{0.27})} < 0.004.$$

The small influence of the nuclear form factor on electrons and the smallness of the corrections for heavy particles was already observed by [53] in the limiting cases $\Lambda \gg m$ for electrons and $\Lambda \ll m$ for muons, using a nuclear form factor

$$F(k) = \frac{\Lambda^2}{\Lambda^2 + k^2}. \tag{6.34}$$

From the corrections to the real photoproduction cross section, the corrections to the bremsstrahlung cross section are obtained via the substitution rules $\varepsilon_+ \to -\varepsilon_1, \varepsilon_- \to \varepsilon_2, \omega \to -\omega$, $d\sigma \to (\omega^2\, d\omega\, /\varepsilon_+^2\, d\varepsilon_+\,)\, d\sigma$, where $x = \varepsilon_+/\omega$ (e. g.,

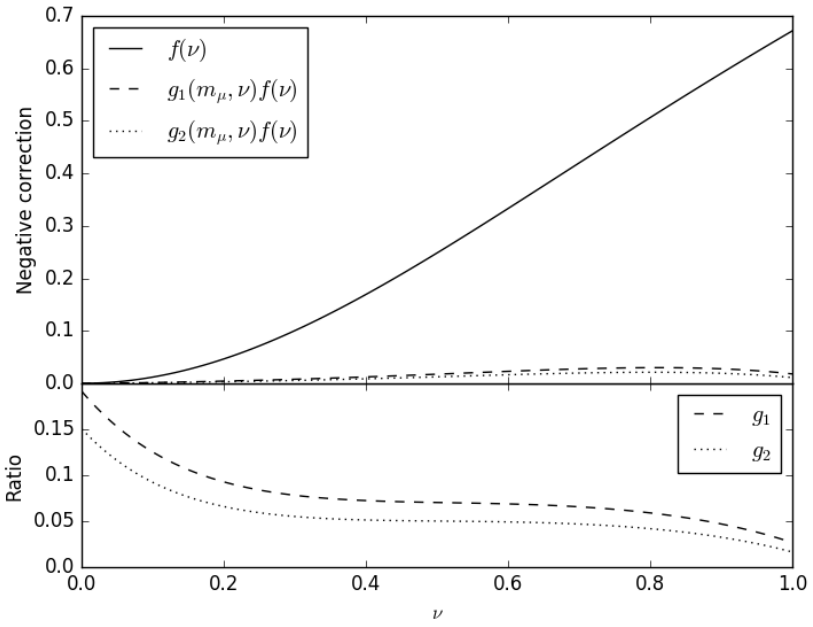

Figure 6.3: Correction to the main logarithm of bremsstrahlung and photoproduction for muons due to Coulomb corrections for a Coulomb field and a screened nucleus. Shown are the correction $f(\nu)$ for a Coulomb field (solid line) and the corrections which account for the screened nucleus $g_1(m_\mu, \nu)f(\nu)$ (dashed line), $g_2(m_\mu, \nu)f(\nu)$ (dotted line).

[84]). Again, the classical result for electrons is obtained, that the function $f(\nu)$ is subtracted from the main logarithm, and it is observed that the correction for muon bremsstrahlung is small, as was found in [11] for a simplified nuclear form factor.

Using the result for the process of pair production by a virtual photon, one can calculate the Coulomb corrections to the cross section of pair production by a charged particle, thus generalizing the corrections calculated by [54] for pair production in a Coulomb field. The correction to the cross section for pair production by a muon is given by

$$d\sigma_2 \;=\; dn_T\,(\omega, Q^2)\sigma_2^T(\omega, Q^2) + \; dn_S\,(\omega, Q^2)\sigma_2^S(\omega, Q^2), \tag{6.35}$$

where the virtual photon fluxes are given by [29]

$$dn_T\,(\omega, Q^2) = \frac{\alpha}{\pi}(1-v)\left(1 - \frac{Q^2_{\min}}{Q^2} + \frac{v^2}{2(1-v)}\right)\frac{d\omega}{\omega}\,\frac{dQ^2}{Q^2}, \tag{6.36}$$

$$dn_S\,(\omega, Q^2) = \frac{\alpha}{\pi}(1-v)\frac{d\omega}{\omega}\,\frac{dQ^2}{Q^2}, \tag{6.37}$$

$$Q^2_{\min} = \frac{m_\mu^2 v^2}{1-v} \leq Q^2 < \infty. \tag{6.38}$$

where $v = \omega/E_\mu$ is the fractional energy loss of the muon. Since σ_2^T, σ_2^S are independent of ω and $dn_T,\ dn_S,\ Q^2_{\min}$ only depend on the fractional energy loss, the correction itself is independent of the incident muon energy, because the singularity for $x \to 0, x \to 1$ is only logarithmic and therefore integrable. Since the contribution in Born approximation is dependent on energy, however, the relative importance of the correction is a function of the energy. Also, the integration over x should only be carried out in the range where the Born contribution is non-negative. The influence of Coulomb corrections on the differential cross section $d\sigma/dv$ for a muon of 100 TeV primary energy in standard rock and lead is shown in Fig. 6.4, 6.5 in comparison to the Born contribution of [67].

The influence of Coulomb corrections on the average energy loss

$$-\frac{dE}{dX} = \frac{N_A}{A}\int \omega \frac{d\sigma}{d\omega}\, d\omega\ , \tag{6.39}$$

where N_A is Avogadro's constant, A is the mass number of the material, and $X = x/\varrho$ is the depth, is shown in Fig. 6.6 for standard rock[3] and in Fig. 6.7 for lead, integrated in the appropriate energy-dependent limits of the Born approximation cross section of [67].

6.4 Discussion

We have calculated Coulomb corrections to the cross sections of pair production and bremsstrahlung on extended screened nuclei. These calculations generalize the work of [14, 53, 54] with regard to pair production and the work of [11] with regard to muon bremsstrahlung.

[3] Standard rock is assumed as a mixture of $MgCO_3$ and $CaCO_3$ consisting of 52% oxygen, 27% calcium and 9% magnesium.

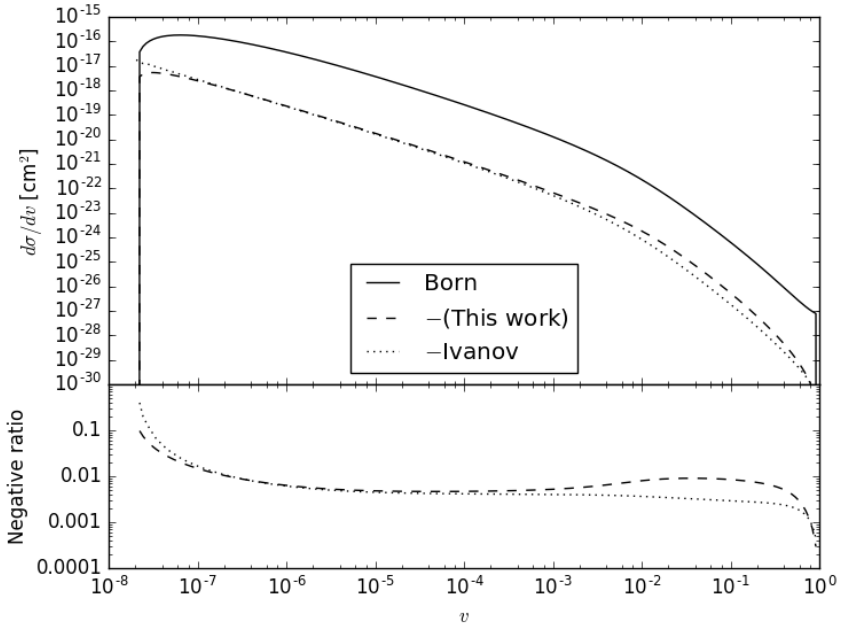

Figure 6.4: Differential cross section $d\sigma/dv$ for a muon of 100 TeV primary energy in standard rock. Shown are the cross section in Born approximation [67] (solid line), our Coulomb corrections (dashed line), and the corrections of [54] (dotted line).

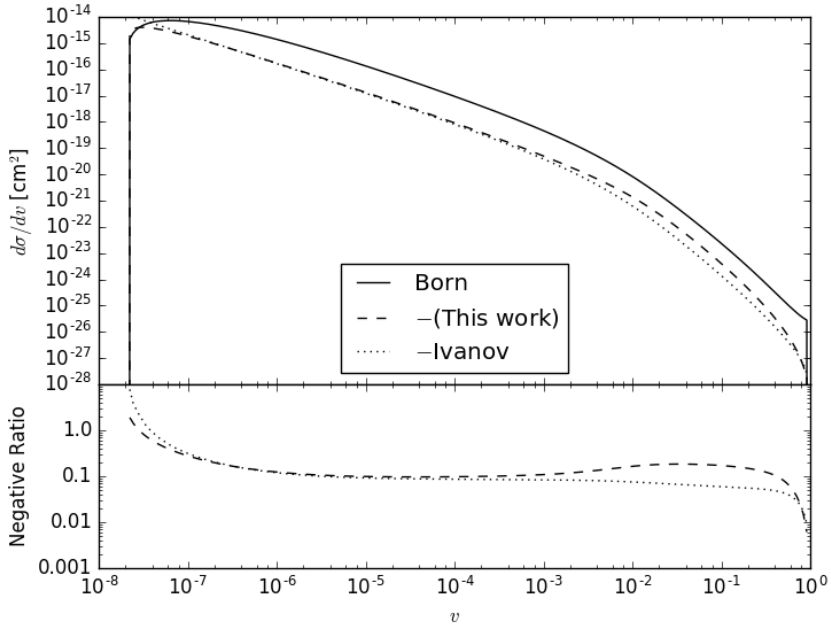

Figure 6.5: Differential cross section $d\sigma/dv$ for a muon of 100 TeV primary energy in lead. Shown are the cross section in Born approximation [67] (solid line), our Coulomb corrections (dashed line), and the corrections of [54] (dotted line).

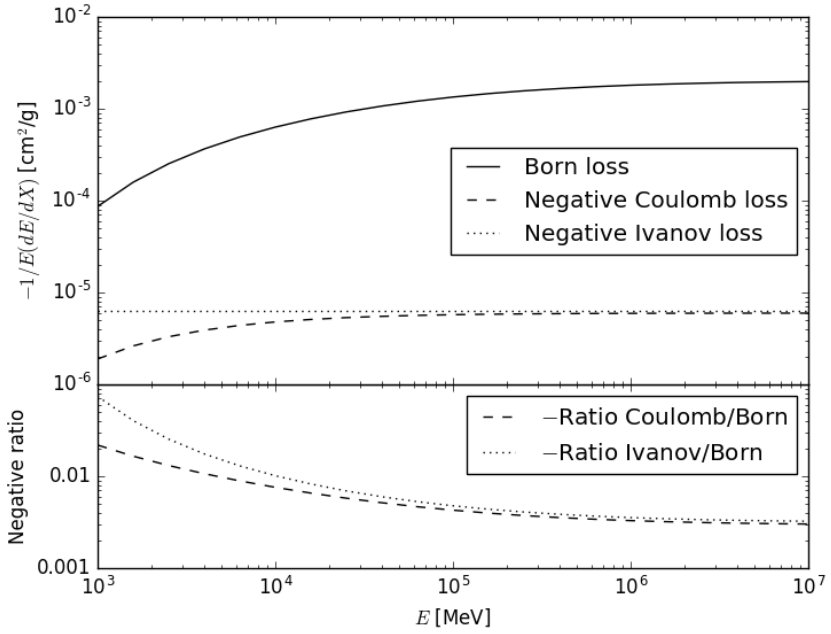

Figure 6.6: Average energy loss through pair production in standard rock, calculated using the Born cross section of [67] (solid line) and the negative Coulomb corrections calculated in this work (dashed line) and in [54] (dotted line).

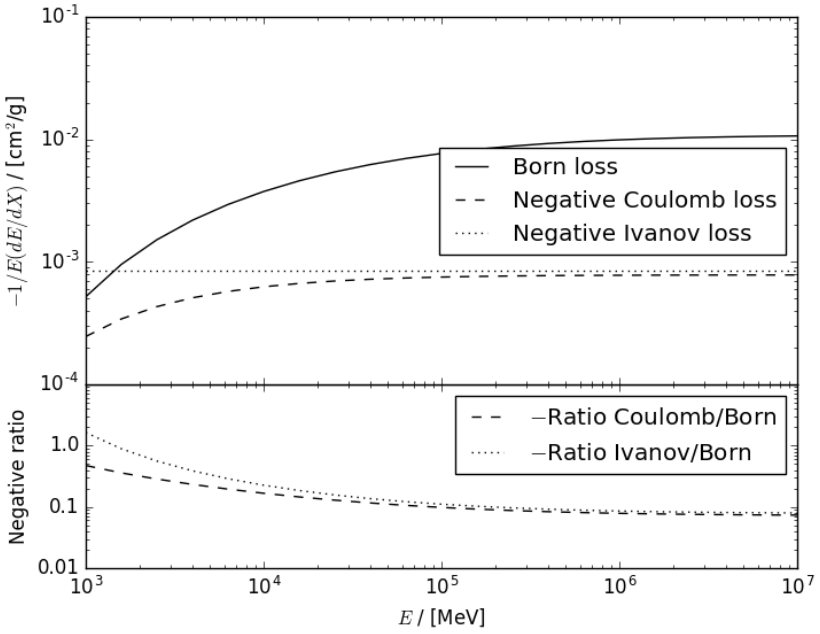

Figure 6.7: Average energy loss through pair production in lead, calculated using the Born cross section of [67] (solid line) and the negative Coulomb corrections calculated in this work (dashed line) and in [54] (dotted line).

Our results confirm that the Coulomb corrections to the muon bremsstrahlung cross section are negligible with very high accuracy. This coincides qualitatively with the results of [11], who applied a very simple model for the charge distribution of the nucleus and used a different method based on wave functions. However, here a more realistic charge distribution was used; therefore a direct comparison of the numerical results is difficult. In contrast to the results of [68], the corrections do not vanish identically in our calculation.

Our results on electron pair production by high-energy muons confirm the importance of Coulomb corrections established by [54] for this process in precise calculations of muon transport. Our calculations differ in two aspects from [54]:

- the correction in the cross section is integrated only over values of x, v, for which the Born cross section is positive;
- the atomic and nuclear form factor is taken into account.

The effect of the first aspect decreases with energy; however, as shown in Fig. 6.4, the effect of correct limits is still noticeable at a muon energy of 100 TeV in standard rock. The second point leads to an additional decrease of the Coulomb correction which does not decrease with energy. As shown in Fig. 6.7, for lead the correction to the energy loss is smaller by more than 10%, amounting to about a percent of the Born loss. For the differential cross section, the effect is even greater, as shown in Fig. 6.5.

Chapter 7

Discussion and outlook

In this thesis corrections to the energy loss cross sections of high-energy muons have been calculated. Muons loose energy by ionization, pair production, bremsstrahlung and inelastic nuclear interaction. Ionization dominates the energy loss at low energies, while the other processes dominate at higher energies. Over a large part of the energy range investigated by very large volume neutrino telescopes such as IceCube, pair production and bremsstrahlung dominate the energy loss, with inelastic nuclear interaction being a subdominant process.

The leading-order cross sections of bremsstrahlung and pair production have been determined more accurately by dropping the approximation that the two screening functions are equal. For bremsstrahlung, the effect on high-energy muons is negligible compared to the parametrization of [58]; for pair production, in addition to this, the analytical approximation by [66] to the non-logarithmic terms of the cross section has been replaced by the exact expression calculated in [55], and the nuclear formfactor corrections calculated in [67] have been replaced by later more exact calculations of [58]. Together these improvements lead to changes of a several percent to the simply differential cross section $d\sigma/dv$.

For bremsstrahlung, the next-to-leading-order (NLO) corrections have been calculated for the average energy loss and the differential cross section. The average energy loss is increased by about 2% in the high-energy limit due to these corrections. The relative effect on the differential cross section $d\sigma/dv$ is independent of the energy of the muon in the approximation used in this work; the NLO corrections increase the cross section most pronounced for the emission of photons with $v \sim 0.1$, i. e. large energy losses.

For the inelastic nuclear interaction, NLO corrections have also been calculated. The correction to the cross section is also most pronounced for large v; the average energy loss is increased by 2–3%. The uncertainties on the cross section of this process are however, much larger than in the case of pair production and bremsstrahlung, therefore these corrections are less important.

For bremsstrahlung and pair production, Coulomb corrections, i. e. corrections to all orders in the coupling $Z\alpha$ to the electric field of the nucleus have been calculated and parametrized, taking into account the nuclear formfactor. For muon bremsstrahlung, the result of previous approximate calculations [11] are confirmed that Coulomb corrections are negligible. For pair production, the result show that the calculations of [53, 54] are valid for light nuclei and describe accurately the cross section and energy loss, if the limits of integration are cho-

sen appropriately. For heavy nuclei such as lead, however, the nuclear formfactor cannot be neglected and the Coulomb corrections to the cross section decrease. Although the qualitative behavior has been predicted earlier using simplified models for the nuclear charge distribution, this is the first quantitative calculation of Coulomb corrections for realistic extended nuclei.

The theoretical uncertainties on the energy loss cross sections influence the experimental results as systematic uncertainties. These corrections are important for the energy reconstruction of high-energy muons which are observed in particle and astroparticle detectors.

Further work in this direction should include the calculation of radiative corrections to the pair production cross section. The method of equivalent photons applied here to the bremsstrahlung cross section is not applicable to this problem [29]. Therefore this problem is much more complex to solve due to the large number of particles in the final state and the corresponding large number of degrees of freedom.

Appendix A

Analytical cross section for main contribution of pair production

A.1 Cross section differential in q^2, k^2

The contribution of the e-diagrams to the pair production is given by

$$\begin{aligned}\frac{d^2\sigma}{d\omega\ d\varepsilon_1} = \frac{Z^2\alpha^4 m^4}{32\pi^2 k^* p_3^2}\int\frac{dk^2\ dq^2\ d\nu}{k^4 q^4}\{&W_1 L_1 \mathscr{M}_1{}^{\mu\mu}_{\alpha\alpha} + W_2 L_2 \mathscr{M}_1{}^{44}_{44} \\ &- W_1 L_2 \mathscr{M}_1{}^{\mu\mu}_{44} - W_2 L_1 \mathscr{M}_1{}^{44}_{\alpha\alpha}\}\end{aligned} \tag{A.1}$$

where in the case of a screened heavy nucleus [31]

$$W_1 = 0, \quad W_2 = -[F_n(q^2) - F_a(q^2)]^2\delta(\nu), \tag{A.2}$$

$$L_1 = -4\left\{\frac{k^2}{2} - \mu^2 - \frac{k^2}{k^{*2}}\left(-\varepsilon_3\varepsilon_4 + \frac{k^2}{4}\right)\right\}, \tag{A.3}$$

$$L_2 = -4\left\{\frac{k^2}{2} - \mu^2 - 3\frac{k^2}{k^{*2}}\left(-\varepsilon_3\varepsilon_4 + \frac{k^2}{4}\right)\right\}, \tag{A.4}$$

$$-\frac{1}{8}\mathscr{M}_1{}^{44}_{44} = \frac{8\pi}{m^6\omega\Gamma}\varepsilon_1^2\varepsilon_2^2\left(1 - \frac{1}{y} - \frac{\delta^2\Gamma}{m^2}\ln y - \ln x\right), \tag{A.5}$$

$$\begin{aligned}-\frac{1}{8}\mathscr{M}_1{}^{44}_{\alpha\alpha} = &\frac{4\pi}{m^4\omega\Gamma}\varepsilon_1\varepsilon_2\left(2 - \frac{k^2}{m^2}\right)\left(1 - \frac{1}{y} - \frac{\delta^2\Gamma}{m^2}\ln y - \ln x\right) \\ &+ \pi(\varepsilon_1^2 + \varepsilon_2^2)\left\{\frac{J_3'}{2\varepsilon_1^2\varepsilon_2^2} + \frac{2q^2}{\pi m^4}J_2 + \frac{4\delta\nu}{m^6\omega}\ln y\right\}.\end{aligned} \tag{A.6}$$

with

$$\begin{aligned}J_3' &= -\frac{\omega\Gamma}{m^2}\left[\sqrt{y^2 - 8\xi y + 16\xi(1+\xi)y^2} - 1 - 4\xi\right] \\ &= -\frac{\omega\Gamma}{m^2}(y-1) + \mathscr{O}(\xi),\end{aligned}$$

$$
\begin{aligned}
J_2 &= \frac{\pi}{m^2\omega\Gamma}\ln x,\\
\ln x &= \frac{1}{4\sqrt{\xi(1+\xi)}}\\
&\quad\times\ln\frac{1+4\xi+4\sqrt{\xi(1+\xi)}-\sqrt{\xi/(1+\xi)}}{\sqrt{1-8\xi/y+16\xi(1+\xi)/y^2}+4\sqrt{\xi(1+\xi)}/y-\sqrt{\xi/(1+\xi)}},\\
\delta &= \frac{m^2\omega}{2\varepsilon_1\varepsilon_2},\quad \Gamma = 1+\frac{k^2\varepsilon_1\varepsilon_2}{m^2\omega^2},\quad y=\frac{1}{\delta\Gamma}(\sqrt{q^2+\nu^2}+\nu),\quad \xi=\frac{q^2}{4m^2\Gamma}\\
k^* &= \sqrt{k^2+\omega^2}.
\end{aligned}
$$

The integration region is given by the relations

$$
\begin{aligned}
(\delta\Gamma)^2 - 2\nu\delta\Gamma < q^2 < \infty,\\
\frac{\mu^2\omega^2}{\varepsilon_3\varepsilon_4} < k^2 < 4\varepsilon_3\varepsilon_4.
\end{aligned}
$$

$\ln x$ can be expanded in two overlapping regions

$$
\ln x \approx 1-\frac{1}{y}-\frac{2}{3}\xi\left(1+\frac{3}{y^2}-\frac{4}{y^3}\right), \qquad \xi \ll 1, \tag{A.7}
$$

$$
\ln x \approx \frac{1}{\sqrt{\xi(1+\xi)}}\ln(\sqrt{1+\xi}+\sqrt{\xi}), \qquad y \gg 1. \tag{A.8}
$$

Since the mass of electrons is much lighter than the inverse radius of nuclei, it is reasonable to set $F_n = 1$. The form factor (Tsai 74)

$$
F_a(q^2) = \frac{1}{1+b^2q^2} \tag{A.9}
$$

leads to the correct behavior in the limiting cases of complete screening and absence of screening.

A.2 No Screening

As a first step, the cross section is calculated for the case of on unscreened point nucleus, such that

$$
W_2 = -\delta(\nu). \tag{A.10}
$$

We start with the evaluation of $\mathscr{M}_{144}^{44}$, since the terms also occur in $\mathscr{M}_{1\alpha\alpha}^{44}$.

We split the integration over q^2 at an auxiliary momentum q_0 subject to the conditions $q_0 \gg \delta\Gamma, q_0^2 \ll 4m^2\Gamma$. We obtain

$$
\begin{aligned}
&\int_{(\delta\Gamma)^2}^{\infty}\left(1-\frac{1}{y}-\frac{\delta^2\Gamma}{m^2}\ln y-\ln x\right)\frac{dq^2}{q^4}\\
&=\left(\int_{(\delta\Gamma)^2}^{q_0^2}+\int_{q_0^2}^{\infty}\right)\left(1-\frac{1}{y}-\frac{\delta^2\Gamma}{m^2}\ln y-\ln x\right)\frac{dq^2}{q^4}
\end{aligned}
$$

$$\approx 2\int_{\delta\Gamma}^{q_0}\left[\frac{2}{3}\xi\left(1+\frac{3}{y^2}-\frac{4}{y^3}\right)-\frac{\delta^2\Gamma}{m^2}\ln y\right]\frac{dq}{q^3}$$
$$+\int_{q_0^2}^{\infty}\left(1-\frac{1}{y}-\frac{\delta^2\Gamma}{m^2}\ln y-\frac{1}{\sqrt{\zeta(1+\zeta)}}\ln(\sqrt{1+\zeta}+\sqrt{\zeta})\right)\frac{dq^2}{q^4}.$$

We consider these integrals separately. In the region $\delta\Gamma < q < q_0$

$$2\int_{\delta\Gamma}^{q_0}\left[\frac{2}{3}\xi\left(1+\frac{3}{y^2}-\frac{4}{y^3}\right)-\frac{\delta^2\Gamma}{m^2}\ln\frac{q}{\delta\Gamma}\right]\frac{dq}{q^3}$$
$$=\frac{1}{3m^2\Gamma}\int_{\delta\Gamma}^{q_0}\left(\frac{1}{q}+3(\delta\Gamma)^2\frac{1}{q^3}-4(\delta\Gamma)^3\frac{1}{q^4}\right)dq\;-\frac{2\delta^2\Gamma}{m^2}\int_{\delta\Gamma}^{q_0}\frac{dq}{q^3}\ln\frac{q}{\delta\Gamma}$$
$$=\frac{1}{3m^2\Gamma}\left[\ln q-\frac{3(\delta\Gamma)^2}{2q^2}+\frac{4(\delta\Gamma)^3}{3q^3}\right]_{\delta\Gamma}^{q_0}+\frac{\delta^2\Gamma}{m^2}\left[\frac{\ln(q/\delta\Gamma)}{q^2}+\frac{1}{2q^2}\right]_{\delta\Gamma}^{q_0}$$
$$=\frac{1}{3m^2\Gamma}\left[\ln\frac{q_0}{\delta\Gamma}-\frac{3(\delta\Gamma)^2}{2q_0^2}+\frac{3}{2}+\frac{4(\delta\Gamma)^3}{3q_0^3}-\frac{4}{3}\right]$$
$$+\frac{\delta^2\Gamma}{m^2}\left[\frac{1}{q_0^2}\ln\frac{q_0}{\delta\Gamma}+\frac{1}{2q_0^2}-\frac{1}{2(\delta\Gamma)^2}\right]$$
$$=\frac{1}{3m^2\Gamma}\left[\left(1+3\frac{(\delta\Gamma)^2}{q_0^2}\right)\ln\frac{q_0}{\delta\Gamma}+\left(1-\frac{(\delta\Gamma)^2}{q_0^2}\right)\frac{3}{2}-\left(1-\frac{(\delta\Gamma)^3}{q_0^3}\right)\frac{4}{3}\right.$$
$$\left.-\left(1-\frac{(\delta\Gamma)^2}{q_0^2}\right)\frac{3}{2}\right]$$
$$\approx\frac{1}{3m^2\Gamma}\left(\ln\frac{q_0}{\delta\Gamma}-\frac{4}{3}\right).$$

In the region $q_0^2 < q^2 < \infty$

$$\int_{q_0^2}^{\infty}\left(1-\frac{\delta^2\Gamma}{m^2}\ln y-\frac{1}{\sqrt{\zeta(1+\zeta)}}\ln(\sqrt{1+\zeta}+\sqrt{\zeta})\right)\frac{dq^2}{q^4}$$
$$=\frac{1}{4m^2\Gamma}\left\{\int_{\zeta_0=q_0^2/4m^2\Gamma}^{\infty}\left(1-\frac{1}{\sqrt{\zeta(1+\zeta)}}\ln(\sqrt{1+\zeta}+\sqrt{\zeta})\right)\frac{d\zeta}{\zeta^2}\right.$$
$$\left.-\frac{2\delta^2\Gamma}{m^2}\int_{q_0}^{\infty}\frac{dq}{q^3}\ln\frac{q}{\delta\Gamma}\right\}$$
$$=\frac{1}{4m^2\Gamma}\left\{\int_0^{\eta_0=1/\zeta_0}\left(1-\frac{\eta}{\sqrt{1+\eta}}\ln\frac{1+\sqrt{1+\eta}}{\sqrt{\eta}}\right)d\eta\right.$$
$$\left.+\frac{\delta^2\Gamma}{m^2}\left[\frac{1}{q^2}\ln\frac{q}{\delta\Gamma}+\frac{1}{2q^2}\right]_{q_0}^{\infty}\right\}$$

$$
\begin{aligned}
&= \frac{1}{4m^2\Gamma}\left\{\frac{2}{3}\left[\eta+\ln\eta+(2-\eta)\sqrt{\eta+1}\ln\frac{\sqrt{\eta+1}+1}{\sqrt{\eta}}\right]_0^{\eta_0}\right.\\
&\quad\left.-\frac{\delta^2\Gamma}{m^2q_0^2}\ln\frac{q_0}{\delta\Gamma}-\frac{\delta^2\Gamma}{2m^2q_0^2}\right\}\\
&= \frac{1}{6m^2\Gamma}\left\{\left[\frac{4m^2\Gamma}{q_0^2}+\ln\frac{4m^2\Gamma}{q_0^2}+\left(2-\frac{4m^2\Gamma}{q_0^2}\right)\sqrt{\frac{4m^2\Gamma}{q_0^2}+1}\right.\right.\\
&\quad\left.\left.\times\ \ln\frac{\sqrt{4m^2\Gamma+q_0^2}+q_0}{\sqrt{4m^2\Gamma}}-\ln 4\right]-\frac{\delta^2\Gamma}{m^2q_0^2}\ln\frac{q_0}{\delta\Gamma}-\frac{\delta^2\Gamma}{2m^2q_0^2}\right\}\\
&\approx \frac{1}{6m^2\Gamma}\left[\ln\frac{m^2\Gamma}{q_0^2}+\frac{5}{3}\right]
\end{aligned}
$$

The final result is therefore

$$
\begin{aligned}
&\int_{(\delta\Gamma)^2}^{\infty}\left(1-\frac{1}{y}-\frac{\delta^2\Gamma}{m^2}\ln y-\ln x\right)\frac{dq^2}{q^4}\\
&\approx \frac{1}{3m^2\Gamma}\left(\ln\frac{q_0}{\delta\Gamma}-\frac{4}{3}\right)+\frac{1}{6m^2\Gamma}\left(\ln\frac{m^2\Gamma}{q_0^2}+\frac{5}{3}\right) \qquad \text{(A.11)}\\
&= \frac{1}{6m^2\Gamma}\left(\ln\frac{m^2}{\delta^2\Gamma}-1\right).
\end{aligned}
$$

We now calculate the integral occurring in $\mathscr{M}_1{}^{44}_{\alpha\alpha}$ besides the one already calculated. Retaining only the lowest order of ξ in J_3', we have

$$
\int_{(\delta\Gamma)^2}^{\infty}\left[\frac{\omega\Gamma}{2m^2\varepsilon_1^2\varepsilon_2^2}(1-y)+\frac{2q^2}{m^6\omega\Gamma}\ln x\right]\frac{dq^2}{q^4}=\int_{\delta\Gamma}^{\infty}\frac{4}{m^6\omega\Gamma}[(\delta\Gamma)^2(1-y)+q^2\ln x]\frac{dq}{q^3} \qquad \text{(A.12)}
$$

We again split up the integration at q_0^2 and obtain for $(\delta\Gamma)^2<q^2<q_0^2$

$$
\begin{aligned}
&\frac{4}{m^6\omega\Gamma}\left\{\int_{\delta\Gamma}^{q_0}\frac{(\delta\Gamma)^2-(\delta\Gamma)q}{q^3}\,dq\ +\int_{\delta\Gamma}^{q_0}\left[1-\frac{1}{y}-\frac{2}{3}\xi\left(1+\frac{3}{y^2}-\frac{4}{y^3}\right)\right]\frac{dq}{q}\right\}\\
&= \frac{4}{m^6\omega\Gamma}\left\{\left[-\frac{(\delta\Gamma)^2}{2q^2}+\frac{\delta\Gamma}{q}\right]_{\delta\Gamma}^{q_0}+\left[\ln q+\frac{\delta\Gamma}{q}-\frac{q^2}{12m^2\Gamma}-\frac{(\delta\Gamma)^2}{2m^2\Gamma}\ln q\right.\right.\\
&\quad\left.\left.-\frac{2(\delta\Gamma)^3}{3m^2\Gamma q}\right]_{\delta\Gamma}^{q_0}\right\}\\
&\approx \frac{4}{m^6\omega\Gamma}\left(\ln\frac{q_0}{\delta\Gamma}-\frac{3}{2}\right)
\end{aligned}
$$

and for the region $q_0^2<q^2<\infty$

$$
\frac{2}{m^6\omega\Gamma}\int_{q_0^2}^{\infty}\left[(\delta\Gamma)^2(1-y)+\frac{q^2}{\sqrt{\zeta(1+\zeta)}}\ln(\sqrt{1+\zeta}+\sqrt{\zeta})\right]\frac{dq^2}{q^4}
$$

$$= \frac{2}{m^6\omega\Gamma}\left\{2\int_{q_0}^{\infty}\left[\frac{(\delta\Gamma)^2}{q^3}-\frac{\delta\Gamma}{q^2}\right]dq \;+\int_{q_0^2/4m^2\Gamma}^{\infty}\frac{1}{\sqrt{\zeta(1+\zeta)}}\ln(\sqrt{1+\zeta}+\sqrt{\zeta})\frac{d\zeta}{\zeta}\right\}$$

$$= \frac{2}{m^6\omega\Gamma}\left\{2\left[-\frac{(\delta\Gamma)^2}{2q^2}+\frac{\delta\Gamma}{q}\right]_{q_0}^{\infty}+\int_0^{4m^2\Gamma/q_0^2}\frac{d\eta}{\sqrt{\eta(1+\eta)}}\ln\frac{\sqrt{\eta+1}+1}{\sqrt{\eta}}\right\}$$

$$= \frac{2}{m^6\omega\Gamma}\left\{\frac{(\delta\Gamma)^2}{q_0^2}-\frac{\delta\Gamma}{q_0}+\left[2\sqrt{\eta+1}\ln\frac{\sqrt{\eta+1}+1}{\sqrt{\eta}}+\ln\eta\right]_0^{4m^2\Gamma/q_0^2}\right\}$$

$$\approx \frac{2}{m^6\omega\Gamma}\left(\ln\frac{4m^2\Gamma}{q_0^2}+2-\ln 4\right)$$

$$= \frac{2}{m^6\omega\Gamma}\left(\ln\frac{m^2\Gamma}{q_0^2}+2\right).$$

Thus the final result is

$$\int_{(\delta\Gamma)^2}^{\infty}\left[\frac{\omega\Gamma}{2m^2\varepsilon_1^2\varepsilon_2^2}(1-y)+\frac{2q^2}{m^6\omega\Gamma}\ln x\right]\frac{dq^2}{q^4}\approx\frac{2}{m^6\omega\Gamma}\left(\ln\frac{m^2}{\delta^2\Gamma}-1\right). \quad (A.13)$$

Therefore in the absence of screening

$$\int\frac{dq^2\;d\nu}{q^4}W_2\mathscr{M}_1{}^{44}_{44}=\frac{32\pi}{3m^8\Gamma^2}\frac{\varepsilon_1^2\varepsilon_2^2}{\omega}\left(\ln\frac{m^2}{\delta^2\Gamma}-1\right), \quad (A.14)$$

$$\begin{aligned}\int\frac{dq^2\;d\nu}{q^4}W_2\mathscr{M}_1{}^{44}_{\alpha\alpha}&=\frac{16\pi}{m^6\Gamma^2}\frac{\varepsilon_1\varepsilon_2}{\omega}\left(2-\frac{k^2}{m^2}\right)\left(\ln\frac{m^2}{\delta^2\Gamma}-1\right)\\&\quad+\frac{16\pi}{m^6\Gamma}\frac{\varepsilon_1^2+\varepsilon_2^2}{\omega}\left(\ln\frac{m^2}{\delta^2\Gamma}-1\right).\end{aligned} \quad (A.15)$$

A.3 Partial screening

The cross section differential in k^2 can be expressed using two dimensionless functions

$$\Phi_1(\delta,\Gamma)=\frac{1}{2}\int_{(\delta\Gamma)^2}^{\infty}[q^2\ln x-(\delta\Gamma)^2(y-1)]\frac{b^4q^4}{(1+b^2q^2)^2}\frac{dq^2}{q^4}, \quad (A.16)$$

$$\Phi_2(\delta,\Gamma)=3m^2\Gamma\int_{(\delta\Gamma)^2}^{\infty}\left(1-\frac{1}{y}-\ln x-\frac{\delta^2\Gamma}{m^2}\ln y\right)\frac{b^4q^4}{(1+b^2q^2)^2}\frac{dq^2}{q^4} \quad (A.17)$$

which also occur in bremsstrahlung. As shown above, in the absence of screening

$$\Phi_1(\delta,\Gamma)=\Phi_2(\delta,\Gamma)=\frac{1}{2}\left(\ln\frac{m^2}{\delta^2\Gamma}-1\right)$$

and the cross section is given by

$$\int W_2\mathscr{M}_1{}^{44}_{44}\frac{dq^2}{q^4}=\frac{64\pi}{3m^8\omega\Gamma^2}\Phi_2(\delta,\Gamma), \quad (A.18)$$

$$\int W_2 \mathscr{M}_{1\alpha\alpha}^{44} \frac{dq^2}{q^4} = \frac{16\pi}{3m^4\delta\Gamma^2}\left(2 - \frac{k^2}{m^2}\right)\Phi_2(\delta,\Gamma) + \frac{32\pi(\varepsilon_1^2+\varepsilon_2^2)}{m^6\omega\Gamma}\Phi_1(\delta,\Gamma). \tag{A.19}$$

The result of the calculation in the preceding section is independent of the value of the auxiliary momentum q_0^2. Therefore we can give any value to it and in particular $m^2\Gamma$, such that the atomic formfactor at the cutoff momentum is practically zero and the logarithms in the high-q^2 terms vanish such that we obtain

$$\Phi_1(\delta,\Gamma) = \frac{1}{2}\int_{(\delta\Gamma)^2}^{m^2\Gamma} (q-\delta\Gamma)^2 \frac{b^4q^4}{(1+b^2q^2)^2}\frac{dq^2}{q^4} + 1, \tag{A.20}$$

$$\Phi_2(\delta,\Gamma) = 3m^2\Gamma \int_{(\delta\Gamma)^2}^{m^2\Gamma} \left[\frac{2}{3}\xi\left(1+\frac{3}{y^2}-\frac{4}{y^3}\right) - \frac{\delta^2\Gamma}{m^2}\ln y\right]\frac{b^4q^4}{(1+b^2q^2)^2}\frac{dq^2}{q^4} + \frac{5}{3}. \tag{A.21}$$

In analogy to [10, 11] we obtain

$$\begin{aligned}
\Phi_1(\delta,\Gamma) &= \frac{1}{2}\left\{\ln\frac{1+b^2m^2\Gamma}{1+(b\delta\Gamma)^2} - 2b\delta\Gamma[\arctan(bm\sqrt{\Gamma}) - \arctan(b\delta\Gamma) \right. \\
&\quad \left. + 1]\right\} + 1 \qquad (A.22) \\
&\approx \frac{1}{2}\left[1 + \ln\frac{b^2m^2\Gamma}{1+b^2(\delta\Gamma)^2}\right] - b\delta\Gamma\arctan\frac{1}{b\delta\Gamma}, \\
\Phi_2(\delta,\Gamma) &= 2(b\delta\Gamma)^3[\arctan(b\delta\Gamma) - \arctan(bm\sqrt{\Gamma})] \\
&\quad + \frac{3(b\delta\Gamma)^2+1}{2}\ln\frac{1+b^2m^2\Gamma}{1+(b\delta\Gamma)^2} \\
&\quad - 3(b\delta\Gamma)^2\left(1+\frac{1}{1+b^2m^2\Gamma}\right)\ln\frac{m}{\delta\sqrt{\Gamma}} \\
&\quad + \frac{12\Gamma^3b^4\delta^2m^2 + 7\Gamma b^2m^2 - 12(b\delta\Gamma)^3bm\sqrt{\Gamma} + 3(b\delta\Gamma)^2 + 10}{6(1+b^2m^2\Gamma)} \\
&\approx \frac{1}{2}\left(\frac{2}{3} + \ln\frac{b^2m^2\Gamma}{1+b^2(\delta\Gamma)^2}\right) + 2(b\delta\Gamma)^2\left(1 - \arctan\frac{1}{b\delta\Gamma}\right. \\
&\quad \left. + \frac{3}{4}\ln\frac{(b\delta\Gamma)^2}{1+(b\delta\Gamma)^2}\right). \qquad (A.23)
\end{aligned}$$

A.4 Interpolation between full screening and no screening

The integration over k^2 can be carried out analytically [55] in the limiting cases of full screening and no screening. It was shown in [87], that the function $\Phi = \Phi_1 \approx \Phi_2$ in the bremsstrahlung cross section, which assumes the limiting values

$$\Phi_{\mathrm{NS}} = \ln\frac{\mu}{\delta} - \frac{1}{2} \tag{A.24}$$

in the absence of screening and

$$\Phi_{\mathrm{FS}} = \ln\left(\frac{\mu}{m} 183 Z^{-1/3}\right) \tag{A.25}$$

for full screeening, can approximate the numerical results for a Thomas-Fermi atom for any degree of screening with the function

$$\Phi = \ln \frac{(\mu/m) B Z^{-1/3}}{1 + B Z^{-1/3} \delta / m}. \tag{A.26}$$

This describes the behavior of a Thomas-Fermi atom better than the form factor in the previous section, which deviates by several percent in the partial screening region, but leads to the correct limiting behavior.

This interpolation was later applied by [66] on the pair production cross section, based on the cross section integrated over k^2 and in the approximation $\Phi_1 \approx \Phi_2$, thus leading to an uncertainty of 1–3%.

To improve this parametrization we apply this analytical interpolation to the functions Φ_1, Φ_2 separately, without using $\Phi_1 \approx \Phi_2$. The integration over k^2 is dominated by small values of k^2 due to the factor $1/k^4$ in the integrand, similar to the q^2 integration. The lower limit of k^2, $\mu^2\omega^2/\varepsilon_3\varepsilon_4$, is not small compared to m^2 for $\omega \gtrsim (m/\mu)\varepsilon_3$, and we cannot neglect k^2 compared to m^2. In the region $\varepsilon_{3,4}^2 \gg \mu^2$, however, we can neglect k^2 compared to ω^2, such that $k^* = \sqrt{k^2 + \omega^2} \approx \omega$.

In the chosen accuracy

$$\begin{aligned}
\int \frac{dk^2\ dq^2\ d\nu}{k^4 q^4} W_2 L_2 \mathscr{M}_{1\,44}^{\,44} &= \int -4\frac{k^2}{\omega^2}\left\{\frac{k^2}{2} - \mu^2 - 3\frac{k^2}{\omega^2}\left(-\varepsilon_3\varepsilon_4 + \frac{k^2}{4}\right)\right\} \\
&\quad \times \frac{64\pi}{3m^8\omega\Gamma^2}\varepsilon_1^2\varepsilon_2^2\Phi_2\frac{dk^2}{k^4}, \\
-\int \frac{dk^2 dq^2 d\nu}{k^4 q^4} W_2 L_1 \mathscr{M}_{1\,\alpha\alpha}^{\,44} &= \int 4\left\{\frac{k^2}{2} - \mu^2 - \frac{k^2}{\omega^2}\left(-\varepsilon_3\varepsilon_4 + \frac{k^2}{4}\right)\right\} \\
&\quad \times \left[\frac{16\pi}{3m^4\delta\Gamma^2}\left(2 - \frac{k^2}{m^2}\right)\Phi_2 + 32\pi\frac{\varepsilon_1^2 + \varepsilon_2^2}{m^6\omega\Gamma}\Phi_1\right]\frac{dk^2}{k^4}
\end{aligned} \tag{A.27}$$

The Integration over k^2 can be reduced to the following integrals

$$\begin{gathered}
\int \frac{k^2\Phi_2 dk^2}{\Gamma^2}, \quad \int \frac{\Phi_2 dk^2}{\Gamma^2}, \quad \int \frac{\Phi_2 dk^2}{k^2\Gamma^2}, \quad \int \frac{\Phi_2\, dk^2}{k^4\Gamma^2} \\
\int \frac{\Phi_1 dk^2}{\Gamma}, \quad \int \frac{\Phi_1 dk^2}{k^2\Gamma}, \quad \int \frac{\Phi_1\, dk^2}{k^4\Gamma},
\end{gathered}$$

as detailed in the following equations

$$\int \frac{dk^2\ dq^2\ d\nu}{k^4 q^4} W_2 L_2 \mathscr{M}_1{}^{44}_{44} = -\frac{256\pi}{3m^8\omega^3}\varepsilon_1^2\varepsilon_2^2 \left\{ \left[\frac{1}{2} + 3\frac{\varepsilon_3\varepsilon_4}{\omega^2}\right] \int \frac{\Phi_2}{\Gamma^2}\, dk^2 \right.$$
$$- \mu^2 \int \frac{\Phi_2}{k^2\Gamma^2}\, dk^2$$
$$\left. - \frac{3}{4\omega^2} \int \frac{k^2\Phi_2}{\Gamma^2}\, dk^2 \right\}, \tag{A.28}$$

$$-\int \frac{dk^2\ dq^2\ d\nu}{k^4 q^4} W_2 L_1 \mathscr{M}_1{}^{44}_{\alpha\alpha} = \frac{128\pi}{3m^6\omega}\varepsilon_1\varepsilon_2 \left\{ \left(1 + \frac{\mu^2}{m^2} + 2\frac{\varepsilon_3\varepsilon_4}{\omega^2}\right) \int \frac{\Phi_2}{k^2\Gamma^2}\, dk^2 \right.$$
$$- \left(\frac{1}{2m^2} - \frac{\varepsilon_3\varepsilon_4}{m^2\omega^2} - \frac{1}{2\omega^2}\right) \int \frac{\Phi_2}{\Gamma^2}\, dk^2$$
$$- 2\mu^2 \int \frac{\Phi_2}{k^4\Gamma^2}\, dk^2$$
$$\left. + \frac{1}{4m^2\omega^2} \int \frac{k^2\Phi_2}{\Gamma^2}\, dk^2 \right\}$$
$$+ 128\pi \frac{\varepsilon_1^2 + \varepsilon_2^2}{m^6\omega} \left\{ \left(\frac{1}{2} + \frac{\varepsilon_3\varepsilon_4}{\omega^2}\right) \int \frac{\Phi_1}{k^2\Gamma}\, dk^2 \right.$$
$$- \mu^2 \int \frac{\Phi_1}{k^4\Gamma}\, dk^2$$
$$\left. - \frac{1}{4\omega^2} \int \frac{\Phi_1}{\Gamma}\, dk^2 \right\}. \tag{A.29}$$

Using the integrals below we obtain the following resulting cross section for the limiting cases of complete (no) screening, corresponding to the upper (lower) sign in $\pm$:

$$\int \frac{dk^2\ dq^2\ d\nu}{k^4 q^4} L_2 W_2 \mathscr{M}_1{}^{44}_{44} = \frac{256\pi}{3m^6\omega^3}\varepsilon_1^2\varepsilon_2^2 \left\{ \tilde{\Psi}_2 \left[\frac{\mu^2}{m^2} \left(\ln\frac{1+\xi}{\xi} - \frac{1}{1+\xi} \right) \right.\right.$$
$$\left. - \frac{\omega^2}{\varepsilon_1\varepsilon_2} \left(\frac{1}{2} + 3\frac{\varepsilon_3\varepsilon_4}{\omega^2}\right) \frac{1}{1+\xi} \right] \pm \frac{1}{2} \left[\frac{\mu^2}{m^2} \left(\mathrm{Li}_2\, \frac{1}{1+\xi} - \frac{1}{1+\xi} \right) \right.$$
$$\left.\left. - \frac{\omega^2}{2\varepsilon_1\varepsilon_2(1+\xi)} \left(\frac{1}{2} + 3\frac{\varepsilon_3\varepsilon_4}{\omega^2}\right) \right] \right\}, \tag{A.30}$$

$$-\int \frac{dk^2\ dq^2\ d\nu}{k^4 q^4} L_1 W_2 \mathscr{M}_1{}^{44}_{\alpha\alpha} = 128\pi \frac{\varepsilon_1\varepsilon_2}{3m^6\omega^3}\varepsilon_3\varepsilon_4 \left\{ \tilde{\Psi}_2 \left[\ln\frac{1+\xi}{\xi} \right.\right.$$
$$\left.\left(\frac{\omega^2}{\varepsilon_3\varepsilon_4} + \frac{\mu^2\omega^2}{m^2\varepsilon_3\varepsilon_4} + 2 + 4\xi \right) - \frac{1}{1+\xi} \left(\frac{\omega^2}{\varepsilon_3\varepsilon_4} + \frac{\mu^2\omega^2}{m^2\varepsilon_3\varepsilon_4} + 2 + \frac{\omega^4}{2\varepsilon_1\varepsilon_2\varepsilon_3\varepsilon_4} \right.\right.$$

$$
\begin{aligned}
&-\frac{\omega^2}{\varepsilon_1\varepsilon_2}\Big) - 2\Big] \pm \frac{1}{2}\left[\mathrm{Li}_2\,\frac{1}{1+\xi}\left(\frac{\omega^2}{\varepsilon_3\varepsilon_4} + \frac{\mu^2\omega^2}{m^2\varepsilon_3\varepsilon_4} + 2 + 4\xi\right)\right.\\
&\left.-\frac{1}{1+\xi}\left(\frac{\omega^2}{\varepsilon_3\varepsilon_4} + \frac{\mu^2\omega^2}{m^2\varepsilon_3\varepsilon_4} + 2 + \frac{\omega^4}{2\varepsilon_1\varepsilon_2\varepsilon_3\varepsilon_4} - \frac{\omega^2}{\varepsilon_1\varepsilon_2}\right) - 2\xi\ln\frac{1+\xi}{\xi}\right]\Big\}\\
&+ 128\pi\frac{\varepsilon_1^2+\varepsilon_2^2}{3m^6\omega^3}\varepsilon_3\varepsilon_4\left\{\tilde{\Psi}_1\left[\ln\frac{1+\xi}{\xi}\left(\frac{\omega^2}{2\varepsilon_3\varepsilon_4} + 1 + \xi\right) - 1\right]\right.\\
&\left.\pm\frac{1}{2}\left[\mathrm{Li}_2\,\frac{1}{1+\xi}\left(\frac{\omega^2}{2\varepsilon_3\varepsilon_4} + 1 + \xi\right) - \xi\ln\frac{1+\xi}{\xi}\right]\right\}, \qquad \text{(A.31)}
\end{aligned}
$$

$$
\tilde{\Psi}_i = \Phi_i|_{\Gamma=1+\xi}. \qquad \text{(A.32)}
$$

Changing to the notation used in [66], the expressions by [55] are obtained.

To obtain the correction for the nuclear formfactor, $\Phi_{1,2}$ are changed to $\Phi_{1,2} - \mathit{\Delta}_{1,2}$, where $\mathit{\Delta}_{1,2}$ are given by (3.24) with $= m_e\sqrt{\Gamma}$. Numerical calculations show that the cross section is described with good accuracy by the expressions in the main text.

A.5 Integrals over k^2 in the pair production cross section

The Φ_i can be split into a constant term and $\ln\Gamma$, such that the necessary indefinite integrals are

$$
\begin{aligned}
\int\frac{k^2\,dk^2}{\Gamma^2} &= \left(\frac{k^2}{\Gamma-1}\right)^2\left(\ln\Gamma + \frac{1}{\Gamma}\right),\\
\int\frac{dk^2}{\Gamma^2} &= \frac{k^2}{\Gamma(1-\Gamma)},\\
\int\frac{dk^2}{k^2\Gamma^2} &= -\ln\Gamma + \ln k^2 + \frac{1}{\Gamma},\\
\int\frac{dk^2}{k^4\Gamma^2} &= \frac{2(\Gamma-1)}{k^2}\left(\ln\Gamma - \ln k^2 - \frac{1}{\Gamma}\right) - \frac{1}{k^2\Gamma},\\
\int\frac{dk^2}{\Gamma} &= \frac{k^2}{\Gamma-1}\ln\Gamma,\\
\int\frac{dk^2}{k^2\Gamma} &= \ln k^2 - \ln\Gamma,\\
\int\frac{dk^2}{k^4\Gamma} &= \frac{\Gamma-1}{k^2}(\ln\Gamma - \ln k^2) - \frac{1}{k^2},
\end{aligned}
$$

$$
\begin{aligned}
\int\frac{k^2\ln\Gamma}{\Gamma^2}\,dk^2 &= \left(\frac{k^2}{\Gamma-1}\right)^2\frac{2+2\Gamma\ln\Gamma+\ln^2\Gamma}{2\Gamma},\\
\int\frac{\ln\Gamma}{\Gamma^2}\,dk^2 &= \frac{k^2}{\Gamma(1-\Gamma)}(1+\ln\Gamma),\\
\int\frac{\ln\Gamma}{k^2\Gamma^2}\,dk^2 &= \frac{1}{\Gamma} + \frac{\ln\Gamma}{\Gamma} + \mathrm{Li}_2\,\frac{\Gamma-1}{\Gamma},
\end{aligned}
$$

$$
\begin{aligned}
\int \frac{\ln \Gamma}{k^4 \Gamma^2}\, dk^2 &= \frac{\Gamma - 1}{k^2}\left[2\,\mathrm{Li}_2(1-\Gamma) + \ln^2 \Gamma + \ln k^2 - \frac{1}{\Gamma}\right] - \frac{\Gamma^2 + \Gamma - 1}{k^2 \Gamma}\ln \Gamma, \\
\int \frac{\ln \Gamma}{\Gamma}\, dk^2 &= \frac{k^2}{2(\Gamma - 1)}\ln^2 \Gamma, \\
\int \frac{\ln \Gamma}{k^2 \Gamma}\, dk^2 &= -\frac{1}{2}\ln^2 \Gamma - \mathrm{Li}_2(1-\Gamma), \\
\int \frac{\ln \Gamma}{k^4 \Gamma}\, dk^2 &= \frac{\Gamma - 1}{k^2}\left(\ln k^2 + \frac{1}{2}\ln^2 \Gamma - \frac{\Gamma}{\Gamma - 1}\ln \Gamma + \mathrm{Li}_2(1-\Gamma)\right),
\end{aligned}
$$

Appendix B

Improved cross section parametrizations

For convenience, this appendix lists the complete cross sections for bremsstrahlung and pair production with all corrections calculated in this thesis.

In this appendix, we use the following symbols:

B	radiation logarithm (≈ 183)
B'	inelastic radiation logarithm (≈ 1429)
$D_n = 1.54A^{0.27}$	nuclear formfactor parametrization
μ	mass of the incoming particle

B.1 Bremsstrahlung

This parametrization takes into account: elastic atomic and nuclear formfactors, inelastic nuclear formfactors, bremsstrahlung on atomic electrons (μ-diagrams only), and radiative corrections. The Coulomb corrections, which are important for electrons[1], are negligible for muons and therefore neglected.

$$\begin{aligned}\frac{d\sigma}{dv} = 4Z^2\alpha\left(r_e\frac{m_e}{\mu}\right)^2\frac{1}{v}\Bigg\{\left[(2-2v+v^2)\Phi_1(\delta) - \frac{2}{3}(1-v)\Phi_2(\delta)\right] \\ + \frac{1}{Z}s_{\text{atomic}}(v,\delta) + \frac{\alpha}{4}\Phi_1(\delta)s_{\text{rad}}(v)\Bigg\},\end{aligned} \tag{B.1}$$

where

$$\Phi_1(\delta) = \ln\frac{\frac{\mu}{m_e}BZ^{-1/3}}{1+BZ^{-1/3}\sqrt{e}\delta/m_e} - \mathit{\Delta}_1\left(1-\frac{1}{Z}\right), \tag{B.2}$$

$$\Phi_2(\delta) = \ln\frac{\frac{\mu}{m_e}BZ^{-1/3}e^{-1/6}}{1+BZ^{-1/3}e^{1/3}\delta/m_e} - \mathit{\Delta}_2\left(1-\frac{1}{Z}\right), \tag{B.3}$$

$$\mathit{\Delta}_1 = \ln\frac{\mu}{q_c} + \frac{\varrho}{2}\ln\frac{\varrho+1}{\varrho-1}, \tag{B.4}$$

[1] For electrons, $\Phi_{1,2}$ are to be replaced by $\Phi_{1,2} - f(\alpha Z)g_{1,2}(\mu/\text{MeV}, \alpha Z)$, where $f(\nu) = \nu^2\sum_{n=1}^{\infty}[n(n^2+\nu^2)]^{-1}$ and $g_{1,2}(x,\nu)$ is given in 6.

n	0	1	2	3	4	5
a_n	−0.00349	148.84	−987.531			
b_n	0.1642	132.573	−585.361	1407.77		
c_n	−2.8922	−19.0156	57.698	−63.418	14.1166	1.84206
d_n	2134.19	581.823	−2708.85	4767.05	1.52918	0.361933

Table B.1: Parameters of the parametrization for the radiative corrections to the bremsstrahlung cross section.

$$\mathcal{A}_2 = \ln\frac{\mu}{q_c} + \frac{3\varrho-\varrho^3}{4}\ln\frac{\varrho+1}{\varrho-1} + \frac{2\mu^2}{q_c^2}, \tag{B.5}$$

$$\varrho = \sqrt{1+\frac{4\mu^2}{q_c^2}}, q_c = m_\mu e/D_n, \tag{B.6}$$

$$s_{\text{atomic}}(\delta) = \left[\frac{4}{3}(1-v)+v^2\right]\left[\ln\frac{\mu/\delta}{\mu\delta/m_e^2+\sqrt{e}} - \ln\left(1+\frac{m_e}{\delta B' Z^{-2/3}\sqrt{e}}\right)\right], \tag{B.7}$$

$$s_{\text{rad}}(v) = \begin{cases} \sum_{n=0}^{2} a_n v^n & v < 0.02, \\ \sum_{n=0}^{3} b_n v^n & 0.02 \le v < 0.1, \\ \sum_{n=0}^{2} c_n v^n + c_3 v\ln v + c_4\ln(1-v) + c_5\ln^2(1-v) & 0.1 \le v < 0.9, \\ \sum_{n=0}^{2} d_n v^n + d_3 v\ln v + d_4\ln(1-v) + d_5\ln^2(1-v) & v \ge 0.9, \end{cases} \tag{B.8}$$

where the values of the fit parameters a_n, b_n, c_n, d_n are given in table B.1.

B.2 Pair production

This parametrization of the pair production cross section takes into account: elastic atomic and nuclear formfactors, and pair production on atomic electrons[2].

$$\frac{d^2\sigma}{dv\,d\varrho} = \frac{2}{3\pi}Z(Z+\zeta)\frac{1-v}{v}\left[\Phi_e + \frac{m_e^2}{m_\mu^2}\Phi_\mu\right], \tag{B.9}$$

where

$$\Phi_e = C_1^e L_1^e + C_2^e L_e^2, \tag{B.10}$$

$$C_1^e = C_e - C_2^e, \tag{B.11}$$

$$C_2^e = [(1-\varrho^2)(1+\beta)+\xi(3-\varrho^2)]\ln\left(1+\frac{1}{\xi}\right) + 2\frac{1-\beta-\varrho^2}{1+\xi} - (3-\varrho^2), \tag{B.12}$$

$$L_1^e = \ln\frac{BZ^{-1/3}\sqrt{1+\xi}}{X_e + \frac{2m_e\sqrt{e}BZ^{-1/3}(1+\xi}{Ev(1-\varrho^2}} - \frac{\mathcal{A}_e}{C_e} - \frac{1}{2}\ln\left[X_e + \left(\frac{m_e}{m_\mu}D_n\right)^2(1+\xi)\right] \tag{B.13}$$

[2]The way this calculation is set up it is impossible to take into account the inelastic nuclear formfactor and the atomic electron contribution simultaneously.

$$L_2^e = \ln \frac{BZ^{-1/3}e^{-1/6}\sqrt{1+\xi}}{X_e + \frac{2m_e e^{1/3}BZ^{-1/3}(1+\xi}{Ev(1-\varrho^2)}} - \frac{\mathit{\Delta}_e}{C_e} - \frac{1}{2}\ln\left[X_e + \left(\frac{m_e}{m_\mu}D_n\right)^2 e^{1/3}(1+\xi)\right] \tag{B.14}$$

$$X_e = \exp\left(-\frac{\mathit{\Delta}_e}{C_e}\right), \tag{B.15}$$

$$C_e = [(2+\varrho^2)(1+\beta) + \xi(3+\varrho^2)]\ln\left(1+\frac{1}{\xi}\right) + \frac{1-\varrho^2-\beta}{1+\xi} - (3+\varrho^2), \tag{B.16}$$

$$\mathit{\Delta}_e = [(2+\varrho^2)(1+\beta) + \xi(3+\varrho^2)]\,\mathrm{Li}_2\,\frac{1}{1+\xi} - (2+\varrho^2)\xi\ln\left(1+\frac{1}{\xi}\right) - \frac{\xi+\varrho^2+\beta}{1+\xi}, \tag{B.17}$$

where $L_{1,2}^e$ can be equivalently expressed in the case of large X_e as

$$L_1^e = \ln \frac{BZ^{-1/3}\sqrt{1+\xi}}{1 + \frac{2m_e\sqrt{e}BZ^{-1/3}(1+\xi)}{Ev(1-\varrho^2)}X_e^{-1}} - \frac{1}{2}\frac{\mathit{\Delta}_e}{C_e} - \frac{1}{2}\ln\left[1 + \left(\frac{m_e}{m_\mu}D_n\right)^2 (1+\xi)X_e^{-1}\right], \tag{B.18}$$

$$L_2^e = \ln \frac{BZ^{-1/3}e^{-1/6}\sqrt{1+\xi}}{1 + \frac{2m_e e^{1/3}BZ^{-1/3}(1+\xi)}{Ev(1-\varrho^2)}X_e^{-1}} - \frac{1}{2}\frac{\mathit{\Delta}_e}{C_e} - \frac{1}{2}\ln\left[1 + \left(\frac{m_e}{m_\mu}D_n\right)^2 e^{1/3}(1+\xi)X_e^{-1}\right], \tag{B.19}$$

and

$$\mathit{\Phi}_\mu = C_1^\mu L_1^\mu + C_2^\mu L_2^\mu, \tag{B.20}$$

$$L_1^\mu = \ln \frac{B\frac{\mu}{m_e}Z^{-1/3}/D_n}{X_\mu + \frac{2m_e\sqrt{e}BZ^{-1/3}(1+\xi)}{Ev(1-\varrho^2)}} - \frac{\mathit{\Delta}_\mu}{C_\mu}, \tag{B.21}$$

$$L_2^\mu = \ln \frac{B\frac{\mu}{m_e}Z^{-1/3}/D_n}{X_\mu + \frac{2m_e e^{1/3}BZ^{-1/3}(1+\xi)}{Ev(1-\varrho^2)}} - \frac{\mathit{\Delta}_\mu}{C_\mu}, \tag{B.22}$$

$$C_1^\mu = C_\mu - C_2^\mu, \tag{B.23}$$

$$C_2^\mu = [(1-\beta)(1-\varrho^2) - \xi(1+\varrho^2)]\frac{\ln(1+\xi)}{\xi} - 2\frac{1-\beta-\varrho^2}{1+\xi} + 1 - \beta - (1+\beta)\varrho^2, \tag{B.24}$$

$$C_\mu = \left[(1+\varrho^2)\left(1+\frac{3}{2}\beta\right) - \frac{1}{\xi}(1+2\beta)(1-\varrho^2)\right]\ln(1+\xi) + \frac{\xi(1-\varrho^2-\beta)}{1+\xi} + (1+2\beta)(1-\varrho^2), \tag{B.25}$$

$$X_\mu = \exp\left(-\frac{\mathit{\Delta}_\mu}{C_\mu}\right), \tag{B.26}$$

$$\begin{aligned}\mathit{\Delta}_\mu = {} & \left[(1+\varrho^2)\left(1+\frac{3}{2}\beta\right) - \frac{1}{\xi}(1+2\beta)(1-\varrho^2)\right]\mathrm{Li}_2\left(\frac{\xi}{1+\xi}\right) \\ & + \left(1+\frac{3}{2}\beta\right)\frac{1-\varrho^2}{\xi}\ln(1+\xi) + \left[1-\varrho^2-\frac{\beta}{2}(1+\varrho^2) + \frac{1-\varrho^2}{2\xi}\beta\right]\frac{\xi}{1+\xi},\end{aligned} \tag{B.27}$$

where $L_{1,2}^{\mu}$ can be expressed for large X_{μ} equivalently as

$$L_1^{\mu} = \ln \frac{B\frac{\mu}{m_e} Z^{-1/3}/D_n}{1 + \frac{2m_e\sqrt{e}BZ^{-1/3}(1+\xi)}{Ev(1-\varrho^2)} X_{\mu}^{-1}}, \tag{B.28}$$

$$L_2^{\mu} = \ln \frac{B\frac{\mu}{m_e} Z^{-1/3}/D_n}{1 + \frac{2m_e e^{1/3}BZ^{-1/3}(1+\xi)}{Ev(1-\varrho^2)} X_{\mu}^{-1}}, \tag{B.29}$$

with the abbreviations

$$\beta = \frac{v^2}{2(1-v)}, \tag{B.30}$$

$$\xi = \left(\frac{\mu v}{m_e}\right)^2 \frac{1-\varrho^2}{1-v}, \tag{B.31}$$

$$\zeta = \frac{0.073 \ln \frac{E/\mu}{1+\gamma_1 Z^{2/3} E/\mu} - 0.26}{0.058 \ln \frac{E/\mu}{1+\gamma_2 Z^{1/3} E/\mu} - 0.14}, \tag{B.32}$$

$$\gamma_1 = 1.95 \times 10^{-5}, \quad \gamma_2 = 5.3 \times 10^{-5} \text{ for } Z \neq 1, \tag{B.33}$$

$$\gamma_1 = 4.4 \times 10^{-5}, \quad \gamma_2 = 4.8 \times 10^{-5} \text{ for } Z = 1. \tag{B.34}$$

The dilogarithm $\mathrm{Li}_2(x)$ is defined as

$$\mathrm{Li}_2(x) = -\operatorname{Re} \int_0^x \frac{\ln(1-t)}{t} dt. \tag{B.35}$$

Appendix C

Constants used in this work

This appendix lists the numerical values of fundamental constants and material constants.

Constant	Value
α	$1/137.035\,999\,074$
r_e	$2.817\,940\,326\,7 \times 10^{-13}\,\mathrm{cm}$
N_A	$6.022\,141\,29 \times 10^{23}\,\mathrm{mol}^{-1}$
K	$0.307\,075\,\mathrm{MeV\,cm^2/g}$
$m_e c^2$	$0.510\,998\,928\,\mathrm{MeV}$
$m_\mu c^2$	$105.658\,371\,5\,\mathrm{MeV}$
$m_\tau c^2$	$1776.82\,\mathrm{MeV}$
$m_\pi c^2$	$139.570\,18\,\mathrm{MeV}$
$m_N c^2$	$938.272\,046\,\mathrm{MeV}$
τ_τ	$290.3 \times 10^{-15}\,\mathrm{s}$

Table C.1: Natural constants. Values are taken from [83].

Material	Z	A	I [eV]	$-C$	a
Water	1+8	1.007 94 + 15.9994	75.0	0.091 16	
Ice	1+8	1.007 94 + 15.9994	75.0	0.091 16	
Rock	11	22	136.4	3.7738	0.083 01
Fréjus rock	10.12	20.34	149.0	5.053	0.078
Material	m	X_0	X_1	ϱ [g/cm^3]	δ_0
Water	3.4773	0.2400	2.8004	1.000	0
Ice	3.4773	0.2400	2.8004	0.917	0
Rock	3.4120	0.0492	3.0549	2.650	0
Fréjus rock	3.645	0.288	3.196	2.740	0

Table C.2: Material constants. Values are taken from [49, 77].

Z	B	Z	B	Z	B	Z	B	Z	B
1	202.4	8	173.4	15	172.2	22	176.8	53	178.6
2	151.9	9	170.0	16	173.4	26	175.8	74	177.6
3	159.9	10	165.8	17	174.3	29	173.1	82	178.0
4	172.3	11	165.8	18	174.8	32	173.0	92	179.8
5	177.9	12	167.1	19	175.1	35	173.5		
6	178.3	13	169.1	20	175.6	42	175.9	other	182.7
7	176.6	14	170.8	21	176.2	50	177.4		

Table C.3: Radiation logarithm in the Hartree-Fock model. Values are taken from [60].

Parameter	Value	Parameter	Value
a_{P1}	-0.0808	a_{P3}	1.1709
a_{R1}	0.584 00	a_{R3}	2.6063
b_{P1}	$0.602\,43^2$	b_{P3}	1.8439
b_{R1}	$0.107\,11^2$	b_{R3}	0.493 38
c_{P1}	0.280 67	c_{P3}	2.1979
c_{R1}	0.801 07	c_{R3}	3.4942
m_P^2	49.457 GeV^2	m_0^2	0.319 85 GeV^2
m_R^2	0.150 52 GeV^2		
a_{P2}	$-0.448\,12$		
a_{R2}	0.378 88		
b_{P2}	1.3754^2		
b_{R2}	1.9386^2		
c_{P2}	0.222 91		
c_{R2}	0.973 07		
$\mathcal{A}^2$	0.065 27 GeV^2		
$Q_0^2 - \mathcal{A}^2$	0.460 17 GeV^2		

Table C.4: Parameters of the parametrization of inelastic nuclear interaction according to [6].

A note of thanks/Acknowledgments

This thesis would not have been possible without the help of many people: my parents, who continuously supported me throughtout all my life; Wolfgang Rhode, my supervisor, and Kevin Kröninger, the second examiner of my thesis; Stanislav Richardovich Kelner, Rostislav Pavlovich Kokoulin and Anatoliy Afanasyevich Petrukhin, with whom it was a pleasure to collaborate during my stay at the National Research Nuclear University Moscow Engineering Physics Institute; and the whole astroparticle physics group at Dortmund, for numerous discussions and a pleasant working environment. I want to especially thank those who have undertaken the onerous work of proofreading my thesis, in particular Jan Benjamin Soedingrekso.

Furthermore, useful discussions with Spencer Klein on the giant dipole resonance are acknowledged. This work was supported in part by the Helmholtz Allianz für Astroteilchenphysik under grant number HA-301. The author is grateful for the accomodation provided by the NRNU MEPhI during part of this work.

Bibliography

[1] A. Aab et al. “The Pierre Auger Cosmic Ray Observatory”. In: *Nucl. Instr. Meth. Phys. Res. A* 798 (2015), p. 172.

[2] M. G. Aartsen et al. “Characterization of the Atmospheric Muon Flux in IceCube”. In: *Astropart. Phys.* 78 (2016), p. 1.

[3] M. G. Aartsen et al. “Observation and Characterization of a Cosmic Muon Neutrino Flux from the Northern Hemisphere Using Six Years of IceCube Data”. In: *Astrophys. J.* 833 (2016), p. 3.

[4] M. G. Aartsen et al. “The IceCube Neutrino Observatory: instrumentation and online systems”. In: *J. Instrumentation* 12 (2017), P03012.

[5] R. Abbasi et al. “An improved method for measuring the muon energy using the truncated mean of dE/dx”. In: *Nucl. Instr. Meth.* A703 (2013), pp. 190–198.

[6] H. Abramowicz and A. Levy. *The ALLM parametrization of $\sigma_{tot}(\gamma^* p)$: an update*. arXiv:hep-ph/9712415. 1997.

[7] H. Abramowicz et al. “A parametrization of $\sigma_T(\gamma^* p)$ above the resonance region for $Q^2 \geq 0$”. In: *Phys. Lett. B* 269 (1991), pp. 465–476. doi: doi:10.1016/0370-2693(91)90202-2.

[8] T. Abu-Zayyad et al. “The surface detector array of the Telescope Array experiment”. In: *Nucl. Instr. Meth. Phys. Res. A* 689 (2012), p. 87.

[9] A. I. Akhiezer and V. B. Berestetskii. *Квантовая электродинамика (Quantum Electrodynamics)*. 4th ed. Moscow: Nauka, 1981.

[10] Yu. M. Andreev, L. B. Bezrukov, and E. V. Bugaev. “Excitation of a target in muon bremsstrahlung”. In: *Phys. At. Nucl.* 57 (1994), pp. 2066–2074.

[11] Yu. M. Andreev and E. V. Bugaev. “Muon bremsstrahlung on heavy atoms”. In: *Phys. Rev. D* 55 (1997), pp. 1233–1243.

[12] A. B. Arbuzov. “Radiative corrections to high energy muon bremsstrahlung on heavy nuclei”. In: *JHEP* 01 (2008), p. 031.

[13] V. N. Baier, V. M. Katkov, and V. S. Fadin. *Излучение релятивистских электронов*. Moscow: Атомиздат, 1973.

[14] S. Bakmaev et al. “Electron-positron pair production by linearly polarized photon in the nuclear field”. In: *Phys. Lett. B* 660 (2008), pp. 494–500.

[15] Paul H. Barrett et al. “Interpretation of Cosmic-Ray Measurements Far Underground”. In: *Rev. Mod. Phys.* 24 (1952), pp. 133–178. doi: doi:10.1103/RevModPhys.24.133.

[16] J. F. Beacom et al. “Measuring Flavor Ratios of High-Energy Astrophysical Neutrinos”. In: *Phys. Rev. D* 68 (2003), p. 093005.

[17] V. B. Berestetskii, E. M. Lifshitz, and L. P. Pitaevskii. *Квантовая Электродинамика (Quantum Electrodynamics)*. Moscow: Nauka, 1980.

[18] Jarle Berntsen, Terje O. Espelid, and Alan Genz. “DCUHRE – An Adaptive Multidimensional Integration Routine for a Vector of Integrals”. In: *ACM Transactions on Mathematical Software* 17 (1991), pp. 452–456.

[19] H. Bethe. “Zur Theorie des Durchgangs schneller Korpuskularstrahlen durch Materie”. In: *Ann. Phys.* 397 (1930), p. 325.

[20] H. A. Bethe and L. C. Maximon. “Theory of Bremsstrahlung and Pair Production. I. Differential Cross Section”. In: *Phys. Rev.* 93 (1954), p. 768.

[21] H. Bethe and W. Heitler. “On the Stopping of Fast Particles and on the Creation of Positive Electrons”. In: *Proc. Roy. Soc. Lond. A.* 146 (1934), p. 83.

[22] L. B. Bezrukov and E. V. Bugaev. “Nucleon shadowing effects in photonuclear interactions”. In: *Sov. J. Nucl. Phys.* 33 (1981), p. 635.

[23] H. J. Bhabha. “The Scattering of Positrons by Electrons with Exchange on Dirac’s Theory of the Positron”. In: *Proc. Roy. Soc. A* 154 (1936), p. 195.

[24] Arunava Bhadra and Prabir Banik. *High energy leptonic originated neutrinos from astrophysical objects*. arXiv:1801.07677 [astro-ph.HE]. 2018.

[25] Atri Bhattacharya et al. “The Glashow resonance at IceCube: signatures, event rates and pp vs. $p\gamma$ interactions”. In: *JCAP* 10 (2011), p. 017.

[26] M. M. Block, L. Durand, and P. Ha. “Connection of the virtual $\gamma^* p$ cross section of ep deep inelastic scattering to real γp scattering, and the implications for νN and ep total cross sections”. In: *Phys. Rev. D* 89 (2014), p. 094027.

[27] J. Breitweg et al. “ZEUS results on the measurement and phenomenology of F_2 at low x and low Q^2”. In: *Eur. Phys. J. C* 7 (1999), p. 609.

[28] L. M. Brown and R. P. Feynman. “Radiative Corrections to Compton Scattering”. In: *Phys. Rev.* 85 (1952), p. 231.

[29] V. M. Budnev et al. “The Two-Photon Particle Production Mechanism. Physical Problems. Applications. Equivalent Photon Approximation”. In: *Phys. Rep.* 3 (1975), pp. 181–282.

[30] E. V. Bugaev et al. “Atmospheric muon flux at sea level, underground, and underwater”. In: *Phys. Rev. D* 58 (1998), p. 054001.

[31] E. V. Bugaev. “Effect of target recoil and excitation in bremsstrahlung and pair production processes”. In: *Sov. Phys. J. Exp. Theor. Phys.* 45 (1977), pp. 12–16.

[32] E. V. Bugaev and Yu. V. Shlepin. “Photonuclear interaction of high energy muons and tau leptons”. In: *Nucl. Phys. B Proc. Suppl.* 122 (2003), pp. 341–344. doi: 10.1016/S0920-5632(03)80414-0.

[33] E. V. Bugaev et al. “Propagation of tau neutrinos and tau leptons through the Earth and their detection in underwater/ice neutrino telescopes”. In: *Astropart. Phys.* 21 (2004), p. 491.

[34] A. P. Bulmahn. “Lepton pair production in high energy μA scattering: cross sections, energy loss, and applications to underground lepton production”. PhD thesis. University of Iowa, 2010.

[35] A. V. Butkevich et al. “Comments on multiple scattering of high-energy muons in thick layers”. In: *Nucl. Instr. Meth. in Phys. Res. A* 488 (2002), p. 282.

[36] M. Cerruti et al. *Lepto-hadronic single-zone models for the electromagnetic and neutrino emission of TXS 0506+056*. arXiv:1807.04335 [astro-ph.HE]. Submitted to Mon. Not. Roy. Astron. Soc. 2018.

[37] Xiao-Chuan Chang, Ruo-Yu Liu, and Xiang-Yu Wang. “Star-forming Galaxies as the Origin of the IceCube PeV Neutrinos”. In: *Astrophys. J.* 805 (2015), p. 95.

[38] G. F. Chew and S. C. Frautschi. “Regge Trajectories and and the Principle of Maximum Strength for Strong Interactions”. In: *Phys. Rev. Lett.* 8 (1962), pp. 41–44.

[39] D. Chirkin and W. Rhode. *Propagating leptons through matter with Muon Monte Carlo (MMC)*. arXiv:hep-ph/0407075. 2004.

[40] S. D. Drell and J. D. Walecka. “Electrodynamic Processes with Nuclear Targets”. In: *Ann. Phys.* 28 (1964), p. 18.

[41] L. R. B. Elton. *Nuclear Sizes*. Oxford University Press, 1961.

[42] R. Enberg, M. H. Reno, and I. Sarcevic. “Prompt neutrino fluxes from atmospheric charm”. In: *Phys. Rev. D* 78 (2008), p. 043005.

[43] Anatoli Fedynitch et al. “Calculation of conventional and prompt lepton fluxes at very high energy”. In: *Proceedings, 18th International Symposium on Very High Energy Cosmic Ray Interactions (ISVHECRI 2014): Geneva, Switzerland, August 18–22, 2014*. Vol. 99. 2015, p. 08001. eprint: 1503.00544.

[44] Enrico Fermi. “Über die Theorie des Stoßes zwischen Atomen und elektrisch geladenen Teilchen”. In: *Z. Phys.* 29 (1924), p. 315.

[45] Thomas K. Gaisser. “Atmospheric leptons. the search for a prompt component”. In: *European Physical Journal Web of Conferences*. Vol. 52. June 2013, p. 09004. doi: 10.1051/epjconf/20125209004. arXiv: 1303.1431.

[46] Thomas K. Gaisser, Ralph Engel, and Elisa Resconi. *Cosmic rays and particle physics*. 2nd edition. Cambridge University Press, 2016.

[47] G. Giacinti, M. Kachelrieß, and D. V. Semikoz. “Escape model for Galactic cosmic rays and an early extragalactic transition”. In: *Phys. Rev. D* 91 (2015), p. 083009.

[48] D. E. Groom and S. R. Klein. “Passage of particles through matter”. In: *Chin. Phys. C.* 38 (2014), p. 090001.

[49] D. E. Groom, N. V. Mokhov, and S. I. Striganov. “Muon Stopping Power and Range Tables 10 MeV–100 TeV”. In: *Atomic Data and Nuclear Data Tables* 78 (2001), p. 183.

[50] R. Hofstadter. “Electron Scattering and Nuclear Structure”. In: *Rev. Mod. Phys.* 28 (1952), p. 214.

[51] Mirco Hünnefeld. “Online Reconstruction of Muon Neutrino Events in IceCube using Deep Learning Techniques”. MA thesis. Technische Universität Dortmund, 2017.

[52] D. Yu. Ivanov. Private communications. Mar. 23, 2016.

[53] D. Ivanov and K. Melnikov. “Lepton pair production by a high energy photon in a strong electromagnetic field”. In: *Phys. Rev. D* 57 (1998), p. 4025.

[54] D. Ivanov et al. “Production of e^+e^- pairs to all orders in $Z\alpha$ for collisions of high-energy muons with heavy nuclei”. In: *Phys. Lett. B* 442 (1998), pp. 453–458.

[55] S. R. Kelner. “Pair Production in Collisions Between a Fast Particle and a Nucleus”. In: *Sov. J. Nucl. Phys.* 5 (1967), p. 778.

[56] S. R. Kelner. “Pair Production in Collisions between Muons and Atomic Electrons”. In: *Phys. At. Nucl.* 61 (1998), pp. 448–456.

[57] S. R. Kelner, R. P. Kokoulin, and A. A. Petruhkin. “Direct Production of Muon Pairs by High-Energy Muons”. In: *Phys. At. Nucl.* 63 (2000), pp. 1603–1611.

[58] S. R. Kelner, R. P. Kokoulin, and A. A. Petrukhin. *About Cross Section for High-Energy Muon Bremsstrahlung*. Preprint MEPhI 024-95. Moscow, 1995.

[59] S. R. Kelner, R. P. Kokoulin, and A. A. Petrukhin. “Bremsstrahlung from Muons scattered by Atomic Electrons”. In: *Phys. At. Nucl.* 60 (1997), pp. 576–583.

[60] S. R. Kelner, R. P. Kokoulin, and A. A. Petrukhin. “Radiation Logarithm in the Hartree-Fock Model”. In: *Phys. At. Nucl.* 62 (1999), pp. 1894–1898.

[61] S. R. Kelner and Yu. D. Kotov. “Muon energy loss to pair production”. In: *Sov. J. Nucl. Phys.* 7 (1968), pp. 237–240.

[62] S. Klein. “Suppression of bremsstrahlung and pair production due to environmental factors”. In: *Rev. Mod. Phys.* 71 (1999), p. 1501.

[63] J.-H. Koehne et al. “PROPOSAL: A tool for propagation of charged leptons”. In: *Comput. Phys. Commun.* 184 (2013), pp. 2070–2090.

[64] J.-H. Köhne. “Der Leptonpropagator PROPOSAL”. PhD thesis. TU Dortmund, 2013.

[65] R. P. Kokoulin. “Uncertainties in underground muon flux calculations”. In: *Nucl. Phys. B Proc. Suppl.* 70 (1999), p. 475.

[66] R. P. Kokoulin and A. A. Petrukhin. “Analysis of the cross section of direct pair production by fast muons”. In: *Proc. 11th Int. Conf. on Cosmic Rays, Budapest 1969*. Vol. 29, Suppl. 4. Acta Phys. Acad. Sci. Hung., 1970, pp. 277–284.

[67] R. P. Kokoulin and A. A. Petrukhin. “Influence of the nuclear formfactor on the cross section of electron pair production by high-energy muons”. In: *Proc. 12th Int. Conf. on Cosmic Rays, Hobart 1971*. Vol. 6. 1971, pp. 2436–2444.

[68] P. A. Krachkov and A. I. Milstein. “Charge asymmetry in the differential cross section of high-energy bremsstrahlung in the field of a heavy atom”. In: *Phys. Rev. A* 91 (2015), p. 032106.

[69] P. A. Krachkov and A. I. Milstein. “Coulomb effects in high-energy e^+e^- electroproduction by a heavy charged particles in an atomic field”. In: *Phys. Lett. B* 771 (2017), pp. 5–8.

[70] V. A. Kudryavtsev. “Muon simulation codes MUSIC and MUSUN for underground physics”. In: *Comp. Phys. Commun.* 180 (2008), pp. 339–346.

[71] V. A. Kudryavtsev, E. V. Korolkova, and N. J. C. Spooner. “Narrow muon bundles from muon pair production in rock”. In: *Phys. Lett. B* 471 (1999), pp. 251–256.

[72] L. D. Landau and I. Ya. Pomeranchuk. “Пределы применимости теории тормозного излучения электронов и образования пар при больших энергиях”. In: *Доклады академии наук СССР* 92 (1953), p. 535.

[73] J. G. Learned and S. Pakvasa. “Detecting ν_τ Oscillations at PeV Energies”. In: *Astropart. Phys.* 3 (1995), p. 267.

[74] P. Lipari and T. Stanev. “Propagation of multi-TeV muons”. In: *Phys. Rev. D* 44 (1991), p. 3543.

[75] L. N. Lipatov and G. V. Frolov. “Some Processes in Quantum Electrodynamics at High Energies”. In: *Sov. J. Nucl. Phys.* 13 (1971), pp. 333–339.

[76] Ruo-Yu Liu et al. *A hadronuclear interpretation of a high-energy neutrino event coincident with a blazar flare*. arXiv:1807.05113 [astro-ph.HE]. 2018.

[77] W. Lohmann, R. Kopp, and R. Voss. CERN 85-03. 1985.

[78] F. Mandl and T. H. R. Skyrme. “Theory of the Double Compton Effect”. In: *Proc. Roy. Soc. Lond. A Math. Phys. Sci.* 215 (1952), p. 497.

[79] Theo Mayer-Kuckuk. *Kernphysik. Eine Einführung*. Teubner, 2002.

[80] Maximilian Meier. Private communications.

[81] A. B. Migdal. “Bremsstrahlung and Pair Production at High Energies in Condensed Media”. In: *Sov. Phys. J. Exp. Theor. Phys.* 5 (1957), p. 527.

[82] K. Mork and H. Olsen. “Radiative Corrections. I. High-Energy Bremsstrahlung and Pair Production”. In: *Phys. Rev.* 140 (1965), B 1661.

[83] K. A. Olive et al. “Review of Particle Physics”. In: *Chin. Phys. C* 38 (2014), p. 090001.

[84] H. Olsen. “Outgoing and Ingoing Waves in Final States and Bremsstrahlung”. In: *Phys. Rev.* 167 (1968), p. 1159.

[85] Andrea Palladino et al. *Interpretation of the diffuse astrophysical neutrino flux in terms of the blazar sequence*. arXiv:1806.04769 [astro-ph.HE].

[86] B. Peters. “Primary Cosmic Radiation and Extensive Air Showers”. In: *Nuovo Cimento* XXII (1961), p. 800.

[87] A. A. Petrukhin and V. V. Shestakov. “The influence of nuclear and atomic form factors on the muon bremsstrahlung cross section”. In: *Canad. J. Phys.* 46 (1968), S377.

[88] A. A. Petrukhin and V. V. Shestakov. “К вопросу о сечении тормозного излучения мюонов при больших энергиях”. In: *Физика элементарных частиц*. Ed. by V. D. Mikhaylov and I. L. Rozental’. Moscow: Атомиздат, 1966, p. 102.

[89] Robert Piessens et al. *QUADPACK: A subroutine package for automatic integration*. Springer-Verlag, 1983.

[90] S. Polityko et al. “Muon cross-sections with both the LPM and Ter-Mikaelyan effect at extremely high energies”. In: *J. Phys. G: Nucl. Part. Phys.* 28 (2002), p. 427.

[91] G. Racah. “Sulla Nascita di Coppie per Urti di Particelle Elettrizzate”. In: *Il Nuovo Cimento* 14 (1937), p. 93.

[92] M. H. Reno, I. Sarcevic, and S. Su. “Propagation of supersymmetric charged sleptons at high energies”. In: *Astropart. Phys.* 24 (2005), p. 107.

[93] W. Rhode. “Measurements of the Muon-Flux with the Fréjus-Detector”. In: *Nucl. Phys. B Proc. Suppl.* 35 (1994), p. 250.

[94] Wolfgang Rhode. “Untersuchung der Energiespektren hochenergetischer Muonen im Fréjusdetektor”. WUB-DIS-93-11. PhD thesis. Universität Wuppertal, 1993.

[95] A. Sandrock, S. R. Kelner, and W. Rhode. “Radiative corrections to the average bremsstrahlung energy loss of high-energy muons”. In: *Phys. Lett. B* 776 (2018), pp. 350–354.

[96] Alexander Sandrock and Wolfgang Rhode. *Coulomb corrections to the bremsstrahlung and electron pair production cross section of high-energy muons on extended nuclei*. arXiv:1807.08475. Submitted to Phys. Lett. B.

[97] L. I. Schiff. “Energy-Angle Distribution of Thin-Target Bremsstrahlung”. In: *Phys. Rev.* 83 (1951), p. 252.

[98] Jan Benjamin Soedingrekso. Private communications.

[99] I. A. Sokalski, E. V. Bugaev, and S. I. Klimushin. “MUM: flexible precise Monte Carlo algorithm for muon propagation through thick layers of matter”. In: *Phys. Rev. D* 64 (2001), p. 074015.

[100] T. Stanev et al. “Development of ultrahigh-energy electromagnetic cascades in water and lead including the Landau-Pomeranchuk-Migdal effect”. In: *Phys. Rev. D* 25 (1982), p. 1291.

[101] R. M. Sternheimer and R. F. Peierls. “General Expression for the Density Effect for the Ionization Loss of Charged Particles”. In: *Phys. Rev.* B3 (1971), p. 3681.

[102] V. V. Sudakov. “Vertex parts at Very High Energies in Quantum electrodynamics”. In: *Sov. Phys. J. Exp. Theor. Phys.* 3 (1956), pp. 65–71.

[103] M. L. Ter-Mikaelian. In: *Доклады академии наук СССР* 94 (1954), p. 1033.

[104] F. F. Ternovskiĭ. “Effect of multiple scattering on pair production by high energy particles in a medium”. In: *Sov. Phys. J. Exp. Theor. Phys.* 10 (1960), p. 718.

[105] Y. S. Tsai. “Pair production and bremsstrahlung of charged leptons”. In: *Rev. Mod. Phys.* 46 (1974), pp. 815–851.

[106] C. F. v. Weizsäcker. “Ausstrahlung bei Stößen sehr schneller Elektronen”. In: *Z. Physik* 88 (1934), pp. 612–625. doi: 10.1007/BF01333110.

[107] E. J. Williams. “Nature of the High Energy Particles of Penetrating Radiation and Status of Ionization and Radiation Formulae”. In: *Phys. Rev.* 45 (1934), pp. 729–730. doi: 10.1103/PhysRev.45.729.

[108] R. Yennie, S. C. Frautschi, and H. Suura. “The infrared divergence phenomena and high-energy processes”. In: *Ann. Phys. (N. Y.)* 13 (1961), p. 379.

[109] Chengchao Yuan et al. “Cumulative Neutrino and Gamma-Ray Backgrounds from Halo and Galaxy Mergers”. In: *Astrophys. J.* 857 (2018), p. 50.